CARIBBEAN PRECIPITATION IN OBSERVATIONS AND IPCC AR4 MODELS

A Dissertation

by

ELINOR RUTH MARTIN

Submitted to the Office of Graduate Studies of
Texas A&M University
in partial fulfillment of the requirements for the degree of

DOCTOR OF PHILOSOPHY

August 2011

Major Subject: Atmospheric Sciences

CARIBBEAN PRECIPITATION IN OBSERVATIONS AND IPCC AR4 MODELS

A Dissertation

by

ELINOR RUTH MARTIN

Submitted to the Office of Graduate Studies of
Texas A&M University
in partial fulfillment of the requirements for the degree of

DOCTOR OF PHILOSOPHY

Approved by:

Chair of Committee,	Courtney Schumacher
Committee Members,	Ping Chang
	Andrew Dessler
	Bradford Wilcox
Head of Department,	Kenneth P. Bowman

August 2011

Major Subject: Atmospheric Sciences

ABSTRACT

Caribbean Precipitation in Observations and IPCC AR4 Models. (August 2011)

Elinor Ruth Martin, B.Sc., University of Reading;

M.S., Colorado State University

Chair of Advisory Committee: Dr. Courtney Schumacher

A census of 24 coupled (CMIP) and 13 uncoupled (AMIP) models from the Intergovernmental Panel on Climate Change (IPCC) fourth assessment report (AR4) were compared with observations and reanalysis to show varied ability of the models to simulate Caribbean precipitation and mechanisms related to precipitation in the region. Not only were errors seen in the annual mean, with CMIP models underestimating both rainfall and sea surface temperature (SST) and AMIP models overestimating rainfall, the annual cycle was also incorrect. Large overestimates of precipitation at all SSTs (and particularly above 28°C) and at vertical circulations less than -10 hPa/day (the deep convective regime) were inherent in the atmospheric models with models using spectral type convective parameterizations performing best. In coupled models, however, errors in the frequency of occurrence of SSTs (the distribution is cold biased) and deep convective vertical circulations (reduced frequency) lead to an underestimation of Caribbean mean precipitation. On daily timescales, the models were shown to produce too frequent light rainfall amounts (especially less than 1 mm/day) and dry extremes and too few heavy rainfall amounts and wet extremes. The simulation of the mid-summer drought (MSD) proved a challenge for the models, despite their ability to produce a Caribbean low-level jet (CLLJ) in the correct location. Errors in the CLLJ, such as too strong magnitude and weak semi-annual cycle, were worse in the CMIP models and were attributed to problems with the location

and seasonal evolution of the North Atlantic subtropical high (NASH) in both CMIP and AMIP models. Despite these discrepancies between models and observations, the ability of the models to simulate the correlation between the CLLJ and precipitation varied based on season and region, with the connection with United States precipitation particularly problematic in the AMIP simulations. An observational study of intraseasonal precipitation in the Caribbean showed an explicit connection between the Madden-Julian oscillation (MJO) and Caribbean precipitation for the first time. Precipitation anomalies up to 50 % above (below) the annual mean are observed in phases 1 and 2 (5 and 6) of the MJO and are related to changes in the CLLJ, that is also modulated by the MJO. Considerable progress has been made on identifying both problems and successes in the simulation of Caribbean climate in general circulation models, but many areas still require investigation.

ACKNOWLEDGMENTS

I would like to thank my advisor and committee chair, Dr. Courtney Schumacher, without whom I would be neither the scientist nor person I am today. Considerable thanks also go to my other committee members, Drs. Ping Chang, Andy Dessler and Brad Wilcox for their role and advice in shaping my dissertation. Additional thanks go to Dr. Rusty Feagin for his role as a substitute committee member. I also thank all the members of the department, my friends, my family, and of course my fellow A-Team members, for all the support they have given during my time at A&M.

This research was supported by NASA Grants NNX06AE23G and NNX10AG89G. The author acknowledges the modeling groups, the PCMDI and the World Climate Research Programme's Working Group on Coupled Modelling (WGCM) for their roles in making available the WCRP CMIP3 multi-model dataset. Support of this dataset was provided by the Office of Science, U.S. Department of Energy. The monthly GPCP combined precipitation data were developed and computed by the NASA/Goddard Space Flight Center's Laboratory for Atmospheres as a contribution to the GEWEX Global Precipitation Climatology Project. NCEP_Reanalysis 2 data were provided by the NOAA/OAR/ESRL PSD, Boulder, Colorado, USA, from their Web site at http://www.esrl.noaa.gov/psd/. Wavelet software is available at URL: http://atoc.colorado.edu/research/wavelets/ and was developed by C. Torrence and G. Compo.

TABLE OF CONTENTS

CHAPTER Page

LIST OF TABLES

LIST OF FIGURES

FIGURE Page

FIGURE Page

FIGURE Page

FIGURE Page

FIGURE Page

FIGURE Page

CHAPTER I

INTRODUCTION

The Caribbean is one of many regions of the world where it is vital to understand precipitation patterns, extremes and variability. The low-lying coastal regions of Caribbean islands are densely populated and development pressure is increasing. The region is also vulnerable to many natural hazards that are related to and exacerbated by precipitation variations, such as hurricanes, earthquakes, mudslides and drought. There is also evidence that precipitation patterns can influence the spread of Dengue fever in the region (Jury, 2008). Planning, policy and management of these events are extremely dependent on knowledge of the precipitation of the region. These social and economic reasons provide considerable motivation for increasing and expanding current knowledge of precipitation in the Caribbean.

Lying between South and North America, bordered by the Atlantic ocean and the central American highlands (Fig. 1, Caribbean climate is influenced by a wide range of phenomena. The Caribbean is defined throughout this study as lying between 55 and 90°W and 10 to 25°N (black box in Fig. 1). This includes the Greater and Lesser Antilles, a portion of central America and northern South America in addition to the Caribbean Sea and far western subtropical Atlantic ocean.

In order to simulate future climate change, general circulation models (GCMs) need to accurately represent observed climate. Whilst GCMs simulate temperature well, precipitation is considerably more challenging, especially in the tropics as the small sub-grid scale processes associated with precipitation (and convection in particular) require parameterization. For example, most models from the 4th Assessment

---

The journal model is *Journal of Climate*.

Report (AR4) of the Intergovernmental Panel on Climate Change (IPCC) predict a decrease in precipitation across the Caribbean region whilst also underestimating current precipitation amounts in the region (Neelin et al., 2006; Christensen et al., 2007).

The trend in precipitation during June, July and August (JJA) from a subset of IPCC AR4 models was investigated by Neelin et al. (2006). They show that not only is Caribbean precipitation projected to decrease, the Caribbean is one of a handful of tropical regions where there is large inter-model agreement in the trend. Observed trends in precipitation in the Caribbean are unclear from the literature. Whilst Neelin et al. (2006) identify a small but statistically significant drying trend during JJA in recent decades in three datasets, Peterson et al. (2002) found no statistically significant trends in mean precipitation amounts, indicating the need for further analysis of precipitation in the region.

However, as noted previously, the IPCC AR4 also found that models underestimated the monthly observed precipitation amounts in the Caribbean by approximately 30% when compared to the Climate Prediction Center Merged Analysis of Precipitation (CMAP). The spatial and temporal distribution of this underestimation, in addition to mechanisms causing the underestimation by the AR4 models, has not been fully investigated. The inability of models to correctly simulate both precipitation amount and variability in the current climate is a significant stumbling block for future climate simulations and could influence how much we trust output of current climate change simulations.

A variety of GCMs with differing parameterization, resolutions and flux corrections were used for the IPCC AR4 report. Much of the report concerning the Caribbean is focused on the results from coupled (atmosphere and ocean models) simulations. However, results from uncoupled simulations, which force the atmo-

spheric only model with observed sea surface temperatures (SSTs), are also available for the latter part of the 20th century and can be used to provide insight into potential sources of error in the coupled simulations. This study is focused on simulations of 20th century climate, precipitation in particular, to assess the ability of models to simulate current climate and identify biases that may propagate into the future simulations.

A review of the literature has shown that the IPCC AR4 models are not accurately representing mean Caribbean precipitation, however, a detailed study of which features and mechanisms are not well represented has not yet been undertaken. Whilst initial thoughts may lead to the lack of tropical cyclone activity within GCMs, the IPCC AR4 shows an underestimation of precipitation across all seasons (Christensen et al., 2007), indicating a more complex problem.

It is the aim of this research to develop and extend current understanding of precipitation climatology, extremes and variability in the Caribbean. This will be accomplished by investigating mechanisms and phenomenon in both observations and IPCC AR4 model output. The following key objectives will be the focus of this research:

- Characterize the precipitation climatology, extreme events and variability in observations and IPCC AR4 GCMs with special emphasis on the Madden-Julian Oscillation (MJO).

- Determine what significant differences exist between the observations and models. Are differences due to problems with parameterizations, resolution or mechanisms?

The research is split into three areas. The precipitation climatology (average and extremes), including investigations into mechanisms behind errors in the IPCC

AR4 model simulation of precipitation is discussed in Chapter II. The simulation of the Caribbean low-level jet (CLLJ), an important regional feature that is important for control of both local and United States precipitation is investigated in Chapter III. The third research area, contained in Chapter IV, is an observational study of intraseasonal variability in Caribbean precipitation and its relationship with the MJO. Conclusions and suggestions for future work are contained in Chapter V.

CHAPTER II

CARIBBEAN PRECIPITATION CLIMATOLOGY AND IPCC AR4 MODEL COMPARISONS

A. Background

The structure of the precipitation in the Caribbean (defined as 10-25°N, 55-90°W, see Fig. 1) is relatively well known, although mechanisms behind the climatology are still being understood. Annual rainfall exhibits a bimodal structure, with an initial maximum around May, a minimum around July-August, and a second maximum in September-October (Jury et al., 2007; Gamble et al., 2008). The minimum that separates the two peaks in rainfall has been termed the 'mid-summer' drought (MSD) and is thought to be caused by expansion of the North Atlantic subtropical high (NASH) and the Caribbean low-level jet (CLLJ) (Magaña et al., 1999). The MSD and specifically its relationship with the CLLJ is addressed more thoroughly in Chapter III.

The dominant cause for spatial variations in precipitation across the region is land-sea and orography effects. Sobel et al. (2011) show using Tropical Rainfall Measuring Mission (TRMM) precipitation radar (PR) data that the rainfall enhancement is more significant over larger (greater than 315 km^2) islands than smaller islands in the Caribbean. Smaller islands have a negligible or even negative change in rainfall intensity and frequency while large islands have increases close to 30% the the daily mean.

The dominant synoptic influence for Caribbean precipitation is the NASH. The location of the NASH shifts zonally and meridionally and also varies in intensity. These variations affect the strength of the trade winds and subsidence which act to

modify precipitation amounts in the Caribbean region (Gamble et al., 2008). On interannual timescales, precipitation in the region is also influenced by the El Niño-Southern Oscillation (ENSO) and the North Atlantic Oscillation (NAO) (Chen and Taylor, 2002; Jury et al., 2007). ENSO impacts the Caribbean through changes in convergence patterns and sea surface temperatures (SSTs) in the Caribbean that cause changes in rainfall (Giannini et al., 2000; Taylor et al., 2002; Chen and Taylor, 2002). The second rainfall season (September and October) tends to be drier in El Niño years and wetter in La Niña years (Giannini et al., 2000). However, the first rainfall season in May and June tends to be wetter in the year after an El Niño and drier in a La Niña year (Chen and Taylor, 2002). The phase of the NAO modulates the behavior of warm ENSO events (Giannini et al., 2001).

The region is influenced on timescales of days to weeks by the propagation of easterly waves, which can mature into tropical storms and hurricanes, representing a large contribution to rainfall in the Caribbean and the main contribution to the second rainfall peak in the annual cycle (Gamble et al., 2008). Recent evidence also suggests a quasi-decadal (7 - 10 year) cycle in Caribbean rainfall that may be related to hemispheric-scale features such as the Hadley Cell and the inter-tropical convergence zone (ITCZ) (Jury, 2009b). It is apparent that the climatology of this region is complex with variability on a range of spatial and temporal scales.

The Caribbean Sea is part of the Atlantic Warm Pool (AWP) with SSTs exceeding 28.5°C and has maximum extent in boreal summer, when it is positively correlated with precipitation not only over the Caribbean, but Central America, southeast Pacific and the US (Wang and Enfield, 2001; Wang et al., 2008). However, (Misra et al., 2009) show that in 8 of the IPCC AR4 coupled simulations for summer, the SSTs have a large cold bias. Although coupled models underestimate Caribbean precipitation, it has been shown the uncoupled models forced with observed SSTs overestimate

Caribbean precipitation (Biasutti et al., 2006; Martin and Schumacher, 2011a).

A number of comparisons will also be made between the AWP and the West Pacific Warm Pool (WPWP).In the WPWP, SSTs are higher and have a greater spatial extent than the AWP, as seen in Fig. 2. The WPWP not only has higher SSTs, but also high relative humidity in the lower free troposphere and weaker surface winds (Sobel et al., 2011). The warm SSTs of the WPWP are associated with large amounts of water vapor, column ice and a larger areal coverage of rainfall events. Clouds are deeper and higher in the WPWP than the East Pacific and Caribbean and much of the rainfall is from convective rather than stratiform rainfall (Berg et al., 2002). Both the West Pacific and Caribbean contain a large number of islands and show enhanced rain frequency and total rainfall over larger islands compared to the surrounding ocean (Sobel et al., 2011).

Similar modeling results to the Caribbean, although less extreme, have been shown in the Western Pacific Warm Pool (WPWP) (Lin, 2007). Although most models get the general large-scale structure in the West Pacific, the well known double ITCZ structure over the tropical Pacific and associated westward extension of the East Pacific cold tongue is a major problem in the IPCC AR4 simulations (Lin, 2007). The WPWP is also more directly influenced by ENSO than the Caribbean, and hence the poor simulation of ENSO in the IPCC AR4 models (AchutaRao and Sperber, 2002) may impact the WPWP more than the AWP. Despite the similarities between the regions, the IPCC AR4 report predicts precipitation to increase in the West Pacific (Christensen et al., 2007). Further differences and similarities between the regions in observations and IPCC AR4 models will be investigated in this study.

In addition to SSTs, the connection between precipitation and the large-scale vertical circulation (as represented by ω_{500}) is also of importance. Correctly representing large-scale vertical circulations is essential for correctly reproducing heat and

moisture transport and thus impacts on stability and precipitation. The relationship between precipitation and both SST and ω_{500} will be investigated using the regime sorting (or compositing) technique of Bony et al. (2004) to determine the source of the precipitation errors.

The correct simulation of Caribbean climate, in particular, its moisture budget and SST, is important not only for the Caribbean but also for weather and climate in the United States. The amount of moisture transport to the central U.S. by the Great Plains low-level jet is strongly influenced by the Caribbean moisture budget (Mestas-Nuñez et al., 2007; Wang et al., 2008) and hence the correct simulation of precipitation by GCMs in the Caribbean is critical for accurate simulations of both local and remote climate. It is the aim of this chapter to thoroughly investigate how a range of IPCC AR4 models represent precipitation in the Caribbean, including mean values, extremes, and relationships with SSTs and vertical circulation.

This chapter will begin with a brief discussion of the observational and IPCC AR4 data (Section B), followed by an analysis of mean rainfall and annual cycles (Section C) and connections with local and remote SSTs (Section D). Mechanisms are analyzed using a regime sorting analysis in Section E, and daily data is used to investigate precipitation distributions in Section F.

B. Data and Model Information

1. Observations

Several observational and reanalysis datasets are used to obtain the most accurate and spatially complete climatology of Caribbean precipitation, with which the model output can be compared. All data is monthly resolution for the period 1979-2008. Vertical pressure velocity (500 hPa) is obtained from NCEP/DOE Reanalysis II

(Kanamitsu et al., 2002) at 2.5° resolution. Precipitation data is from the Global Precipitation Climatology Project (GPCP), which is a combination of satellite products and gauge observations (Huffman et al., 2001). Monthly GPCP data is available at 2.5° resolution. Jury (2009a) show that the GPCP monthly data better captures the features of the Caribbean precipitation climatology than the CPC Merged Analysis of Precipitation (CMAP) dataset, justifying the use of the GPCP product for comparisons with the IPCC AR4 output. The third dataset used was the Hadley Centre Sea Ice and Sea Surface Temperature data set 1 (HadISST1) to investigate the links between the CLLJ and SST. The HadISST dataset is at 1° resolution and uses a combination of in situ and satellite observations to provide global coverage (Rayner et al., 2003). Daily precipitation data is also used for analyzing the daily distribution of precipitation from the GCMs (Section F). Daily precipitation is also from the GPCP dataset and is available at 1° resolution for the period 1997-2008.

Regions with equal numbers of grid points were chosen to represent the Caribbean (AWP) and West Pacific (WPWP) and are shown by the boxes in Fig. 2. The Caribbean is defined as 10-25^{o}N, 55-90^{o}W, and the West Pacific as 10^{o}S-5^{o}N, 130-165^{o}E. These regions were chosen as they are both influenced by the surrounding land and/or islands.

2. IPCC AR4 Models

Output from 24 coupled ocean-atmosphere GCMs (coupled model intercomparison project; CMIP type) and 13 atmospheric only GCMs (atmosphere model intercomparison project; AMIP type) are examined. These models are a subset of those used as part of the IPCC AR4 and are available through the Program for Climate Model Diagnostics and Intercomparison (PCMDI). Vertical large-scale circulation (ω_{500}), SST and precipitation monthly and daily means are used. Monthly mean values for the

last 30 years of the CMIP climate of the 20th century simulations (20C3M) are used in order to make a fair comparison with the observational data. For the AMIP simulation, 1979-2000 are used (except GFDL_2_1 and NCAR_PCM, which were available for 1980-1999 and 1979-1999 respectively). Daily data, which is used in Section F, is for the last 12 years of the CMIP and AMIP simulations.

All models are configured differently with varying resolutions and parameterizations. A summary of the models used, as well as pertinent information concerning their configuration and parameterizations (convective and closure), is shown in Tables 1 and 2. While some models had multiple ensembles, only one realization from each model is used to ensure model mean results are not skewed towards models with a large number of ensembles. All model output is kept at its original resolution (unless otherwise specified), rather than interpolating onto a consistent grid, in order to make conclusions about the impact of resolution.

In order to determine whether the type of convective parameterization scheme significantly influences precipitation and its relationships with SST and the large-scale vertical circulation, models were grouped by four different convective parameterization types as shown in Table 2. Bulk parameterizations (e.g. Gregory and Rowntree (1990)) use one cloud model to represent the average over the convective ensemble. Spectral parameterizations (e.g. Moorthi and Suarez (1992)) are similar to Arawaka and Schubert (1974), which parameterizes deep convection with ensembles of clouds. A number of models use the Zhang and McFarlane (1995) scheme (ZM) which applies techniques from both the spectral and bulk methods. Three models use convective parameterizations that are not classified as 'bulk', 'spectral' or 'ZM' and thus are classified as 'other' in this study.

C. Climatology

A climatology of precipitation rate by season (DJF, MAM, JJA, and SON) across the Caribbean region was developed from GPCP monthly data and is shown in Fig. 3. A climatology was also developed for the shorter time period, higher resolution daily GPCP data, but as the main features compared well (Fig. 33a), output from the longer term monthly data only is used throughout much of the discussion of climatology in this chapter.

Figure 3 shows the complex nature of the precipitation pattern across the Caribbean throughout the year. The most obvious feature is the increase in precipitation over land, which is seen clearly over the large (e.g. Cuba and Hispaniola) islands and Central America.. Despite the low horizontal resolution, a hint of precipitation increase over the smaller Lesser Antilles islands (60°W) is also seen throughout the annual cycle. Orography and land-sea differences clearly play an important role in precipitation in this region. The area with the lowest average precipitation rates is located in the south central Caribbean Sea, to the north of Venezuela. The spatial pattern of precipitation remains relatively constant throughout the annual cycle, with precipitation rates lowest during the winter (DJF) and largest in the fall (SON). Jury (2009a) identifies five key features in Caribbean rainfall that can be identified in Fig. 3 that are necessary to correctly simulate (although the domain used in this study is broader in all direction). The five features are:

1. Topographically enhanced convection (Greater Antilles)
2. Narrow dry zone in wind shadow of Hispaniola
3. Broad dry zone extending from east Atlantic through northern Lesser Antilles
4. Broad dry zone with easterly trade wind north of Venezuela

5. Moist tongue extending northward from South America through Lesser Antilles

The DJF and JJA average precipitation rate from two IPCC AR4 CMIP and AMIP simulations are shown in Figs. 4 and 5, respectively. The two models shown (CNRM and MIROC_HI) are representative of the entire model ensemble. Precipitation output from the IPCC AR4 models captures the general structure of the precipitation distribution (i.e. key feature 3) on the large scale, considering the low horizontal resolution of the model output and the representation of both islands and topography in the models (difficultly in representing key features 1, 2, and 5). This lack of islands and topography in the IPCC AR4 models leads to a more uniform precipitation pattern across the region as seen in Figs. 4 and 5 with the IPCC models in general underestimating precipitation on and close to land, and overestimating ocean based precipitation, particularly in the central Caribbean Sea (key feature 4).

The wintertime (DJF) climatology produced by the IPCC models, tends to overestimate the precipitation in both the CMIP and AMIP models, clearly seen in the CNRM simulations (Figs. 4a, c). This is a strong indication that errors in precipitation simulation are not simply due to the misrepresentation of tropical storms. The simulations for JJA (Fig. 5) are representative of all seasons aside from DJF, where once again precipitation patters are more uniform than observations, CMIP models tend to underestimate precipitation rates and AMIP models overestimate precipitation. The CNRM model is one of the few CMIP models (Fig. 5a) that overestimate JJA precipitation. The area-averaged annual cycle of precipitation from the IPCC models and observations is further investigated in Fig. 6.

The observed annual cycle of precipitation in the Caribbean (Fig. 6, black solid line) shows the bimodal distribution as seen in the literature, with peaks in June and October, separated by a period of midsummer drought (Gamble et al., 2008; Jury

et al., 2007). Perhaps the most striking result from Fig. 6 is the overestimation by AMIP models (dashed line) and underestimation by CMIP models (dotted line) throughout the entire annual cycle (except January through March when both overestimate). This agrees with the IPCC report and previous studies (Biasutti et al., 2006; Christensen et al., 2007) but extends the findings to the whole ensemble of CMIP and AMIP models and the entire annual cycle. The large range of both the AMIP (Fig. 6, left panel) and CMIP (Fig. 6, right panel) ensembles is evident, particularly in the summer months when differences between the models with the largest and smallest area-averaged monthly values can be in excess of 4 mm/day.

An additional feature that is evident from both the CMIP and AMIP mean annual cycles and the individual models annual cycles is the poor representation of the MSD, particularly in the CMIP models. The two maxima are less pronounced in the models and in many cases the annual cycle is unimodal with a peak in September or October. The AMIP models show a more distinct MSD, although not all models produce a MSD. More analysis concerning the MSD and the relationship with the CLLJ can be found in Chapter III.

The observed annual cycle of monthly standard deviations (i.e. standard deviation of all January's, February's etc.) indicates a similar bimodal structure to the mean annual cycle with the first maxima in May and June (Fig. 7, black line). However, the second maxima in standard deviation is one month later than the annual mean and is seen is October, possibly due to the impact of tropical storms being more variable in October. The IPCC AR4 models capture the magnitude of the standard deviation annual cycle but similar problems to the mean annual cycle are seen (i.e. weaker bimodal or unimodal), with AMIP simulations (Fig. 7, red lines) more accurately representing the standard deviation annual cycle.

Additional analysis of variability was performed using Wavelet analysis (Torrence

and Compo, 1998) of the area-averaged Caribbean precipitation to analyze the main periods and timescales of enhanced variability. The wavelet analysis for both the observations (Fig. 8) and a selection of IPCC AR4 models (Fig. 9) shows clear evidence of observed enhanced power in the 2-4 year range associated with ENSO and the 8 year period discussed in Jury (2009b). The representation of these features is generally poor in the IPCC AR4 models, which tend to underestimate power at all timescales and the ENSO signal tends to be at at shorter timescales (AchutaRao and Sperber, 2002). This underestimation is particularly the case for the CMIP models. Further discussion of variability in the 30-90 day range is contained in Chapter IV.

D. Sea Surface Temperature

1. Local SST Relationships

Precipitation in the tropics is dependent on SST, and as discussed previously, Misra et al. (2009) has shown that in 8 of the IPCC AR4 coupled simulations for summer, SSTs have a large cold bias in the Caribbean. This section aims to further understand this cold SST bias in the Caribbean and how it impacts precipitation in the region.

The observed (from HadISST) seasonal mean SST distribution in the Caribbean and northern tropical Atlantic is shown in Fig. 10. The development of the AWP (often distinguished by the 28.5°C isotherm) in the eastern Pacific is seen in MAM (Fig. 10b) and it extends into the Gulf of Mexico and Caribbean Sea in JJA (Fig. 10c). This warming of the SSTs in the Caribbean matches well with the increasing precipitation throughout the seasons seen in Fig. 3.

The simulation of summer SST in the Caribbean in a small number of IPCC AR4 coupled models is shown in Misra et al. (2009). This study extends that work to look at the whole CMIP ensemble for all seasons. Two model examples are shown

here. The first (Fig. 11, CSIRO_3_0), is the model with the lowest area-mean SSTs and the second (Fig. 12, MPI), is one of the models with the highest area mean SSTs. These are chosen to illustrate the huge range of results from the CMIP simulation.

Figures 11 and 12 show that whilst the magnitudes of the SST are clearly incorrect, the general pattern shows some similarities with observations in the majority of the models. Both show the warmest waters initially appearing in the eastern Pacific prior to the Gulf of Mexico and Caribbean Sea warming in JJA, along with a region of high SSTs across the tropical Atlantic. In many of the models, as seen in these two examples, the Caribbean Sea to the north of Venezuela has a region of cold SSTs that is much more distinct than the observations. This may be a result of incorrect upwelling in the region due to the CLLJ being too strong in the models (see Chapter III). It is evident that errors in the SST are not just confined to the summer season and are likely to impact precipitation throughout the year.

The climatology of annual mean Caribbean area-averaged precipitation and SST is shown in Fig. 13a for observations (OM) and model output. The strong cold bias of the CMIP models is evident, exceeding 1.5°C in 9 of the models. This bias occurs throughout the annual cycle (not shown). The CMIP model results do not show a simple relationship between SST and precipitation, as models with the largest SST bias (over 2°C) do not necessarily produce the lowest mean precipitation amounts. The CMIP multi-model ensemble mean (CM) SST is biased cold (26.1°C versus 27.5°C) and the multi-model ensemble mean precipitation is biased dry (2.38 mm/day versus 2.71 mm/day). This oversensitivity of precipitation to SST is demonstrated in the AMIP model output also shown in Fig. 13a. In this case, and much of the later discussion, oversensitivity is regarded as too much precipitation for a given value of SST, unless otherwise specified. Despite forcing with observed SST, the range of precipitation produced by the AMIP ensemble is larger than the CMIP ensemble, with

the multi-model ensemble mean (AM) 0.86 mm/day larger than observed.

The impact of the convective parameterization type is more obvious on precipitation than SST. Models using bulk parameterizations tend to produce higher than average precipitation and models using spectral parameterizations produce lower precipitation amounts, for both CMIP and AMIP models. Models using the ZM scheme tend to overestimate precipitation in AMIP models, and underestimate in CMIP models. When analyzing by mean SST in which convective parameterization is not the main factor in determining value, it seen that the four models with the best Caribbean averaged SST values (CSIRO_3_5, INGV, MPI, and UKMO_HADCM) all use bulk parameterizations. However, the three models with the lowest Caribbean averaged SST values (CSIRO_3_0, GISS_ER, and CNRM) also use the bulk parameterizations, suggesting no simple relationship between convective parameterization type and SST in the region, as may be expected due to the complex interactions and feedbacks between precipitation and SST. More rigorous testing of the impact of convective parameterization on SST (and precipitation) could be performed by using the same model framework and varying the convective parameterization. This relationship between SST, precipitation and convective parameterization will be returned to in Section E.

The climatology for the West Pacific is shown in Fig. 13b and shows similarities with the Caribbean although it is both warmer and wetter. The majority of the CMIP models produce SSTs that are biased cold, although unlike the Caribbean, most of the models are within 1°C of the observed mean. The CMIP models also produce too dry conditions in the West Pacific and wetter than observed conditions in the AMIP simulations. In addition to the weaker cold bias in the West Pacific, the main difference between the climatology of the regions is the impact of the convective parameterizations. Again, the bulk parameterizations produce both the warmest

and coldest annual mean SSTs, but the impact of parameterization on precipitation is reversed from the Caribbean. The spectral parameterization group produces the most rainfall, with the ZM and bulk groups producing less. This result suggests that processes controlling deep convection differ in the two regions and hence, the performance of the parameterizations is not consistent in the two warm pool regions.

2. Global SST Relationships

As discussed previously, rainfall in the Caribbean is influenced by a number of remote climate features in both the Pacific and Atlantic such as ENSO and the NAO (Giannini et al., 2000; Taylor et al., 2002; Chen and Taylor, 2002). The relationship between local Caribbean precipitation and global SSTs is investigated using a regression analysis between the area-averaged Caribbean precipitation anomalies (seasonal cycle removed) and the global grid point SST anomalies (seasonal cycle removed). The SSTs are also detrended, however, this makes little difference to the patterns calculated. Regressions were also calculated for lagged seasons (SST leading precipitation) but results were again similar. The instantaneous regression values are calculated for each season and are shown in Fig. 14 for observations.

Focusing on the Pacific first, in all seasons (except for MAM) an equatorially centered region of negative correlations is seen in the eastern Pacific, extending as far as the dateline. This significant (not in DJF) and negative relationship indicates when SSTs are high in this region, Caribbean precipitation tends to be reduced in all seasons (except MAM when the regression values are significantly positive). This qualitatively agrees with the results of Giannini et al. (2000) and Chen and Taylor (2002) that the second Caribbean rainfall season tends to be drier in El Niño years and the first rainfall season tends to be drier in La Niña years. Certainly this is an important relationship for GCMs to be able to reproduce, even if the representation

of ENSO has flaws.

In the Atlantic, a quite different pattern is seen in all seasons and is strongest and most significant in MAM and JJA. Two different patterns are identifiable in Figs. 14b and c. The first pattern consists of positive regression values in the equatorial and northern Atlantic and negative values between, creating a tripole structure reminiscent of the pattern created by the NAO (Marshall et al., 2001) providing further evidence of the relationship between the NAO and Caribbean rainfall. The second pattern is most evident in MAM, with negative anomalies south of the equator and positive anomalies to the north, characteristic of the interhemispheric Atlantic meridional mode (AMM) (Servain, 1991) which is known to impact hurricane activity (Vimont and Kossin, 2007). The difficultly lies in unraveling the contribution from each of these individual modes (NAO, AMM and ENSO) as they are all interrelated to some degree.

The same analysis was performed on the output from the CMIP and AMIP ensembles, and the results from one representative model (MIROC_MED) are shown in Fig. 15 (CMIP) and Fig. 16 (AMIP). Perhaps the most notable problem in the CMIP simulations is the poor representation of the Pacific (ENSO) relationship with Caribbean rainfall. In DJF (Fig. 15a) the MIROC_MED model has a strong and significant region of positive regression values. Several of the other models do show negative values throughout all seasons, but the area covered is much narrower around the equator. The representation of the Atlantic is generally worse in the CMIP models than the Pacific. Little to no structure is seen, although there is evidence of the tripole structure in MAM in some models (e.g. Fig. 15b), which is consistent with the AMM at a maximum in boreal spring. It is also seen in the Caribbean itself, that the MIROC_MED model produces negative regression values in JJA (Fig. 15c), indicating that even the local relationship is incorrect.

It is perhaps expected that the analysis of the AMIP models should perform well as the SSTs are specified from observations, however, as seen in Fig. 16 this is not the case. The simulations are improved from the CMIP ensemble in many respects, but there are still large errors in the relationships between SST and Caribbean precipitation. As seen in Fig. 16, the spatial structure of the ENSO regression values is much improved (broader), but there are still fundamental errors in the sign of the regression coefficient, especially in DJF (Fig. 16a). The regression coefficients in the Pacific, regardless of sign, are often in excess of those in observations (Figs. 16c,d), indicating too strong of a connection between the two regions. The simulation of the Atlantic is where the greatest improvements over the CMIP simulations are seen. The tripole structure is evident in the majority of the models throughout the year (although the magnitude is too large), and there is evidence of the AMM in the MIROC_MED MAM simulation (Fig. 16b). These results show that simply forcing the atmospheric model with observed SSTs will not produce the correct relationships between SST and Caribbean precipitation. Errors in the atmospheric model's simulation of heating, winds and convergence patterns must be incorrectly relating the remote regions.

E. Regime Sorting

The role of convective parameterizations and the relationship between precipitation and SST is further analyzed by exploring the annual mean precipitation-SST space by regime sorting. This involves three steps; 1) calculating the probability distribution function (PDF) of SST, 2) compositing precipitation by SST, and 3) weighting the composite by the PDF to calculate the regime sorted (or weighted) precipitation. This allows the error in precipitation to be associated with errors affecting either

the frequency of SST or the magnitude of precipitation associated with a given SST (Bony et al., 2004; Bellucci et al., 2010). Regime sorting is performed for all grid points and all months before averaging to create Caribbean and West Pacific area-averaged values.

1. Sea Surface Temperature

The three stages of the regime sorting analysis for the Caribbean and West Pacific are shown in Figs. 17 and 18 for AMIP and CMIP simulations, in addition to the multi-model ensemble mean and observations. Multi-model mean values for each convective parameterization group (bulk, ZM and spectral) are shown in the regime sorting analysis. The standard deviation of the precipitation for each SST is calculated and plus/minus one standard deviation is indicated by gray shading in the appropriate plots. The PDFs of AMIP SSTs (Fig. 17a and 18a) have slight variations from the HadISST data, however these do not affect the results.

The observed composite of precipitation at a given SST in the AMIP simulations is shown in Figs. 17c and 18c by the solid black line. As expected, convection increases with SST but this increase is not constant across the range of SSTs observed in the Caribbean (Fig. 17c). Precipitation is relatively constant with SST below 27°C, but increases rapidly above this value, similar to the results of Waliser (1993), Zhang (1993) and Lin et al. (2006a). This observation is also seen in the West Pacific (Fig. 18c) although the increase begins at 26°C and increases more rapidly than the Caribbean. Above 30-31°C in each case, the precipitation drops quickly to zero as SSTs are rarely occurring at such high values. In the CMIP models (Figs. 17d and 18d) this SST drop off value varies between the models and hence the multi-model ensemble mean and even the convective parameterization group means are not beneficial above 29°C in the Caribbean and 31°C in the West Pacific.

Figures 17c and 18c shows the overestimation of precipitation at a given SST by the atmospheric component of the model. The overestimation in the Caribbean is smallest below 26°C, but rapidly increases above this value, with maximum overestimation greater than 2 mm/day between 28 and 30°C (Fig. 17c). The multi-model mean shows the increase of precipitation with SST is too large in the models above 26°C. The regime sorted weighted precipitation is shown in Fig. 17e, with the greatest contribution to the observed precipitation at 28 to 29°C. This is also the range where the AMIP models have the greatest oversensitivity to SST.

In the West Pacific, where the SSTs are warmer and the SST distribution is narrower (Fig. 18a), similar results for the AMIP precipitation composite (Fig. 18c) are seen. However, as the extremely high SSTs do not occur frequently and the precipitation composite is not as consistently high biased as the Caribbean, the weighted regime sorted precipitation in Fig. 18e, shows excellent results, particularly in comparison to the Caribbean. These results show that the majority of the overestimation of precipitation by the AMIP models in the West Pacific is at SSTs above 30°C, but this overestimate is small in comparison to the Caribbean.

In the Caribbean, the AMIP models that utilize spectral convective parameterizations produce the regime sorted precipitation that is closest to observations with the bulk and ZM schemes most oversensitive to SST (Figs 17c and 17e). However, in the West Pacific, all schemes perform equally, although the bulk scheme is most oversensitive to precipitation at high SSTs (Figs 18c and 18e). Bulk parameterizations use adiabatic ascent from the lowest model level and hence SST is a much stronger constraint than the spectral schemes that can initiate plumes from multiple levels (Turner and Slingo, 2009). By initiating an ensemble of plumes from multiple levels the spectral parameterizations produce a better precipitation-SST relationship in the AMIP models in the Caribbean, but not in the West Pacific, suggesting differ-

ences between the way deep convection is structured and initialized between the two regions.

The results of the regime sorting analysis using the CMIP models is more complex (particularly when analyzing the impact of the convection parameterizations). The Caribbean SST PDF in Fig. 17b shows the cold bias of the coupled models as seen in Fig. 13a. The bulk group mean appears shifted to warmer temperatures due to the four models with the best SST PDF all being in this group (as discussed previously). The multi-model ensemble mean maximum is over 2°C colder than the observed maximum. The precipitation composite in Fig. 17d shows similar results to the AMIP composite (Fig. 17c), although due to the infrequent occurrence of high SSTs (above 29°C) in the models, the multi-model ensemble mean and parameterization means appear lower than the observations. This is to be expected as the amount of precipitation at a given SST is controlled by the atmospheric component of the coupled model system.

In the West Pacific, the CMIP models are cold biased (Fig. 18b) as expected, but still produce a much narrower distribution than in the Caribbean. The bulk model mean appears broader, not because the individual models produce a broader distribution, but due to two models being centered at SSTs much higher (30-31°C) than the the observed mean and two being centered lower (27°C). It is noted that the models have a longer tail at high SSTs than the observations, which leads to a much slower drop off of precipitation at high SSTs (Fig. 18d). The precipitation composite is similar to that of both the Caribbean and the West Pacific AMIP models, considering the shifted SST distribution.

The regime sorted precipitation in both the Caribbean (Fig. 17f) and West Pacific (Fig. 18f) shows the underestimation of the precipitation by the CMIP multi-model ensemble mean and a shift of the distribution to lower SSTs, with the largest

shift occurring in the Caribbean. The overestimation of precipitation at a given SST that is an inherent part of the atmospheric model in both locations is overcompensated by the cold SST bias in the CMIP models, leading to an underestimation of the precipitation, particularly at SSTs greater than 27.5°C in the Caribbean and between 28 and 30°C in the West Pacific. The individual models that produce the best distribution in the Caribbean and West Pacific use bulk parameterizations because these models have the best SST distribution, however, those that are most different from the observations also use bulk parameterizations (as seen in Fig. 13), illustrating the difficulty of extracting such relationships in coupled model simulations.

2. Vertical Large-Scale Circulation

In addition to precipitation regime sorting by SST, the same methodology was applied to regime sorting by ω_{500} (Fig. 19 for the Caribbean and Fig. 20 for the West Pacific). Figure 19c shows that the AMIP models produce too much rain for a given vertical circulation compared to observations/reanalysis in the Caribbean. This is less evident in the CMIP models (Fig. 19d) due to the severe underestimation of the deep convective (negative) values of ω_{500} (Fig. 19b), particularly those less than -50 hPa/day. Individual models that simulate these strong upward motion regimes overestimate precipitation at these values (not shown), but the multi-model ensemble mean is shifted to lower values of precipitation by averaging these models with those that do not produce these strong upward motion events and hence have composite precipitation values close to zero.

The overestimation of rainfall for a given convective event is the main contributor to the AMIP models overestimating Caribbean precipitation (Fig. 19e) as the ω_{500} PDF (Fig. 19a) is fairly well reproduced by the AMIP multi-model ensemble mean. The spectral parameterization model mean produces the least accurate PDF with

overestimation of shallow convective events and underestimation of deep convective events whereas the bulk and ZM groups overestimate the frequency of deep convective events. Much of this overestimation of precipitation is in deep convective regimes between -10 and -50 hPa/day. As for the regime sorting by SST, AMIP models using the spectral parameterizations outperform other parameterization groups in the Caribbean. However, this good performance of the spectral models is in part because the errors in the ω_{500} PDF (Fig. 19a) are balanced by the errors in the precipitation composite (Fig. 19c).

In the West Pacific, the AMIP models show similar results to the Caribbean, with the ω_{500} PDF (Fig. 20a) being well represented by the multi-model ensemble mean. However, the precipitation composite (Fig. 20c) shows an even larger overestimation and rate of change of precipitation with ω_{500}, far surpassing one standard deviation of the observations below -75 hPa/day. It is also extremely consistent between all three parameterization groups. The result of this overestimation in deep convective regimes is to produce a regime sorted weighted precipitation composite (Fig. 20e) that shows the overestimate of precipitation in the deep convective range (below -50 hPa/day), as seen in the Caribbean.

The CMIP results are, again, more complex in both locations. While too much rainfall for a given vertical circulation is inherent in the atmospheric model in the Caribbean (Fig. 19d) and West Pacific (Fig. 20d), the CMIP models are poorly representing the PDF of vertical circulation in both locations. In the Caribbean, the ω_{500} PDF (Fig. 19b) shows the multi-model ensemble mean, the parameterization group means and the majority of individual models (not shown) below the observations in the deep convective regime (-10 hPa/day and below). Also apparent is the overestimation associated with shallow convection (0 to 20 hPa/day) regimes. These two features essentially produce a narrower PDF in the model output in comparison

to the observations in the Caribbean. In the West Pacific, a different problem is apparent in the ω_{500} PDF (Fig. 20b). Whilst the width of the distribution is similar in the model output and the observations, the multi-model mean, bulk and ZM parameterization group means are skewed towards downward motion, with maxima close to 10 hPa/day compared with -40 hPa/day in the observations. This suggests that the correct simulation of large-scale circulation is a major problem in many of the CMIP models over the West Pacific. This may be due to the poor simulation of ENSO and the East Pacific cold tongue which is know to shift the rising branch of the Walker circulation westward (Cai et al., 2009).

Despite the atmospheric models producing too much rain for a given ω_{500} in both locations (noting the averaging effects in the Caribbean), the differing ω_{500} PDFs produce different regime sorted weighted precipitation composites. In the Caribbean, the underestimation of the frequency of all upward motion events is large enough that the underestimation of precipitation in the CMIP models is mainly during deep convective regimes (Fig. 19f). In the West Pacific, the reduced frequency of upward motion between 0 and -70 hPa/day leads to underestimation of precipitation in this range, which dominates the two overestimating regions above and below this range. The overestimate of downward motion in the West Pacific produces an overestimate of rainfall for positive values of ω_{500}. At the largest upward motion values, below -80 hPa/day, the oversensitivity of precipitation to ω_{500} dominates and produces too much rain at these values. Bellucci et al. (2010) who performed a similar analysis in the southern tropical Pacific (20°S-0°S, 100°-150°W), show results that vary from the West Pacific and the Caribbean. Both AMIP and CMIP models overestimate precipitation in this region and this overestimation is seen in across the entire ω_{500} spectrum.

Once again, the impacts of convective parameterization are considerably more

difficult to discern for the CMIP models, and are not constant between the two regions. The performance of the convective parameterization groups for the regime sorted precipitation in the CMIP models (Figs. 19f and 20f) are dependent on their performance in representing the ω_{500} PDF.

F. Daily Precipitation Analysis

1. Precipitation Distributions

In addition to monthly values of precipitation, information concerning the precipitation distribution can be established using daily data. It is essential to understand the frequency and intensity of precipitation, and how the models reproduce it, to ensure that the models are correctly representing the complex processes associated with tropical convection. Section E provided evidence that the models were underestimating precipitation in deep convective regimes and at high SSTs on a monthly timescale, suggesting that extreme events may be underestimated.

The daily precipitation distribution is analyzed by calculating the percentage contribution to the total precipitation in a range of different categories; less than 1 mm/day (but greater than zero), 1-5 mm/day, 5-10 mm/day, 10-20 mm/day, 20-50 mm/day and greater than 50 mm/day. This is done for each individual grid point and then averaged over the Caribbean domain. These categories were chosen to match those used by Dai (2006) who performed a similar analysis for 50°S-50°N for a select number of CMIP models. Dai (2006) showed evidence that in four IPCC AR4 models the models captured the correct percentage contribution in the 10-20 mm/day range but underestimated in heavy (greater than 20 mm/day) and overestimated in light (less than 10 mm/day) precipitation when compared to TRMM. Others have performed similar analysis for other atmospheric GCMS (Deng et al., 2007; Wilcox and

Donner, 2007) and found similar behavior. Expanding these results to the complete CMIP and AMIP ensembles for the Caribbean will help to identify the precipitation distribution and possible model errors, that are specific to this region. The precipitation distributions are shown in Fig. 21.

Figure 21 shows that the Caribbean receives its largest contribution to the total precipitation (35 %) from the 20-50 mm/day category. Considering the width of this category however, the 10-20 mm/day category that contributes almost 25 % should be considered as the largest contribution to the total precipitation. This is similar to the results shown by Dai (2006) although the values for each category (10-20 mm/day and 20-50 mm/day) were somewhat lower, at approximately 23 and 25 % respectively. The lowest category of precipitation (less than 1 mm/day) contributes to only 2.5% of the total rainfall in the observations of the Caribbean, lower than the larger region used in Dai (2006) where the contribution is approximately 8% (some difference may partly be explained by differences in observing systems). Contributions from the highest precipitation category (greater than 50 mm/day) are larger in the Caribbean than the Dai (2006) domain (12% versus 7%).

Both the CMIP (Fig. 21a) and AMIP (Fig. 21b) models show a similar precipitation distribution with excess precipitation at low rainrates and reduced precipitation at high rainrates. Every CMIP model overestimates the percentage contribution to the total rainfall at rainrates less than 1 mm/day, ranging from 2.4 to 30.8 %, compared to the observed value of 2.2 %. The AMIP models perform better in this lowest category, with no models producing percentages greater than 10 %, although the ensemble mean is still greater than the observations (5.5 %). The same pattern of overestimation is also seen in both the 1-5 and 5-10 mm/day categories in both the CMIP and AMIP models. At rainrates greater than 10 mm/day, and particularly greater than 20 mm/day, both the CMIP and AMIP models severely underestimate

the percentage contribution to the total rainfall, with model ensemble means being an order of magnitude less than the observations (e.g. 34.9 % versus 8.9 % for the observations and CMIP ensemble mean in the 20-50 mm/day category). This underestimation at low rainrates and overestimation at high rainrates agrees with the results of Dai (2006) but both the over and underestimation are more extreme in the Caribbean. The errors are reduced in the AMIP simulations, compared to CMIP, indicating perhaps that the low SSTs and incorrect vertical motion distributions in the CMIP models are leading to a poorer simulation of the precipitation distribution.

The CMIP and AMIP ensembles were divided by the type of closure/trigger mechanism used and one scheme stands out in both the CMIP (Fig. 21a) and AMIP (Fig. 21b) models. Those that use the CAPE with moisture convergence mechanism (MIUB and MPI) consistently outperform other models in almost every category in both CMIP and AMIP simulations, suggesting the importance of closure and trigger schemes for producing a more realistic precipitation distribution. Wilcox and Donner (2007) also showed that changing the closure scheme in an atmospheric GCM can influence the precipitation distribution. The models were also categorized by convective parameterization (not shown). However, none of the convective parameterization groups (spectral, bulk or ZM) perform better than others. A large spread in values in each category is seen within each convective parameterization group, suggesting that the errors in the precipitation distribution are not only (or perhaps not at all) a function of convective parameterization.

2. Precipitation Extremes

Figure 21 illustrates the difficulty the models have in simulating extreme events in the Caribbean. However, this method only assessed the area mean. The spatial distribution of extremes is also important for models to be able to simulate. Methods of evalu-

ating extreme precipitation are varied and a wide range have been developed and used in the literature. This study will use four indices, that were also used by Peterson et al. (2002) in a study of changes in observed Caribbean extremes and Frich et al. (2002) who investigated global extremes. Detailed information and precise definitions of all these indices can be found at http://eca.knmi.nl/indicesextremes/indicesdictionary.php. The indices used in this study are:

- Maximum consecutive dry days (CDD, days). A dry day is defined as precipitation less than 1 mm/day.
- Heavy Precipitation days (R10, days). Days with precipitation greater than 10 mm/day.
- Highest 5-day precipitation amount (R5d, mm).
- Simple daily intensity index (SDII, mm/day). Conditional precipitation rate for days with rain greater than 1 mm/day.

Annual mean maps of the four extreme indices listed above calculated using the GPCP daily data are shown in Fig. 22. The CDD index (Fig. 22a) has a swath of higher consecutive dry days (approximately 50) covering the central Caribbean Sea and northeast into the Atlantic, as would be expected from the annual precipitation map in Fig. 3. The R10 index (Fig. 22b) has maxima up to and exceeding 50 days located predominantly over Central America and the Greater Antilles islands, similar to the annual mean rainfall in the region. The R5D index (Fig. 22c), however, shows a very different structure. The maximum 5 day rainfall total is larger over the ocean than the land and has a maximum between Cuba and Central America of over 150 mm. A seasonal analysis of 5 day rainfall amounts shows that this maximum is found to occur in SON and thus is likely due to tropical storms moving across

the area. The SDII (Fig. 22d) has a very similar structure to the R5D index with a mean of approximately 10 mm. The importance of land-sea contrast, topography and tropical storms in the generation of extreme rainfall events in the Caribbean would suggest that the IPCC AR4 models would have difficulties with simulating the spatial structure of extremes.

Annual mean maps from the GFDL_2_1 CMIP simulation are shown in Fig. 23. This is chosen as representative of both the CMIP and AMIP ensembles as structures were similar across the entire ensemble. Fine scale features, such as land-sea contrasts, were not well represented in the models, as expected. The extremely poor simulation of the magnitude of the extreme indices, was perhaps, worse than expected with the models appearing to produce significantly more dry extremes and fewer wet extremes than the observed climatology. The model simulated values of CDD (Fig. 23a) were often double or more than the observations, as expected from the overestimation of rates less than 1 mm/day seen in Fig. 21. However, the maximum of CDD was often found over the Caribbean Sea as seen in observations.

Indices of R10 (Fig. 23b) and R5D (Fig. 23c) are considerably less than the observations, with maximum values of R5D rarely exceeding 100 mm. The SDII (Fig. 23d) shows results that are expected from Fig. 21. The SDII averages approximately 5 mm/day in the GFDL_2_1 model and equally low values are seen in other models. This implies that the models are raining too frequently and too lightly in the Caribbean, a feature that is also seen in the tropical Atlantic (Biasutti et al., 2006) and is corroborated by calculations of the autocorrelation (not shown). Further analysis of extreme events in the Caribbean is contained in Chapter IV.

G. Summary

An analysis of the climatology of Caribbean rainfall and some of its associated environmental variables (SST and vertical motion) in the IPCC AR4 models shows considerable room for improvement in the next generation of climate models. By analyzing both coupled and uncoupled IPCC AR4 model output, some conclusions were able to be made regarding what aspects of the model need to be improved.

The IPCC AR4 models generally captured the spatial distribution of the rainfall climatology when not including the strong island and land effects (i.e. Greater Antilles, Lesser Antilles and Central America) that are poorly represented by the models due to resolution deficiencies. The models, in general, underestimated precipitation on and close to land, and overestimated ocean-based precipitation, particularly in the central Caribbean Sea. It is shown that the AMIP models overestimate the Caribbean area-averaged rainfall throughout the entire annual cycle, whereas the CMIP models overestimate during winter (DJF) and underestimate the precipitation throughout the rest of the year. The AMIP models also produce a more realistic MSD, mechanisms behind which are discussed in Chapter III.

The mechanisms behind the poor simulation of Caribbean area-averaged precipitation were investigated by first analyzing SST, both locally and globally. Caribbean SST has been shown to be biased cold in summer in a selection of CMIP models (Misra et al., 2009) and this conclusion is extended to almost the entire CMIP ensemble (only five models have annual mean SST within 1°C of observations). While the spatial pattern and seasonal temporal changes in the Caribbean SST are generally correct (the cold bias is seen over the whole domain and throughout the year), one area stands out. The southern Caribbean Sea to the North of Venezuela is regularly significantly colder than it's surroundings in the majority of the models. This may

link to the stronger Caribbean Low-Level Jet seen in many of the models, as discussed in Chapter III.

Caribbean precipitation is known to be influenced by large-scale patterns such as ENSO and the NAO, which impact SSTs in both the Pacific and Atlantic. The connection between rainfall and global SST was investigated using a regression analysis that showed observed evidence of the ENSO connection in the Pacific and the NAO and AMM in the Atlantic. The CMIP models struggled to produce the correct regression values in both the Pacific and the Atlantic. Many of the models produce only weak values in the Pacific and those that were significantly negative are confined too narrowly to the equator. In the Atlantic the performance of CMIP models is worse than the Pacific, with little significant structure, reinforcing the need to improve Atlantic SSTs in CMIP models.

The AMIP models show improvement in comparison to the CMIP models, but they do not perform as well as expected. The Atlantic region is much improved in AMIP simulations although regression values are too large, suggesting that the atmospheric components of the models are too strongly connected or have too large of a sensitivity between Atlantic SST and Caribbean precipitation. This may in part be due to the convective parameterizations not generating correct rainfall and vertical circulation, which impacts the heating structure and hence produces incorrect circulation patterns. Feedbacks between the atmosphere and ocean may also act to adjust convection, winds and heating rates that are not included in the AMIP models.

The relationship between precipitation and SST and precipitation and the large-scale vertical circulation in observations and IPCC AR4 models was investigated using a regime sorting analysis for two tropical warm pool regions: the Caribbean and the West Pacific. The oversensitivity of precipitation to SST was the dominant factor in AMIP models overestimating Caribbean rainfall, with models using spectral

type convective parameterizations performing better than either bulk or ZM type parameterizations. Whilst this oversensitivity of precipitation to SST was still present in CMIP models, the known severe underestimation of SST in the Caribbean leads to a large underestimation of precipitation (particularly at SSTs above 28°C) in the CMIP models.

The same oversensitivity of precipitation to SST was observed in the West Pacific, but the narrowness of the SST distribution lead to only a small overestimation of precipitation in the AMIP models at high SSTs. The CMIP models in the West Pacific also showed a cold bias, although not as strong as the Caribbean, leading to an underestimation of rainfall at SSTs between 28 and 30 °C. Although the relationship between precipitation and SST was similar in the two regions, in both models and observations, the shifting of the SST distribution to colder temperatures is the determining factor in the CMIP simulations. By stratifying the results by type of convective parameterizations, some insights can be gained regarding differences between the deep convective mechanisms in the two regions. The spectral group, which can initiate convection at a range of levels, performed best in the Caribbean. Although no group could be identified as performing best in the West Pacific results from the bulk group, which initiates convective plumes from the surface often performed worse than the two other groups. This stratification by convective parameterization suggests that a bulk approach may not be appropriate to describe warm pool convection and the spectral approach is more successful in the Caribbean than the West Pacific.

Not only was precipitation too sensitive to SST, it was also too sensitive to vertical motion in both regions, which has implications for heating and moisture profiles. The largest disparities were evident in the deep convective regimes (less than -10 hPa/day) and were inherent to the atmospheric models. This oversensitivity is consistent with the results of Bellucci et al. (2010) who performed a similar analysis

in the southern tropical Pacific. The AMIP models were shown to overestimate precipitation due to the incorrect magnitude of rainfall for a given convective event (oversensitivity). Contrary to this results, CMIP models underestimated precipitation due to the reduced frequency of deep convective events in the Caribbean. The results in the West Pacific were similar, but large problems with the ω_{500} distribution in CMIP models (shifted into a downward motion regime) lead to an underestimation of rainfall between 0 and -75 hPa/day. This regime sorting analysis produces similar results when performed by season, although the underestimation of deep convective regimes is further exaggerated in the Caribbean in September to November.

It should be noted that there are a variety of other factors that contribute to rainfall and deep convection in the tropics, not only SST and vertical circulation as discussed here. Precipitation can also be controlled by SST gradients, surface heat and moisture fluxes, and moisture convergence, making the evaluation of precipitation and its errors difficult. Stratification by convective parameterization showed some variation between different parameterizations but with such a small sample size (4-10) in each group, significance of the separation between the groups is likely minimal. This study does not claim that the convective parameterization is the only or leading cause of differences in the precipitation-SST-vertical circulation relationship and other parameterizations are likely to strongly influence convection, particularly the radiation scheme and the type of moisture trigger, which would be the subject of additional studies.

These results suggest that by coupling the models and including atmosphere-ocean feedback, errors occur in the frequency of occurrence of both SST and the large-scale vertical circulation in both warm pool regions, with a reduction in deep convective events and high SSTs, and an increase in low SSTs. The results of the AMIP simulations show that simply improving the SST climatology in future CMIP

models will not be enough. Improvements in convective parameterizations are also necessary as the errors in precipitation magnitude associated with a given SST or vertical circulation are large.

Analysis of daily precipitation data confirmed the lack of extreme events that was suggested by the monthly regime sorting analysis. The models produced significantly more dry extremes and fewer wet extremes than the observed climate. Both AMIP and CMIP models showed a skewed precipitation distribution that had a large overestimation of very light rainfall days (less than 5 mm/day) and an underestimation of large rainfall days (greater than 20 mm/day). This analysis shows that the models are raining too frequently and too lightly in the Caribbean, similar to the results of Dai (2006); Deng et al. (2007) and Wilcox and Donner (2007) but the distribution is more heavily skewed in the Caribbean than the larger region used in Dai (2006). Both CMIP and AMIP models that used a closure and trigger mechanism with CAPE and moisture convergence produced the best daily distribution, suggesting the importance of correctly triggering precipitation in the models as to not produce a constantly drizzling environment.

This analysis of the Caribbean precipitation climatology in the IPCC AR4 models shows the need for improvements, particularly in the convective parameterizations of the atmospheric components of the models and the coupling between the atmosphere and the ocean. While small-scale features such as land-sea and topography effects of the Caribbean islands cannot be expected to be simulated in such low-resolution models, the simulation of regional scale features, in particular the Caribbean low-level jet have not yet been determined and will be investigated in Chapter III.

CHAPTER III

THE CARIBBEAN LOW-LEVEL JET AND ITS RELATIONSHIP WITH PRECIPITATION IN IPCC AR4 MODELS*

A. Background

Low-level jets have been identified in a variety of locations around the globe including North America (Great Plains low-level jet, GPLLJ) (Bonner, 1968; Ting and Wang, 2006), South America (Virji, 1981; Berbery and Collini, 2000) and the easterly low-level jet of the Caribbean (CLLJ) (Amador, 1998; Amador et al., 2000). Interest in the CLLJ has increased in the past decade due to the importance of the CLLJ in transporting moisture from the tropical Atlantic into the Caribbean Sea, Gulf of Mexico, and the continental United States, hence, influencing rainfall both locally in the Caribbean and Central America and remotely in the United States (Mestas-Nuñez et al., 2007; Wang, 2007; Amador, 2008; Cook and Vizy, 2010).

The CLLJ is a localized amplification of the large-scale circulation of the North Atlantic Subtropical high (NASH) and is located in the Caribbean Sea, between northern South America and the islands of the Greater Antilles (70-80^{o}W, 13-17^{o}N, Fig. 24a). Unlike the GPLLJ, the CLLJ is present throughout the year and has two maxima (February and July) and two minima (May and October) in its semiannual cycle (Wang and Lee, 2007; Wang, 2007; Muñoz et al., 2008) (solid line Fig. 25a). For most of the year the maximum wind speed (up to 16 ms^{-1}) is located at 925

*Reprinted with permission from "The Caribbean Low-Level Jet and its Relationship with Precipitation in IPCC AR4 Models" by E.R. Martin and C. Schumacher, 2011. *J. Climate.,* doi:10.1175/JCLI-D-11-00134.1, Copyright 2011 American Meteorological Society.

hPa, but as the jet weakens from its July peak, the jet maximum moves upwards and deepens (Cook and Vizy, 2010). The boreal summer maximum is related to the strengthening and westward extension of the NASH (Wang and Lee, 2007; Wang, 2007; Muñoz et al., 2008; Cook and Vizy, 2010). During boreal summer, the CLLJ splits into two branches. The southerly branch connects with the GPLLJ (Cook and Vizy, 2010) and an easterly branch traverses Central America (Fig. 24a). The boreal winter CLLJ maximum may be in part due to increased heating over northern South America associated with the South American monsoon (Cook and Vizy, 2010).

Although this study will focus predominantly on the local structure and characteristics of the CLLJ in the IPCC AR4 models, there are many connections between the CLLJ and SSTs in both the Atlantic and Pacific. The relationship between ENSO and the CLLJ varies seasonally. During the summer, when the CLLJ is maximum, a strong CLLJ occurs in conjunction with warm Pacific SST anomalies, through teleconnections with SLP in the Atlantic (Amador et al., 1999, 2000, 2006; Wang, 2007; Amador, 2008). Atlantic SSTs may be related to the CLLJ through the North Atlantic Oscillation, again through the SLP (Wang, 2007). In addition to these remote influences, the CLLJ has also been shown to be associated with the Madden-Julian Oscillation (Martin and Schumacher, 2011b).

As noted by Wang (2007) and Cook and Vizy (2010), the CLLJ is geostrophic to first order, thus it is controlled by gradients in pressure (geopotential). As the NASH expands and strengthens the meridional pressure gradient across the Caribbean Sea is increased and the CLLJ strengthens (Wang, 2007; Muñoz et al., 2008; Whyte et al., 2008; Cook and Vizy, 2010). The opposite occurs when the CLLJ contracts. Wang (2007) and Muñoz et al. (2008) show that the semi-annual cycle of the CLLJ is in phase with the semiannual cycle of the meridional SLP gradient across the Caribbean Sea. Meridional gradients in sea surface temperature (SST) across the region also

show a semi-annual cycle that is in phase with that of the CLLJ. This suggests a feedback between the atmosphere and the ocean that acts to reinforce the CLLJ through the effect of opposite values of wind stress curl and hence upwelling on either side of the jets zonal axis (Wang, 2007). Using an idealized modeling study, Wang et al. (2008) also showed that the magnitude of the SST anomaly in the Caribbean influences the strength of the CLLJ through interactions with the NASH. This result is also echoed by the results of Rauscher et al. (2011). When Caribbean SST is anomalously warm (cold), the CLLJ is anomalously weak (strong).

Annual rainfall in the Caribbean exhibits a bimodal structure (solid line in Fig. 25b), with an initial maximum in May, a minimum around July-August, and a second maximum in September-October, (Jury et al., 2007; Gamble et al., 2008). The minimum that separates the two peaks in rainfall has been termed the 'mid-summer' drought (MSD) based on a similar minima of rainfall that occurs on the Pacific coast of Central America (Magaña et al., 1999). The use of MSD in this study will be specific to the Caribbean. The minimum in rainfall associated with the MSD occurs simultaneously with the summer maximum of the CLLJ (solid line in Fig. 25a). It is postulated that the CLLJ is a major contributor to the MSD through the increase in moisture flux divergence in the Caribbean, which acts to suppress convection and decrease rainfall (Magaña et al., 1999; Wang, 2007; Muñoz et al., 2008; Whyte et al., 2008). An anomalously strong CLLJ is also associated with reduced precipitation over the Caribbean throughout the year (Cook and Vizy, 2010). Whilst drying is seen across much of the Caribbean when the CLLJ is strong, the Caribbean coast of Central America has enhanced rainfall (through orographic enhancement and large-scale low level convergence at the jet exit), which deprives the Pacific coast of Central America of moisture and decreases rainfall (Amador, 1998; Cook and Vizy, 2010).

Observational studies of the CLLJ have increased in recent years, including a field

experiment in 2001 (Experimento Climático en las Albercas de Agua Cálida, ECAC; Amador 1998), but there have been limited investigations into its representation in regional or global climate models (GCMs), such as the IPCC fourth assessment report (AR4) models. Wang et al. (2008) used the NCAR Community Atmosphere Model (CAM) to investigate the influence of the size of the Atlantic Warm Pool (AWP) on summer climate, including the CLLJ, as discussed previously. The representation of the climate of the Caribbean by the IPCC AR4 coupled models is somewhat lacking, with SSTs too cold and precipitation underestimated by up to 30 % (Neelin et al., 2006; Christensen et al., 2007). However, the role of the CLLJ in these simulations has not been examined in detail. The relationship between the CLLJ, moisture transport and precipitation both locally and remotely (including extremes and the MSD) (Magaña et al., 1999; Wang, 2007; Cook and Vizy, 2010; Durán-Quesada et al., 2010; Martin and Schumacher, 2011b), in addition to its impact on easterly waves and tropical storms (Serra et al., 2010), highlight the importance of having a realistic CLLJ in GCMs.

This paper will begin with a brief discussion of the observational and IPCC AR4 data (Section B), followed by an analysis of CLLJ properties (Section C) and the connection between the CLLJ and Caribbean precipitation (Section D). Results related to the simulation of the CLLJ impact on the United States is shown in Section E.

B. Data and Methodology

1. Observations

A variety of observational and reanalysis datasets are used to obtain the most accurate and spatially complete climatology of the CLLJ, with which the model output can

be compared. All data is monthly resolution for the period 1979-2008. Wind (1000 hPa to 600 hPa) and sea level pressure are obtained from NCEP/DOE Reanalysis II (Kanamitsu et al., 2002) at 2.5° resolution. Reanalysis data will be referred to as observational throughout this study. Precipitation data is from the Global Precipitation Climatology Project (GPCP), which is a combination of satellite products and gauge observations (Huffman et al., 2001). Monthly GPCP data is available at 2.5° resolution. The third dataset used was the Hadley Centre Sea Ice and Sea Surface Temperature data set 1 (HadISST1) to investigate the links between the CLLJ and SST. The HadISST dataset is at 1° resolution and uses a combination of in situ and satellite observations to provide global coverage (Rayner et al., 2003).

Calculation of area mean values are used in this study to investigate the annual cycle and month-to-month variability of quantities associated with the CLLJ. Three different averaging regions are used: the entire Caribbean region in this study is defined as lying between 55°W to 90°W and 10°N to 25°N (thin black box, Fig. 24a), the CLLJ region is defined as 70°W to 80°W and 11°N to 17°N (white box, Fig. 24a) and the GPLLJ region is defined as 95° to 100° W and 25° to 35° N (thick black box, Fig. 24a). Meridional gradients in the CLLJ region are calculated at each longitude and then averaged over the CLLJ box. The same averaging regions are used for the model output. A CLLJ and GPLLJ index are calculated by removing the average annual cycle of zonal (CLLJ) or meridional (GPLLJ) winds from the time series. The CLLJ index is then multiplied by negative one to create an index where a stronger CLLJ is positive.

2. Model Output

Output from 19 coupled ocean-atmosphere GCMs (coupled model intercomparison project; CMIP type) and 12 atmospheric only GCMs (atmosphere model intercom-

parison project; AMIP type) are examined. These models are a subset of those used as part of the IPCC AR4 and are available through the Program for Climate Model Diagnostics and Intercomparison (PCMDI). All output (wind, SLP, precipitation and SST) are monthly mean values for the last 30 years of the climate of the 20th century simulations (20C3M) in order to make a fair comparison with the observational data. All models are configured differently with varying resolutions and parameterizations. A summary of the models used in this study, as well as pertinent information concerning their configuration, is shown in Tables 1 and 2 in Chapter II. The following models were not included in this analysis as all necessary data was not available: GISS_AOM, GISS_ER, GISS_EH, and MIUB. While some models had multiple ensembles for the 20C3M simulations, we use only one realization from each model to ensure model mean results are not skewed towards models with a large number of ensembles. All model output is kept at its original resolution, rather than interpolating onto a consistent grid, in order to make conclusions about the impact of resolution on the structure of the CLLJ in the models. Throughout this paper, for purposes of brevity, not all model output will be presented in every figure. Presented model output is chosen as representative of the entire model ensemble.

C. CLLJ Properties

1. Location

All CMIP and AMIP models captured an enhancement of the low-level wind field in the Caribbean Sea between South America and the Great Antilles that was evident throughout the annual cycle. As all models were able to produce an enhancement of the low-level wind in the Caribbean, horizontal resolution was not a factor in the ability of models to accelerate the flow in the Caribbean. Climatological JJA 925 hPa

wind speed and direction from example model simulations are shown in Fig. 24. The location of the jet remained constant in other seasons and JJA was chosen as both the CLLJ and GPLLJ are strongest.

Numerous similarities are observed between all simulations in Figs. 24b-e and the observations in Fig. 24a. The strong easterly trade winds across the Atlantic strengthen as they enter the Caribbean Sea, forming a CLLJ. These winds then weaken close to Central America, turn northward across the Yucatan Peninsula, and form a southerly jet across the South-Central United States (the GPLLJ). Details of the IPCC AR4 models representation of the springtime GPLLJ are presented in Cook et al. (2008), who show the ability of the models to produce a realistic GPLLJ.

Despite the clear similarities of the general flow structure in the region, maximum wind speeds in the CLLJ simulations sometimes varied significantly from observations. This variation in wind speeds will be addressed further in Section C2. Figures 24b-e also show that maximum wind speeds are reduced from CMIP to AMIP simulations, while the CLLJ location remained in the Caribbean.

A feature that is clearly seen in Figs. 24b and d and not in the reanalysis (Fig. 24a), is the overly strong easterly flow over Central America and in the East Pacific. The splitting of the CLLJ into an easterly and southerly component over Central America is observed during JJA; however, four of the CMIP models have winds at least 4 ms^{-1} larger than observations in this region (e.g., Figs. 24b and d). A lack of observations in this region may be influencing the reanalysis, as Amador (2008) shows the CLLJ to be strong (in excess of 20 ms^{-1} at 1.5 km in February) at one location in Western Central America using data from the local sounding network.

2. Annual Cycle

The CLLJ has a distinct semi-annual cycle, with maxima in February and July as discussed in Section A. The seasonal cycle of zonal wind in the CLLJ region (white box, Fig. 24a) for observations and the CMIP (dashed) and AMIP (dotted) model means is shown in Fig. 25a. The CMIP and AMIP model means do not capture the semi-annual cycle of the CLLJ; the simulated CLLJ remains almost uniform throughout January to July before reaching a minimum in September/October. The relative peak in CLLJ strength in July is not captured by either the coupled or uncoupled model mean. The weakened semi-annual cycle is also seen in two GCMs in Amador (2008) and four in Amador et al. (2010). The magnitude of the AMIP model mean is also consistently less than that of the CMIP mean and is closer to the observed values, especially in the latter portion of the year.

Figure 25b shows the annual cycle of Caribbean area-averaged precipitation. The CMIP and AMIP models appear unable to accurately produce a MSD in July and August, while simultaneously not producing a peak in the CLLJ. The relationship between the CLLJ, rainfall and the MSD will be addressed further in Section D. Also of importance is the underestimation of precipitation by the CMIP model mean and overestimation by AMIP model means, but that is outside the scope of this investigation (Martin and Schumacher, 2011c).

The annual cycle of several quantities that have been shown to be important in the development and maintenance of the CLLJ, such as SLP and SST, as well as their meridional gradients across the region, are shown in Fig. 25c through f. During the observed July peak in CLLJ, SLP increases due to the expansion of the NASH (Fig. 25c) and SLP and SST gradients also have a distinct peak (Fig. 25d and f), as expected (Wang, 2007; Muñoz et al., 2008). It is well know that the CMIP models

underestimate SSTs in the Caribbean region (Misra et al., 2009) and this is clearly demonstrated in Fig. 25e; however, SST meridional gradients across the Caribbean Sea are overestimated, contributing to the overly strong CLLJ.

Both AMIP and CMIP means show a small peak in SLP during June (a month earlier than observed) and a large dip during September/October. However, the SLP gradient does not show a mid-summer peak in either CMIP or AMIP model means. This uniformity of the SLP gradients from January till July is playing an essential role in the uniformity of the simulated CLLJ during these months. The magnitudes of the SLP gradients are similar to the observations, with the CMIP mean being consistently higher than the AMIP mean leading to the stronger CLLJ in the CMIP models.

The overestimation of the magnitude of the CLLJ in the CMIP models is consistent with results presented by Wang et al. (2008) based upon the theory of Gill (1980). The atmospheric response to an off-equatorial heating anomaly (such as anomalously warm SSTs in the Caribbean) is atmospheric Rossby waves resulting in low SLP to the northwest of the heating (Gill, 1980). Hence, when considering the CMIP simulations which have anomalously weak SSTs in comparison to observations (Fig. 25e), anomalously cold Caribbean SSTs during summer lead to a stronger NASH, a weaker continental low over Mexico and the southwest US, stronger meridional SLP gradients across the Caribbean and hence, a stronger CLLJ. However, this theory does not adequately explain the January through June overestimate in CLLJ magnitude in the AMIP simulations, where SST is prescribed (i.e., not anomalously low as in the CMIP simulations).

While the simple theory of Gill (1980) can explain the overestimate of the CLLJ in CMIP simulations, the lack of a summer peak in magnitude is still unexplained. As seen in Fig. 25c, SLP in the Caribbean increases from a minima in May to a maximum

in July in conjunction with the increase in CLLJ magnitude. The spatial extent of this SLP increase is shown in Fig. 26, maps of the difference between May and July SLP for observations and a selection of models. SLP is observed to increase across much of the Northern Atlantic between May and July as the NASH strengthens (Fig. 26a). Expanding and increasing SLP westward into the Caribbean, Mexico and Central America is essential for increasing the SLP gradient in the Southern Caribbean and causing the observed summer peak in CLLJ magnitude. The models have a wide representation of this May to July SLP difference structure and results are presented from well represented (miroc_hi, Figs. 26b, d) and poorly represented (ncar_ccsm, Figs. 26c, e) simulations.

In general, all models captured the strengthening of the NASH in the northern Atlantic, although this strengthening was often too strong and displaced to the north of observations, as seen in Figs. 26c and e. Although all models showed strengthening of the NASH, the increase in SLP in the western Atlantic and Caribbean was problematic. In the majority of simulations, such as those for ncar_ccsm (Figs. 26c, e), little to no increase in SLP was observed in the western Atlantic and Caribbean. With little to no change in SLP and hence SLP gradients, the CLLJ strength remained relatively constant in these simulations. For the few models that did see a westward expansion of the NASH from May to July (e.g., miroc_hi, Figs. 26b,d), magnitudes were often slightly too large. Little improvement was observed between CMIP and AMIP simulations, with the same problems occurring in both simulation types, as seen in Fig. 26. Possible suggestions as to why this westward expansion is not accurately captured by the models include poor simulation of Amazon or Central American precipitation, which causes weaker overturning. The reduced subsidence over the western Atlantic thus reduces the SLP increase.

3. Vertical Structure

The structure of the CLLJ in the vertical is another metric for assessing the models ability to accurately represent the CLLJ. All material in Section C investigated the CLLJ structure only at 925 hPa. Figure 27a shows the annual cycle of the vertical structure of the zonal wind (averaged over the CLLJ area as shown by the white box in Fig. 24a). The maximum at 925 hPa throughout the year is evident, with a stronger and deeper CLLJ in July as compared to January/February. Minima are observed throughout the lower atmosphere in April and October, as expected from previous studies (Cook and Vizy, 2010). Area-averaged winds reach a maximum of approximately 11 ms^{-1} between 950 and 850 hPa in July. Again, four simulation examples are shown in Figs. 27b through e, which represent the ensemble of model output.

All models were able to capture the CLLJ at 925 hPa. However, due to the overly strong CLLJ in almost all simulations, the depth of the CLLJ (approximated by the 8 ms^{-1} contour, which is shaded in Fig. 27) is too great, extending above 800 hPa throughout the first half of the year. The uniformity of the CLLJ annual cycle, as discussed in Section C2, is evident throughout the lower atmosphere in the majority of simulations and in all four example model outputs shown in Fig. 27.

A positive aspect of the simulations is the deepening of the CLLJ during July. This deepening is observed in all models despite the uniformity and too large magnitude of the CLLJ. In some cases (Figs. 27b, d), the reduction in depth of the CLLJ during April is also captured by the models, even though the magnitude at 925 hPa remains constant. Some models (Fig. 27c) have a secondary peak in summer around 600 hPa that is not seen in observations. Improvement in the strength of the CLLJ at all levels is seen in the AMIP simulations, with some models showing a slight minima

in April (Fig. 27d). However, the general structure of the annual cycle is similar between the two simulation types.

4. Variability

In addition to the climatological structure and annual cycle of the CLLJ, the interannual variability of the CLLJ was studied (Fig. 28). The interannual variability was calculated monthly using the standard deviation of the time series for each month (e.g., the standard deviation of all the Januarys, etc.). The interannual variability of the CLLJ index is presented in Fig. 28a. Similar to Wang (2007) and Muñoz et al. (2008), the largest variance occurs in September and October when the CLLJ is climatologically weak. This strong boreal fall variability may influence the development and track of easterly waves and tropical storms in the region from year to year Wang (2007). The two peaks of variance in February and September seen in Wang (2007), who use NCEP/NCAR reanalysis, is seen in Fig. 28a but a third peak in May is also evident in the NCEP/DOE II reanalysis, which may be due to differences in averaging area and time periods between the two studies. The CMIP and AMIP model means, which are also shown in Fig. 28a, show the ability of the models to represent both the magnitude and annual cycle of the interannual variability of the CLLJ, although the fall peak is one month earlier in the AMIP mean and one month later in the CMIP mean.

As seen in Figs. 28c through f, the dominant quantity affecting the interannual variability of the CLLJ is the SLP gradient (Fig. 28d), which shows a strong October peak and a similar annual cycle to the CLLJ index variability in Fig. 28a. Both the CMIP and AMIP model means underestimate the strength of this peak, but have early (late) peaks corresponding to the early (AMIP) and late (CMIP) peaks in the CLLJ index standard deviation. The timing of the peaks in standard deviation of

precipitation in the models is also incorrect (Fig. 28b). The standard deviations of SLP, SST, and SST gradient are relatively constant throughout the seasonal cycle (aside from a February peak in SLP), which is well represented by the model means. The exception is the magnitude of the SST gradient, which has a standard deviation in the CMIP model mean of approximately twice the observed value, indicating an additional problem with the SSTs in this region.

D. Relationship of the CLLJ with Local Rainfall

1. Annual Correlations

The connection between the CLLJ and Caribbean rainfall has been previously identified, with an anomalously strong CLLJ associated with reduced precipitation over the Caribbean and enhanced precipitation along the Caribbean coast of central America (Amador, 1998; Cook and Vizy, 2010). This is illustrated by the significant (at 95 % level) regression coefficient (-2.57 mm day^{-1} per ms^{-1}) between the annual CLLJ index and Caribbean area-averaged precipitation anomaly time series (Table 3). This significantly negative regression coefficient reinforces the theory that when the CLLJ is strong, moisture divergence in the Caribbean and transport out of the region is large, leading to a reduction in precipitation amounts.

Despite the ability of both the CMIP and AMIP models to develop a CLLJ and precipitation with a similar structures to observations (e.g., Fig. 25), not all models produce a significant negative regression coefficient between the CLLJ index and Caribbean area-averaged precipitation anomalies. Table 3 shows that only 6 CMIP models have a significant negative regression coefficient and 3 CMIP models actually have small positive regressions (although they are not significant). Magnitudes of the regression values were often considerably larger than observed (e.g., -4.32 for mpi),

suggesting that precipitation anomalies reduce too rapidly with an increasingly strong jet.

An improvement is seen in the AMIP models, with 10 out of 12 AMIP models producing significant negative regression values, none having positive coefficients, and magnitudes general closer to that of observations. This suggests that the errors in the relationship between the CLLJ and precipitation seen in the majority of CMIP models were not simply caused by errors in the atmospheric component of the model. The large CMIP and small AMIP errors suggest that the incorrect interaction between the ocean and atmosphere or the anomalously cold SSTs in the CMIP models are affecting the CLLJ-rainfall relationship. It is important to note that local, small-scale connections between the CLLJ and precipitation in the Caribbean are not captured by this annual, area-averaged approach. Higher resolution than is available from both observations, reanalysis and GCM output would be necessary to further investigate these relationships.

2. The Mid-Summer Drought

The CLLJ has an important relationship with precipitation during the MSD, as discussed by Magaña et al. (1999); Wang (2007); Muñoz et al. (2008) and Whyte et al. (2008). In addition to the annual, area-averaged regression coefficients between the CLLJ index and rainfall anomalies, the spatial distribution of correlation values is also important for determining the simulation abilities of the models. The observed correlation map between the CLLJ index and precipitation anomalies for August is shown in Fig. 29a. August was chosen as it coincides with the MSD and a strong CLLJ variation. Results for July were similar but slightly weaker in this dataset. Observations show extensive negative correlations across most of the Caribbean, western tropical Atlantic, and Central America, except for the Caribbean coast of Central America

(orographic and jet exit convergence influence is strong in this region), agreeing well with Cook and Vizy (2010).

Correlation maps from two different models are shown in Figs. 29b through e. These models were chosen to be representative of the model ensemble, with miroc_med (Figs. 29b,d) having a small negative annual regression coefficient in the CMIP run and a significant negative regression in its AMIP run. The ncar_pcm model (Figs. 29c,e) had significant negative regression values in both simulations. It is seen from the model correlation maps that the models produce similar patterns to the observations. Significant negative correlation values across the Caribbean are simulated, although the region of negative correlation in the simulations is not as spatially extensive as the observations. Noticeable improvements are seen in the AMIP simulations in comparison to the CMIP simulations, with a larger spatial extent of the negative correlations across the entire domain. Similar results were observed for other months (not shown).

Primary deficiencies in the model simulations occur in Mexico and the East Pacific. Correlations are close to zero across much of Mexico in many simulations (e.g., 29b,c,d) and any negative correlations that are simulated are not as widespread as observations (e.g., 29e). An interesting region of positive correlations in the models (increased precipitation with a stronger CLLJ) is seen in the East Pacific off the coast of South America that is not in observations. One possible explanation is that the representation of the Central American terrain in the models is lacking, leading to excess moisture transport into the East Pacific. Model errors in this region may also be due to problems in simulation the low-level westerly Choco jet (Poveda and Mesa, 2000; Durán-Quesada et al., 2010) which is an important moisture transport mechanism in the far Eastern Pacific.

In order to further investigate the interaction between the CLLJ and MSD in

the models, composite annual cycles of models with and without a MSD were calculated. Each IPCC AR4 model (both AMIP and CMIP) was categorized by whether it captured the Caribbean MSD. A simple definition for the MSD was established. A model was categorized as MSD if it simulated at least a 0.1 mm/day reduction in area-averaged precipitation between June and July, as the largest reduction in the area-averaged precipitation is seen between June and July (Fig. 25). The AMIP models better captured the MSD, with 7 of 12 categorized as 'MSD'. Only 6 of 19 CMIP models fell into this category (as expected from Fig. 25b). The same variables in Fig. 25 were then calculated for these 'MSD' and 'No MSD' model composites and are shown in Fig. 30.

It is clear from Fig. 30b that the models that capture the MSD (red lines) not only do better at simulating summer rainfall, but the entire annual cycle is improved and both CMIP and AMIP MSD model means are closer to observations. The CLLJ annual cycle is also improved, with a more distinct maximum in July and magnitudes closer to the observations (Fig. 30a). As seen in observations, the CLLJ July peak coincides with the increase in SLP gradients and SST gradients across the Southern Caribbean. The MSD composited models show a much better structure than the 'No MSD' composites (fig. 30d and f), although SLP gradient changes are still weaker than observations.

By compositing the models by those that capture the MSD and those that do not, the representation of the SST in the CMIP models is greatly improved in the MSD composites (Fig. 30e and f). The models with a MSD have larger SSTs (although they are still approximately 1°C below observations) and greatly improved SST gradients in the southern Caribbean. Whether this improvement in SST gradient is the cause or effect of a better CLLJ simulation is not possible to determine from these simulations alone, although the August peak in SST gradient perhaps suggest the SST gradient

is a response to the CLLJ rather than a generating factor. These results reiterate the importance of improving CMIP simulations of SST in this region.

E. Connection with United States Climatology

1. The Great Plains Low-Level Jet

Numerous studies have shown the importance of the CLLJ as a moisture and momentum source to the US and the GPLLJ (Mo et al., 2005; Mestas-Nuñez et al., 2007; Wang et al., 2008; Cook and Vizy, 2010). The observed CLLJ and GPLLJ indices (as described in Section B1 and Fig. 24) were regressed against each other for each month of the year and the results are shown in Table 4. The significant positive regression coefficients in January through April agree with the results of Cook and Vizy (2010), in that the GPLLJ forms temporarily during these cold months when the CLLJ is strong and hence, a positive regression coefficient is observed. Positive values are also seen throughout the rest of the year (except November) and are significant in June, July, and September when both the CLLJ and GPLLJ are strong and the AWP is large (particularly in September).

The connection between the CLLJ and the GPLLJ is important for the accurate simulation of US climate. Figure 31 shows scatter plots and accompanying regression lines between the February CLLJ and GPLLJ indices for observations, as well as each CMIP (Fig. 31a) and AMIP (Fig. 31b) ensemble members. Similar patterns and results were seen for other months (not shown). For the CMIP model ensemble (Fig. 31a), the majority of models (11 of 19) produce a significant positive regression coefficient between the CLLJ and GPLLJ. The AMIP ensemble (Fig. 31a) however, shows quite a different result, with only the minority (4 of 12) models producing a significant positive correlation despite the improved simulation of the February CLLJ

in the AMIP models.

2. Relation with US Rainfall

The ability of the models to simulate the connection between the CLLJ and US precipitation was also investigated for February, as the models produce a strong connection with the GPLLJ and Cook and Vizy (2010) have shown a link with US precipitation in this month. The observed correlation between the CLLJ index and precipitation anomalies for February is shown in Fig. 32, and as for the August maps (Fig. 29) it matches well with the results of Cook and Vizy (2010). A region of significant positive correlations, showing a stronger CLLJ leads to increased precipitation, is evident across the south Central US and the Midwest. Little correlation is observed in the Caribbean itself, but a region of significant negative correlation is seen in the western Atlantic. This negative correlation region is likely due to increased subsidence in this region of the NASH when the CLLJ is strong.

The models produce varying results, as seen in Fig. 32. In both chosen models, the CLLJ and the GPLLJ indices have a significant positive regression coefficient (both CMIP and AMIP), but differing precipitation correlations are evident. The region of negative correlations in the western Atlantic is farther west in all the model simulations, consistent with the westward displacement of the NASH (Fig. 25c) and the overly strong CLLJ in February.

Both CMIP models (Fig. 32b,c) show positive correlations across the central US, although it is shifted southeast in both simulations. The AMIP models (Fig. 32d,e) show little to no positive correlation with precipitation over the central US, despite being significantly correlated with the GPLLJ. This suggests that although the CLLJ itself may be continuing northward into the GPLLJ in the AMIP models, it is not transporting sufficient moisture to influence the central US precipitation. This lack

of moisture may be due to the AMIP models producing too much Caribbean rainfall, which leaves little moisture available for northward transport. It may also be due to inaccurate air-sea moisture fluxes over the Gulf of Mexico that do not input more moisture into the jet as it transitions from the Caribbean to the US.

F. Summary

Using 19 coupled and 12 uncoupled model runs from the IPCC AR4, the ability of the models to produce a CLLJ has been investigated. Previous studies of the CLLJ had either been purely observational (Wang, 2007; Muñoz et al., 2008; Whyte et al., 2008; Cook and Vizy, 2010) or with few GCM studies (Amador, 1998; Wang et al., 2008). The CLLJ is an important feature for IPCC AR4 models to reproduce, as it has a large impact on both local and US climate, including easterly waves and tropical storms (Serra et al., 2010). Although the IPCC AR4 output varied in horizontal resolution from 1.125° to 5°, and contained a multitude of different parameterization configurations, all were able to develop and maintain a CLLJ with similar features to the observed CLLJ, with no clear impact of resolution on the results.

The seasonal cycle of the CLLJ was more challenging for the models to simulate. The observed semi-annual cycle was not seen in either CMIP or AMIP models, with uniform magnitudes between January and July followed by a minimum in September and October. The uniformity of the CLLJ throughout the first half of the year was a result of the NASH being too uniform in its strength and location. The lack of a westward and southward extension of the NASH in July meant that meridional SLP gradients across the Caribbean were not enhanced and hence the CLLJ remained uniform in magnitude. The correct simulation of the structure, strength and evolution of the NASH is essential for the correct development of an accurate CLLJ in the

models. The poor simulation of Atlantic and South American precipitation by the IPCC models (Biasutti et al., 2006; Richter and Xie, 2008) may be impacting the NASH and thus the CLLJ.

The magnitude of the CLLJ was also a problem with the majority of models. At 925 hPa and throughout the lower atmosphere, the models regularly overestimated the strength of the CLLJ with CMIP models having greater magnitudes than AMIP models. This was most evident in the first half of the year. The overestimate of CLLJ strength along with anomalously cold SSTs in the CMIP models agrees with the results presented by Wang et al. (2008) based on the theory of Gill (1980). Despite the overestimate of magnitude by the models, the vertical deepening of the CLLJ during July was well captured by all the models, despite not having a CLLJ peak at this time. This indicates that separate processes must be controlling the deepening and strengthening of the CLLJ, with the deepening better represented in the models.

During the summer months, and particularly August, the CLLJ is highly negatively correlated with precipitation anomalies in the Caribbean. As the CLLJ strength increases, moisture is transported away from the Caribbean leading to drier conditions. Despite some problems with the simulation of precipitation by the models (and the subject of another study), the models showed considerable promise in the simulation of the CLLJ-rainfall relationship in the Caribbean, particularly during August. The AMIP models performed better than the CMIP models in the strength and structure of the precipitation correlations, suggesting that the atmospheric component of the model is performing well and the influence of the cold SSTs and/or incorrect moisture fluxes in the CMIP models may be leading to poorer performance in the CLLJ-rainfall coupling.

A link between the ability of models to produce a summer CLLJ peak and the MSD was established, although the cause and effect could not be explicitly deter-

mined. The models that did produce a distinct MSD produced better area-averaged precipitation throughout the entire annual cycle, had an improved CLLJ annual cycle (although magnitudes were still large in January through June), and had improved magnitudes and annual cycle of SLP and SLP gradients in the Caribbean. These improvements were seen in both the CMIP and AMIP models. An important result from the MSD compositing was the improvement in the SST and especially the SST gradient in the CMIP models that produced a MSD. Although SSTs were still lower than observations in the MSD composite, this highlights the importance of correctly simulating both mean SSTs and SST gradients for reproducing accurate Caribbean climate.

Connections between the CLLJ and US climate in the models were found to be quite variable, with CMIP models outperforming AMIP models. Not only did CMIP models reproduce the positive correlation between the CLLJ and GPLLJ during the cold season, they also showed a better positive correlation between the CLLJ and central US cold season precipitation. Even AMIP models that captured the CLLJ-GPLLJ correlation were unable to accurately reproduce the CLLJ-US rainfall correlations. This leads to the hypothesis that the northward branch of the CLLJ is not transporting enough moisture to the GPLLJ. This may be due to too much moisture being used for precipitation in the Caribbean region (AMIP models overestimate Caribbean precipitation), not enough moisture being fluxed into the lower atmosphere over the Gulf of Mexico or a combination of both. Further investigation into the moisture fluxes and transport in the models is necessary. However, it is also important to consider possible errors in the reanalysis, especially in data sparse regions such as the Caribbean and surrounding areas. Amador (1998) show that NCEP/NCAR reanalysis underestimates moisture flux in the northern Gulf of Mexico between 1973 and 2004, in the entry region to the GPLLJ.

The ability of the IPCC AR4 models to simulate a realistic and accurate CLLJ has been examined in detail and related to local and US climate. Whilst the models show pleasing results across the range of horizontal resolutions and model configurations of the ensemble, further model improvements and understanding of the observations are needed to fully reproduce the observed CLLJ structure and impacts in GCMs. Additional investigations of the relationship between the CLLJ and large-scale climate features such as the NAO and ENSO in the GCMs would be beneficial in further examining the model performance.

CHAPTER IV

MODULATION OF CARIBBEAN PRECIPITATION BY THE MADDEN-JULIAN OSCILLATION*

A. Background

The Caribbean is one of many regions of the world where it is vital to understand precipitation patterns, variability and extremes. The low-lying coastal regions of Caribbean islands are densely populated with development pressure increasing. The region is also vulnerable to many natural hazards that are related to and exacerbated by precipitation, such as hurricanes, earthquakes, mudslides and drought. There is also evidence that precipitation patterns can influence the spread of Dengue fever in the region (Jury, 2008). Planning, policy and management of these events are extremely dependent on knowledge of the precipitation of the region. These social and economic reasons provide considerable motivation for increasing and expanding current knowledge of precipitation in the Caribbean.

Annual rainfall exhibits a bimodal structure, with an initial maximum in May, a minimum around July-August, and a second maximum in September-October (Gamble et al., 2008; Jury et al., 2007). The minimum that separates the two peaks in rainfall has been termed the 'mid-summer' drought (MSD) (Magaña et al., 1999). The precipitation climatology in the Caribbean is well known, and shown in Fig. 33a for reference. Whilst the distribution of the mean rainfall is primarily dominated

---

*Reprinted with permission from "Modulation of Caribbean Precipitation by the Madden-Julian Oscillation" by E.R. Martin and C. Schumacher. *J. Climate.*, **24**, 813-824, Copyright American Meteorological Society.

by location of land,the synoptic influence for Caribbean precipitation is the North Atlantic subtropical high (NAH) whose latitudinal position and strength affects the strength of the trade winds, sea surface temperature and coastal upwelling, which all act to modify precipitation amounts in the region (Mapes et al., 2005; Gamble et al., 2008). Annual average precipitation amounts are as large as 6 mm day^{-1} in the southwestern Caribbean and decrease to 1 mm day^{-1} in the Central Caribbean sea. This structure is primarily due to the Caribbean Low-Level Jet (CLLJ) that dominates the Southern Caribbean region (Amador, 1998; Cook and Vizy, 2010). The CLLJ is an easterly jet that is strongest at 925 hPa and has a semi-annual cycle with maxima in February and July (Amador, 1998; Amador et al., 2000; Magaña and Caetano, 2005; Wang, 2007; Muñoz et al., 2008; Whyte et al., 2008).

Precipitation in this region has variability on a variety of timescales. On the interannual timescale, precipitation in the region is influenced by the El Niño-Southern Oscillation (ENSO) and the North Atlantic Oscillation (NAO) (Chen and Taylor, 2002; Jury et al., 2007). ENSO impacts the Caribbean through changes in convergence patterns and sea surface temperatures (SSTs) in the Caribbean that cause changes in rainfall (Giannini et al., 2000; Taylor et al., 2002; Chen and Taylor, 2002). The second rainfall season tends to be drier in El Niño years and wetter in La Niña years (Giannini et al., 2000; Taylor et al., 2002). However, the first rainfall season tends to be wetter in the year after an El Niño and drier in a La Niña year (Chen and Taylor, 2002). The phase of the NAO modulates the behavior of warm ENSO events (Giannini et al., 2001). The region is also affected on shorter timescales (days to weeks) by the propagation of easterly waves, which can mature into tropical storms and hurricanes that represent a primary rainfall source in the Caribbean contributing to the second rainfall peak in the annual cycle.

A period of variability that has not been intensely studied in the Caribbean is

the intraseasonal range of 30 to 90 days. A connection between the dominant mode of intraseasonal variability in the Pacific, the Madden-Julian Oscillation (Madden and Julian, 1971), and Gulf of Mexico hurricane numbers was identified by Maloney and Hartmann (2000b). In addition, Barlow and Salstein (2006) showed a relationship between the MJO and summertime precipitation in Mexico and Central America. The MJO is suggested to affect central America and modulate hurricane activity in the Gulf of Mexico through generation of a Kelvin wave by the main region of MJO convection in the Indian Ocean. This Kelvin wave propagates across the Pacific and leads to changes in circulation in the Central American region (Matthews, 2000; Kikuchi and Takayabu, 2003; Sperber, 2003). Whilst previous global studies, such as Salby and Hendon (1994); Bantzer and Wallace (1996) and Wheeler and Hendon (2004), indicate changes in circulation and precipitation in the Caribbean in association with the MJO, these changes and their impacts in this region have not been thoroughly documented.

We hypothesize that circulation changes due to the MJO affect precipitation amounts and patterns in the Caribbean region. It is the aim of this paper to investigate the nature of the precipitation changes, including extreme events. Knowledge of a precipitation connection in the Caribbean with the MJO may lead to enhanced forecasting skill due to the predictability of an MJO event being approximately 2 weeks once an event has been initiated.

A brief discussion of the data and methodology is contained in Section B, followed by an analysis of precipitation variability in the region (Section C). The connection between precipitation and the MJO will be analyzed annually (Section D1) and seasonally (Section D2). The role of the CLLJ in relation to the precipitation will be presented in Section E and the relationship between extreme precipitation events and the MJO in Section F.

B. Data and Methodology

The Caribbean region in this study is defined as lying between 55W and 90W, and 10N to 25N (Fig. 33). All data used is at a daily resolution in order to fully investigate the impacts of the MJO on precipitation. As daily precipitation estimates are required, the period of study is a continuous 12 year period from 1997 to 2008, with a strong MJO event occurring on 62 % of days and including approximately 50 MJO cycles (as determined by the Wheeler and Hendon (2004) index described below).

The precipitation data is from the Global Precipitation Climatology Project (GPCP), which is a combination of satellite products and gauge observations (Huffman et al., 2001). Daily GPCP data is available at 1° resolution. This data set was chosen as it has relatively high spatial and temporal resolution and contains the longest time period of daily observations. Wind data at 925 hPa required to investigate circulation changes were acquired from the European Center for Medium Range Weather Forecasting (ECMWF) reanalysis interim (ERA-Interim) dataset at 1.5° resolution. ERA-Interim is a reanalysis product that assimilates observations and model data and is the latest reanalysis product from ECMWF covering the data rich years since 1989. ERA-Interim has been shown to be a significant improvement over previous reanalysis products, especially in the hydrological cycle (Simmons et al., 2007).

In order to characterize the impact of the MJO on the climate of the region, precipitation, circulation and SST anomalies were created. Anomalies were calculated as differences from the annual cycle. This allows for more meaningful comparisons between seasons and prevents the wet season from overwhelming important variability in the dry season. The anomalies were created both annually and seasonally, although only SON (September, October, November) is presented for brevity. This seasonal in-

vestigation is imperative to determine whether intraseasonal variability dominates in any one season (e.g., hurricane season as shown by Maloney and Hartmann (2000b)).

Spectral analysis and wavelet analysis (Torrence and Compo, 1998) were used to create power and variance spectra and time series from area-averaged precipitation anomaly time series' to identify intraseasonal variability. Area-averaging was based on the lettered areas shown in Fig. 33a. Wavelets were chosen in addition to line spectra as wavelet analysis not only identifies timescales of significant variability but how these timescales change throughout a time series, allowing the identification of strong or weak periods of intraseasonal variability within the 12 year time period of investigation.

In order to relate Caribbean precipitation to the MJO, a measure of the MJO is required. There are a variety of methods used to quantify the MJO, but the index developed by Wheeler and Hendon (2004) was used in this study. This index contains daily values of both amplitude (greater than 1 is considered a strong MJO event) and phase (MJO divided into 8 phases according to location as it propagates across the Indian and Pacific Oceans). It is a seasonally independent index derived from lower and upper-level winds and outgoing longwave radiation. Information from all longitudes is used in the MJO index hence it effectively captures the propagation of the MJO convection from the Indian Ocean and into the West Pacific, as well as the variability in winds and precipitation in the East Pacific Precipitation, as discussed by Maloney and Hartmann (2000a) and Maloney and Esbensen (2003). Detailed structure of the evolution of convection and large scale circulation can be seen in Wheeler and Hendon (2004). Circulation and SST anomalies were composited according to phase of the MJO for all strong MJO events to determine how the MJO affects each variable. In addition to this composite analysis, probability distributions functions (PDFs) of rain rates from each grid point during each phase were also

generated to investigate how the rainfall distribution changes between phases, which is of particular use for investigating extreme events.

C. Precipitation Variability

Intraseasonal (defined as 30 to 90 days) variance of annual precipitation in the Caribbean is shown in Fig. 33b. Variance follows the general pattern of annual mean precipitation in the region, being large in the southwestern Caribbean off the coast of central America and small in the east and central Caribbean Sea. However, variance is small over the Caribbean islands and maximized in the Caribbean Sea between central America and Cuba, in contrast to the mean rainfall in Fig. 33a. The variance more closely resembles the precipitation climatology of September, October and November (SON), rather than the annual mean, which will be discussed further in Section D2. This variance climatology suggests large intraseasonal variability in the region but to assess its significance above red noise and relation to other time periods wavelet analysis was used to create line spectra of the annual area-averaged precipitation anomaly time series and is shown in Fig. 34 for each grid box, along with the background spectrum and 90 % confidence level spectrum.

It is seen in Fig. 34g that the region of maximum intraseasonal variance from Fig. 33b has significant power in the intraseasonal range. What is perhaps less obvious from Fig. 33b is that the region directly to the east (box H) also has significant power in the intraseasonal range despite having low variance values in comparison with the surrounding regions. Boxes G and H are in the region of the CLLJ, suggesting a possible link with intraseasonal variability of the CLLJ (further explored in Section E). Although intraseasonal variances are large in many other parts of the Caribbean, it is only boxes G and H that have power in the 30 to 90 days range that

is significantly above the red noise. However, power is still relatively large in most boxes, with a broad peak in the 30 to 90 day range followed by a sharp decrease in power (e.g. Figs. 34a,d,f). These spectra along with the variance map suggest strong precipitation variability at the intraseasonal range and indicates that there is intraseasonal variability in the region that requires further investigation.

The intraseasonal variability that has been identified in Figs. 33b and 34 may be due to local intraseasonal variations or due to the remote influence of the MJO (or a combination of the two). The influence of the MJO will be addressed further in forthcoming sections. The internal or regional intraseasonal variability that may be contributing to this power peak is beyond the scope of this study.

D. Connection with the MJO

1. Annual Composites

As illustrated in Figs. 33b and 34, intraseasonal variability in precipitation is observed in the Caribbean. In order to investigate in what way this intraseasonal variability is connected to the MJO and the spatial patterns of this connection, the compositing technique described in Section B was used on annual precipitation anomalies and is shown in Fig. 35. Precipitation anomalies are composited by the MJO in groups of two phases; phase 1 and 2 (MJO convection located in Africa and the western Indian Ocean), phases 3 and 4 (MJO convection in the eastern Indian Ocean and Maritime continent), phases 5 and 6 (MJO convection in the Western Pacific) and phases 7 and 8 (MJO convection in the western hemisphere).

Precipitation anomalies are composited as percentage differences from the annual average, as it provides a clearer illustration of where the most significant changes are occurring as annual mean precipitation values vary so much across the region (Fig.

33). Precipitation anomalies are observed to reach up to 50 % above normal in phases 1 and 2, and 40 % below normal in phases 5 and 6.

Much of the Caribbean receives above normal precipitation during phases 1 and 2 (Fig. 35a), except the region off the coast of southern Central America where conditions are drier than normal. The reverse pattern is seen in phases 5 and 6 (Fig. 35c), with dry conditions across much of the Caribbean domain and wetter conditions along southern Central America. Whilst the general pattern is reversed between phases 1 and 2 and phases 5 and 6 there are slight differences, including over Cuba. These smaller scale features may be a result of localized differences in wind directions around the islands. The interstitial phases (Figs. 35b and d) show smaller and less coherent precipitation anomalies (although still significant in some locations) and may be acting as transition phases between phases with much larger impact on the region.

To evaluate the causes of the precipitation changes, low-level (925 hPa) wind anomalies and their divergence for different phases are shown in Fig. 36. Significant differences in the wind direction anomalies exist between the two groups of phases, with westerly anomalies in phases 1 and 2 acting to slow down the prevailing trade winds and anomalous easterlies in phases 5 and 6 increasing the strength of the trade winds. The maximum wind speed anomalies are focused in the region of the CLLJ in the southern Caribbean Sea and into Central America. This wind anomaly maximum acts to strengthen (weaken) the jet in phases 5 and 6 (1 and 2), respectively. The wind anomaly reversal is similar to that found in studies of the Eastern Pacific by Maloney and Hartmann (2000a,b).

Changes in the jet strength consequently affect the low-level divergence in the region (shading in Fig. 36). The pattern of divergence and convergence matches the precipitation anomalies rather well as seen in Fig. 35a and c, especially in the

southern Caribbean where precipitation anomalies are largest. Low-level convergence (divergence) is seen in the region of positive (negative) precipitation anomalies. The low-level divergence anomalies begin to appear in the two phases prior to the precipitation anomalies and maximize in the phases with maximum precipitation anomalies (i.e., divergence anomalies consistent with the rainfall pattern in phases 5 and 6 appear in phases 3 and 4 and maximize in phases 5 and 6). This suggests that the cause of the precipitation anomalies is changes in low-level divergence associated with changes in the CLLJ.

Another possible mechanism relating the wind and precipitation anomalies is the relationship between wind and SST, where enhanced wind speeds leads to more evaporative cooling from the sea surface, lower SSTs and hence less convective activity. Composite analysis of the SSTs from the NOAA optimum interpolation product (not shown), show only very small SST anomalies (less than 0.2^{o}C) across the region and little to no SST changes in the region of maximum precipitation anomalies and intraseasonal variability. The largest SSTs are along the coast of Venezuela, where upwelling/downwelling is modulated by wind speed changes.

2. Seasonal Composites

The discussion in Section C, along with the strong bimodality of the precipitation annual cycle in the region, indicate that the intraseasonal variability and the MJO modulation of precipitation may not be constant throughout the seasonal cycle. The seasonal cycle of intraseasonal variance for the same nine grid boxes used in Fig. 34 is shown in Fig. 37 and shows a strong annual cycle across the entire domain. A bimodality similar to that of the precipitation annual cycle is seen at each location, however unlike the annual cycle, the second peak in SON dominates over the earlier peak in May and June in the majority of boxes. The second peak in significantly

above red noise at the 80 % level in 8 locations and above 90 % at 6 locations. This is a strong indication that the MJO is having the largest influence on Caribbean precipitation during late summer and fall (SON).

To investigate the impact the modulation of SON precipitation by the MJO the same analysis as Section D1 was performed on SON precipitation data. Precipitation anomalies for SON composited phase are shown in Fig. 38. It should however be noted that similar patterns of precipitation anomalies that were significantly different from zero were observed in all four seasons, despite the variance being much smaller (Fig. 37). Percentage changes during the other three seasons were of a similar magnitude to those in SON (Fig. 38) but absolute changes were of course less.

Consistent patterns are observed between the SON composites of Fig. 38 and the annual composites of Fig. 35. In phases 1 and 2, wet precipitation anomalies are observed throughout the central Caribbean, and dry anomalies observed along Central America (Fig. 38a) with the reverse pattern in phases 5 and 6 (Fig. 38c). There are differences between the SON and annual composites, however. During phases 1 and 2 (Fig. 38a) precipitation anomalies are not as large (percentage wise) or as significant (due to large standard deviations) in the central Caribbean Sea, but a significant dry anomaly is still observed off the coast of Central America. In phases 5 and 6 (Fig 38c) however, the precipitation anomalies during SON match well with the annual composites in terms of spatial pattern and magnitude. The interstitial phases again show much smaller magnitudes and a less coherent structure across the domain, but the drying in phases 3 and 4 in the annual composite is reduced in both magnitude and extent during SON (Fig. 38b).

In JJA (not shown), a wet precipitation anomaly across almost the whole Caribbean domain is observed in phases 1 and 2 and a dry anomaly in phases 5 and 6. During JJA, the mid-summer drought (Magaña et al., 1999; Gamble et al., 2008) is in effect,

suggesting that the MJO may be impacting the mechanisms behind the mid-summer drought.

E. Role of the Low-Level Jet

The locations of the precipitation, low-level wind and low-level divergence anomalies suggest that the CLLJ is being modulated by the MJO, which then leads to the observed changes in precipitation (particularly in the Southern Caribbean). Previous literature, to the best of the authors' knowledge, has not shown intraseasonal variability of the CLLJ or a relationship with the MJO. To illustrate the seasonal changes in the CLLJ, wind anomalies were composited by season and phases of the MJO and are shown for SON (corresponding to the precipitation anomalies in Fig. 38) in Fig. 39.

In SON, low-level wind direction and speed anomalies are consistent with the annual composites (Fig. 36), with enhanced trade winds during phases 5 and 6 (Fig. 39c) and weaker trade winds during phases 1 and 2 (Fig. 39a). The maxima in wind speed anomalies are focused in the region of the CLLJ in the Southern Caribbean and extend into the eastern Pacific. This is consistent with the location of the precipitation anomalies seen in Fig. 38. In other seasons (not shown), a similar pattern and magnitude of wind speed and direction anomalies are observed in the southern Caribbean in phases 1 and 2 and 5 and 6. The wind speed anomalies are much smaller in phases 3 and 4 and 7 and 8, consistent with the smaller precipitation anomalies. An interesting feature emerges in phases 7 and 8, with large southerly wind anomalies in the western Caribbean possibly influencing transport into the Gulf of Mexico. Anomalies throughout the rest of the domain are weak.

It is well known that the CLLJ undergoes a semi-annual seasonal cycle, with

peaks in February and July (Amador, 1998; Amador et al., 2000; Magaña and Caetano, 2005; Wang, 2007; Muñoz et al., 2008; Whyte et al., 2008; Cook and Vizy, 2010). As seen in Fig. 39, SON wind speed anomalies in the region of the CLLJ are large (1-3 m s^{-1}) and are approximately consistent across other seasons also. This consistency in wind speed anomalies will effect the CLLJ differently in each season due to the semi-annual cycle. It is necessary to determine the influence of the MJO on the CLLJ in each season, as it appears to have a large impact on precipitation in the region.

In order to investigate the influence of the MJO on the CLLJ itself, an index of the CLLJ was defined based on Wang (2007). The CLLJ index is defined by taking the negative of the mean 925 hPa wind anomalies in the region of 12.75°N-17.25°N and 69.25°W-80.5°W (i.e., the thick box in Fig. 39a). Since the 925 hPa winds are easterly in the region of the CLLJ, taking the negative of the wind anomalies makes the index positive (negative) when the CLLJ is stronger (weaker) than average.

Statistics (means and standard deviations) of the CLLJ index by season and phase are shown in Table 5. The large difference between the phases with large precipitation changes (phases 1 and 2, phases 5 and 6) and those with small changes (phases 3 and 4, phases 7 and 8) is apparent in the statistics both annually and seasonally. Jet index means have a larger magnitude for phases with large precipitation changes (e.g. -1.50 for phases 1 and 2 in the annual mean) compared to those with small changes (e.g. -0.46 for phases 7 and 8 in the annual mean), again showing the importance of the CLLJ in the MJO-precipitation connection in the region. For SON, when intraseasonal variance maximizes, the jet index for phases 1 and 2 is -1.47 and is 1.49 for phases 5 and 6, as expected. The jet index means for phases 1 and 2 and phases 5 and 6 are significantly different from each other at the 99.9 % confidence level for each season. These statistics provide evidence that the MJO is modulating

the CLLJ.

Table 5 also shows an interesting anomaly in JJA for phases 7 and 8, with a positive CLLJ index mean (mean is negative in all other seasons and the annual average). Precipitation patterns show drier than average conditions over much of the eastern Caribbean during this time (not shown), further indicating that both the MJO and the CLLJ may have an influence on the mid-summer drought that occurs during JJA (Magaña et al., 1999).

In order to relate the CLLJ, precipitation and intraseasonal variability (the MJO), cross spectral analysis was performed between the CLLJ index and the Caribbean area-averaged precipitation time series. Each time series was divided into twelve 365 day subsets and the cospectra and quadrature spectra for each subset was calculated. These spectra were then averaged together prior to calculating the coherence and phase shown in Fig. 40. Significance was estimated using tables from Amos and Koopmans (1963). The coherence squared is shown in the upper panel of Fig. 40. A clear peak (significant at the 95 % level) in the coherence is seen at frequencies corresponding to the intraseasonal range of 30 to 90 days. By examining the phase (Fig. 40, lower panel) we see that in the intraseasonal time period, the CLLJ and Caribbean area-averaged precipitation are varying approximately in phase. This differs from the significant region of coherence squared between 15 and 20 days (frequencies of approximately 0.06), where the phase suggests the CLLJ is leading area-wide precipitation by approximately 45^o. Whilst this 20 day peak requires further investigation, it is outside the scope of this work.

F. Extreme Events

Extreme precipitation events have important social consequences, and it is essential that we understand them further. Large changes in precipitation associated with the MJO as indicated in Sections D1 and 2, as well as the study of Maloney and Hartmann (2000b) showing hurricane modulation by the MJO, suggest that extreme wet precipitation events may be affected by phase of the MJO. With anomalies in annual and seasonal precipitation up to 50 % of the mean precipitation in some locations, extreme events may be more likely to occur when the MJO is in a certain phase. Two methods are used for determining the MJO impact on extreme events. It should be noted that the precipitation dataset is daily averages over 1° grid-boxes, so it may not be capturing very localized (in both space and time) extreme events.

The PDFs of daily grid-box rain rates across all seasons and all years for phases 1 and 2 and 5 and 6 are shown in Fig. 41. As expected from Figs. 35a and c, daily grid-box rain rates are larger in phases 1 and 2 of the MJO, especially for extremely high rain rates. Differences between the two PDFs are small up to 5 mm day^{-1}, where they begin to diverge. Once rain rates reach approximately 60 mm day^{-1}, they are observed in phases 1 and 2 of the MJO between 50 and 100 % more often than in phases 5 and 6 of the MJO. It is clear from Fig. 41 that the most extreme events, i.e., daily individual grid-box rain rates greater than 100 mm day^{-1}, are more likely to occur when the MJO is is phase 1 or 2.

The most relevant extreme precipitation events to society occur over land. To investigate extreme events over the larger Caribbean islands, the 100 wettest days (corresponding approximately to the 97.5 percentile) across all seasons and all years at four grid points (Cuba, Hispaniola, Puerto Rico and the central Caribbean Sea) were categorized by the MJO phase at the time of the wet event (Fig. 42). Only days

where the MJO was strong (amplitude greater than one) were included.

Figure 42 clearly shows that the wettest days occur when the MJO is in phases 1 and 2 for all of the four locations, as expected from Fig. 41. Cuba has the highest number of wettest days in phases 1 and 2 but it is not well separated from phases 7 and 8, however, the distribution is similar to the other locations if a southeasterly Cuban grid point is chosen as opposed central Cuba as illustrated here, agreeing with the precipitation patterns as shown in Fig. 35a. The proportioning between phases is extremely similar when the wettest 200 days (95th percentile) are used (not shown), although more days fall into phases 1 and 2 in Cuba, making it more in line with the other locations. Strong MJO events affect the large-scale patterns of convergence and divergence in the region which contributes to extreme rainfall events in the region. Weak MJO events account for approximately 30 of the 100 events at each location, comparable with the events in phase 1 and 2. Extreme precipitation events likely occur during weak MJOs due to small-scale localized mechanisms of precipitation enhancement (such as orographic effects) and tropical cyclones.

It is important to be aware of what season the 100 wettest days occur in for each location as they do not all occur during tropical cyclone season. Approximately 50 of the wettest days at each island location occur in SON, with a range of 8 to 12 occurring in the driest season of DJF. The wettest days at each location that were directly due to tropical storms were determined using the National Hurricane Centers archive of storm tracks and the number of storms affecting each location in each phase is shown by the stripped bars in Fig. 42. It is apparent that tropical storms are not always the major contributor to extreme wet events in these locations, further confirming the need for investigation of non tropical storm precipitation variability. The number of tropical storm related wet events follows a similar distribution across the MJO phases, with the most events occurring in phases 1 and 2, suggesting the modulation

of tropical storms in the Caribbean by the MJO. This is consistent with the studies of both Maloney and Hartmann (2000b) and Klotzbach (2010), which investigated hurricanes in the Gulf of Mexico and the Atlantic, respectively.

This modulation of extreme precipitation events by the MJO may play an essential role for prediction of extreme events due to the predictability of MJO phase, which in turn could improve planning and preparation for such events.

G. Summary

Using 12 years of daily observational data, intraseasonal (30-90 day) variability in Caribbean precipitation has been identified. Previous studies of intraseasonal variability in and around the Caribbean had focused only on tropical cyclone variability (Maloney and Hartmann, 2000b; Klotzbach, 2010) and not explicitly precipitation. Intraseasonal variance (and power) is large across much of the western Caribbean, but significant power above red noise is confined to the south west of the region in the vicinity of the CLLJ.

The intraseasonal variability of precipitation in the Caribbean region has been linked to the phase of the Madden-Julian Oscillation. Large positive and negative precipitation anomalies (up to 50 % of the annual mean) were observed in all phases of the MJO based on the index of Wheeler and Hendon (2004). The largest changes and most coherent patterns were observed in phases 1 and 2, when Caribbean precipitation is generally above average, and in phases 5 and 6, when it is below average across much of the region. The intraseasonal variance is maximized during SON across the entire domain, with a secondary smaller peak in variance during the early summer. Precipitation anomalies composited by phase of the MJO are largest in SON (with a similar pattern to the annual composite) when the intraseasonal vari-

ance is maximised. It is speculated that the strength of the MJO during SON in the Caribbean may be a combination of the maximum MJO signal in the East Pacific and Mexico/Central America during Northern Hemisphere summer (Maloney and Hartmann, 2000a; Maloney and Esbensen, 2003; Barlow and Salstein, 2006), as well as the bimodal cycle of precipitation in the Caribbean. As seen in Fig. 37, intraseasonal variance increases in the region during May but does not continue to increase in June and July when the region is subject to Mid-Summer drought conditions. The variance increases again as the climatological rainfall increases, suggesting that the MJO activity favors regions and time periods when climatological rainfall is large. However, precipitation anomalies with phase of the MJO are seen across all seasons, despite the smaller intraseasonal variance.

Investigation into the mechanism behind the precipitation changes using wind data from ERA-Interim reanalysis showed large changes in wind speed and direction at low-levels (925 hPa). When precipitation anomalies were above (below) average in phases 1 and 2 (phases 5 and 6) wind anomalies acted to decrease (increase) the strength of the prevailing easterly trade winds, especially in the southern part of the Caribbean. The maximum wind speed changes (approximately 3 m s^{-1}) are observed in the region of the CLLJ, with the CLLJ being slowed in phases 1 and 2 and increased in phases 5 and 6. These changes in the CLLJ speed influence low-level divergence anomalies, which appear to lead to the observed changes in precipitation with phase of the MJO.

The relationship between the CLLJ and the MJO was explicitly investigated using a jet index to measure the strength of the jet. It was found that the CLLJ varies significantly between phases of the MJO, with the strong CLLJ in phases 5 and 6 being significantly different from the weak CLLJ in phases 1 and 2 at the 99.9 % confidence level. The differences in the CLLJ are observed across all seasons,

including those when the CLLJ is weaker on average. This intraseasonal variability of the CLLJ has not previously been documented. The coherence between the CLLJ index and the precipitation at intraseasonal timescales has also been shown to be significant.

Another interesting feature of the relationship between the MJO and Caribbean precipitation is the modulation of extreme rainfall events by the MJO. High rain rates were more frequently observed during phases 1 and 2 of the MJO, especially compared with phases 5 and 6. Locations over land were specifically chosen to investigate extreme events due to the socio-economic impact of extreme rainfall events over islands. Of the wettest rainfall days at each land station, approximately 30 % were shown to occur in phases 1 and 2 of a strong MJO event, and not all were associated with tropical storms. The number of extreme wet events due to tropical storms followed the same distribution, with the most occurring in phases 1 and 2. This preference for extreme precipitation events to occur in phases 1 and 2 of the MJO may have important implications for predictability of extreme events, as the MJO is predictable out to approximately 2 weeks. Caution must be applied to interpreting the extreme rain results, as the observational data used is at daily, 1 degree resolution and some of the most extreme events may occur at a smaller scale than this.

CHAPTER V

CONCLUSIONS

This research aimed to develop and extend current understanding of the precipitation climatology, extremes and variability in the Caribbean in both observations and the representation of such features in the IPCC AR4 models (both coupled and uncoupled). In the annual area-averaged mean, the CMIP models underestimated precipitation in the region and AMIP models overestimated precipitation, a result discussed in Christensen et al. (2007) and Biasutti et al. (2006). This dissertation investigates the reasons behind these errors in the models in different ways, beginning with the role of SST. The CMIP model ensemble severely underestimates SST (only five models have annual mean SST within 1°C of observations) in the Caribbean region throughout the year. While the spatial pattern and evolution of SST is reasonably well simulated in the models, a major stumbling block in the coupled simulations appears to be the magnitude of SSTs.

Not only do local SSTs play an important role in Caribbean precipitation, but global SSTs also influence the Caribbean due to connections with ENSO, the NAO and the AMM. The simulation of these remote connections was poor in both the CMIP and AMIP models, although the AMIP models outperform the CMIP ensemble. The results of the AMIP ensemble that are forced with observed SSTs shows that either there is an inherent error in the atmospheric component of the model that leads to incorrect remote heating and circulation changes that consequently affect Caribbean precipitation, or air-sea feedbacks are necessary for the processes to correctly occur. Further analysis of heating profiles in the models, both remote and local would be necessary to determine the model deficiencies. Idealized simulations by adding heating to certain regions and investigating the impact on the Caribbean could also help to

identify model problems.

A regime sorting analysis was used to identify Caribbean precipitation, sea surface temperature and large-scale vertical circulation relationships and biases within the CMIP and AMIP ensembles. This allowed the over and under estimates by the AMIP and CMIP models respectively to be studied in more detail. This analysis showed that an oversensitivity of precipitation to both SST and vertical circulation (as represented by ω_{500}) is inherent in the atmospheric models, with models using a spectral type convective parameterization performing best. This error in magnitude of precipitation for a given SST and vertical circulation causes uncoupled AMIP models to overestimate Caribbean mean precipitation, particularly at SSTs greater than 28°C and ω_{500} less than -10 hPa/day. In coupled models, however, errors in the frequency of occurrence of SSTs (the distribution is cold biased) and deep convective vertical circulations (reduced frequency) lead to an underestimation of Caribbean mean precipitation. These results were observed throughout all seasons, suggesting that it is not only the simulation (or non simulation) of tropical storms that is generating these errors.

Evidence from daily precipitation data confirmed the lack of wet extremes in the regime sorting analysis. The models produced significantly more dry extremes and fewer wet extremes than the observed climate, again this was apparent throughout the annual cycle. This analysis shows that the models are raining too frequently and too lightly in the Caribbean, similar to the results of Dai (2006) but the distribution is more heavily skewed in the Caribbean.

The annual cycle of precipitation from the IPCC AR4 CMIP and AMIP models showed a distinct lack of ability in simulating the MSD. It was hypothesized that this may be in part due to the simulation of the CLLJ. However, a census of 19 coupled and 12 uncoupled model runs from the IPCC AR4, showed that all models

have the ability to simulate the general characteristics of the CLLJ in the Southern Caribbean. Despite simulating the CLLJ, the observed semi-annual cycle of the CLLJ magnitude was a challenge for the models to reproduce. In particular, model means failed to capture the strong July CLLJ peak due to the lack of westward and southward expansion of the North Atlantic Subtropical High (NASH) between May and July. The NASH was also found to be too strong, particularly during the first six months of the year in the coupled model runs, which led to increased meridional sea level pressure gradients across the southern Caribbean and hence an overly strong CLLJ. The incorrect simulation of the evolution of the NASH may in part be due to poor simulation of tropical precipitation across the tropical Atlantic region.

The ability of the models to simulate the correlation between the CLLJ and regional precipitation varied based on season and region. During summer months, the negative correlation between the CLLJ and Caribbean precipitation anomalies was reproduced in the majority of models, with uncoupled models outperforming coupled models. The positive correlation between the CLLJ and central United States precipitation during February was more challenging for the models, with the uncoupled models failing to reproduce a significant relationship. This may be a result of overactive convective parameterizations raining out too much moisture in the Caribbean meaning less is available for transport northwards, or due to incorrect moisture fluxes over the Gulf of Mexico. The representation of the CLLJ in general circulation models has important consequences for accurate predictions and projections of future tropical cyclone activity in the region.

Further investigations into the ability of the simulated CLLJ in the CMIP and AMIP models to transport the correct amount of moisture should shed light on its relationship with both local and particularly US precipitation. Moisture budgets for the CLLJ in both models and observations would be needed to investigate how

much moisture was being transported to the US and whether moisture exchange in the Gulf of Mexico was playing a role. Further investigation of the CLLJ and precipitation in the Caribbean can also be carried out on the next generation of IPCC models (CMIP5) that will be the basis of the next IPCC report. It will be important to determine the advances in the simulation ability of the models and important not to degrade features that are currently well simulated. Importantly, advances in convective parameterizations are necessary to eliminate major biases in the atmospheric models.

An observational study of Caribbean precipitation variability using 12 years of daily satellite precipitation data and reanalysis winds showed intraseasonal (30-90 day) variability in Caribbean precipitation is linked to phases of the MJO. Intraseasonal variability is largest during SON, but some modulation of precipitation by the MJO appears throughout all seasons. Precipitation anomalies up to 50 % above (below) the annual mean are observed in phases 1 and 2 (5 and 6) of the MJO.

The changes in Caribbean precipitation associated with the MJO are shown to be related to changes in the low-level (925 hPa) winds. When precipitation anomalies are above (below) average in phases 1 and 2 (5 and 6) wind anomalies act to decrease (increase) the strength of the prevailing easterly trade winds. The changes in the low-level winds are most apparent in the region of the CLLJ and divergence anomalies associated with the entrance and exit region of the CLLJ precede the precipitation anomalies. The CLLJ itself is also shown to be subject to intraseasonal variability, and its magnitude varies with phase of the MJO. Again, intraseasonal variability in the CLLJ associated with the MJO is observed in all seasons and shows a significant coherence with intraseasonal variability in the precipitation. Extreme rainfall events over islands in the Caribbean show a strong relationship with MJO phase, with extreme events being most common in phases 1 and 2 of an MJO event.

This relationship between the MJO and extreme events has important implications for predictability of precipitation extremes in the Caribbean.

Due to the inability of the CMIP and AMIP ensemble to simulate an MJO (Lin et al., 2006b), the intraseasonal variability of Caribbean rainfall in the IPCC models was not thoroughly investigated. Wavelet analysis of the model precipitation suggests a major lack of variability across all scales including the intraseasonal range. The next generation of IPCC models may produce a better MJO, allowing the connection with the CLLJ and Caribbean rainfall to be investigated. Regional or idealized simulations with a realistic MJO may also provide useful for investigation the influence of the MJO on the Caribbean.

Initial investigations into the ability of regional models to correctly simulate Caribbean precipitation and the CLLJ show varied results (Appendix C). Data from a regional coupled simulation of the Atlantic, using WRF and ROMS and forced with climatological conditions for May and run through October, was analyzed. Precipitation across the Atlantic domain and precipitation and SST in the Caribbean was overestimated, with errors apparently growing with time. The atmospheric model precipitation was strongly oversensitive to SST, greater than even the IPCC AR4 models. The CLLJ while simulated correctly during the first two months, rapidly weakened and eventually reversed and generated a strong westerly jet in the Eastern Pacific. The weakening and reversal of the CLLJ was primarily due to a low pressure developing in the Gulf of Mexico and reversing the SLP gradients, which may be a response to the over active convection. Further regional modeling studies, with different configurations of parameterizations may help to identify potential model errors and mechanisms that are not being simulated correctly.

Precipitation in the Caribbean is complex both in space and time and IPCC AR4 models have numerous successes and failures in its simulation. The analysis

of these similarities and differences between observations and model output shed light on mechanisms and processes that need improvement. Naturally, the relatively low horizontal resolution of the models prevented them from simulating small scale features such as the enhancement of rainfall over the Antilles, but this was found to be only a part of the problems with the model simulations.

REFERENCES

AchutaRao, K. and K. Sperber, 2002: Simulation of the El Niño southern oscillation: Results from the coupled model intercomparison project. *Clim. Dyn.*, **19**, 191–209, doi:10.1007/s00 382–001–0221–9.

Amador, J., 1998: A climatic feature of the tropical Americas: The trade wind easterly jet. *Top. Meteor. Oceanogr.*, **5**, 91–102.

_____, 2008: The Intra-Americas sea low level jet: Overview and future research. *Ann. N.Y. Acad. Sci.*, **1146**, 153–188.

_____, V. Magaña, and J. Pérez, 1999: Dynamics of the low-level jet over the Caribbean sea. Preprints, *23rd Conf. on Hurricanes and Tropical Meteorology, Dallas, TX*, Amer. Meteor. Soc., 868–869.

_____, _____, and _____, 2000: The low level jet and convective activity in the Caribbean. Preprints, *24th Conf. on Hurricanes and Tropical Meteorology, Fort Lauderdale, FL*, Amer. Meteor. Soc., 114–115.

_____, E. Alfaro, O. Lizano, and V. Magaña, 2006: Atmospheric forcing of the eastern tropical Pacific: A review. *Prog. Oceanogr.*, **69**, 101–142.

_____, _____, E. Rivera, and B. Calderón, 2010: Climatic features and their relationship with tropical cyclones over the Intra-Americas seas. *Hurricanes and climate change*, J. Elsner, R. Hodges, J. Malmstadt, and K. Scheitlin, Eds., Spring Dordrecht, Heidelberg, 149-173.

Amos, D. and L. Koopmans, 1963: Tables of the distributions of the coefficient of

coherence for stationary bivariate gaussian processes. Sandia Corporation Monogr., SCR-483.

Arawaka, A. and W. Schubert, 1974: Interaction of a cumulus cloud ensemble with the large-scale environment, part I. *J. Atmos. Sci.*, **31**, 674–701.

Bantzer, C. and J. Wallace, 1996: Intraseasonal variability in tropical mean temperature and precipitation and their relation to the tropical 40-50 day oscillation. *J. Atmos. Sci.*, **53**, 3032–3045.

Barlow, M. and D. Salstein, 2006: Summertime influence of the Madden-Julian oscillation on daily rainfall over Mexico and Central America. *Geophys. Res. Lett.*, **33**, L21708, doi:10.1029/2006GL027 738.

Bellucci, A., S. Gualdi, and A. Navarra, 2010: The double ITCZ syndrome in coupled general circulation models: The role of large-scale vertical circulation regimes. *J. Climate*, **23**, 1127–1145.

Berbery, E. and E. Collini, 2000: Springtime precipitation and water vapor flux over over southeastern South America. *Mon. Wea. Rev.*, **128**, 1328–1346.

Berg, W., C. Kummerow, and C. Morales, 2002: Differences between East and West Pacific rainfall systems. *J. Climate*, **15**, 3659–3672.

Betts, A., 1986: A new convective adjustment scheme. part I: Observational and theoretical basis. *Quart. J. Roy. Meteor. Soc.*, **112**, 677–691.

Biasutti, M., A. Sobel, and Y. Kushir, 2006: AGCM precipitation biases in the tropical Atlantic. *J. Climate*, **19**, 935–958.

Bonner, W., 1968: Climatology of the low level jet. *Mon. Wea. Rev.*, **96**, 833–850.

Bony, S., J. Dufresne, H. L. Treut, J. Morcrette, and C. Senior, 2004: On dynamic and thermodynamic components of cloud changes. *Climate Dyn.*, **22**, 71–86.

Bougeault, P., 1985: A simple parameterization of the large-scale effects of cumulus convection. *Mon. Wea. Rev.*, **113**, 2108–2121.

Cai, W., A. Sullivan, and T. Cowan, 2009: Rainfall teleconnections with Indo-Pacific variability in the WCRP CMIP3 models. *J. Climate*, **22**, 5046–5071.

Chen, A. and M. Taylor, 2002: Investigating the link between early season Caribbean rainfall and the El Niño + 1 year. *Int. J. Climatol.*, **22**, 87–106.

Christensen, J., B. Hewitson, A. Busuioc, A. Chen, X. Gao et al., 2007: Regional Climate Projections. *Climate Change 2007: The Physical Science Basis. Contribution of Working Group I to the Fourth Assessment Report of the Intergovernmental Panel on Climate Change*, S. Solomon, D. Qin, M. Manning, Z. Chen, M. Marquis, K.B. Averyt, M. Tignor and H.L. Miller eds., Cambridge University Press, Cambridge, UK.

Cook, K. and E. Vizy, 2010: Hydrodynamics of the Caribbean low-level jet and its relationship to precipitation. *J. Climate*, **23**, 1477–1494.

_____, _____, Z. S. Launer, and C. Patricola, 2008: Springtime intensification of the Great Plains low-level jet and Midwest precipitation in GCM simulations of the twenty-first century. *J. Climate*, **21**, 6321–6340.

Dai, A., 2006: Precipitation characteristics in eighteen coupled climate models. *J. Climate*, **19**, 4605–4630.

Deng, Y., K. Bowman, and C. Jackson, 2007: Differences in rain rate intensities be-

tween trmm observations and community atmosphere model simulations. *Geophys. Res. Lett.*, **34**, L01808, doi:10.1029/2006GRL027 246.

Durán-Quesada, A., L. Gimeno, J. Amador, and R. Nieto, 2010: Moisture sources for Central America: Indentification of moisture sources using a lagrangian analysis technique. *Geophys. Res. Lett.*, **115**, D05103, doi:10.1029/2009JD012 455.

Emmanuel, K., 1991: A scheme for representing cumulus convection in large-scale models. *J. Atmos. Sci.*, **48**, 2313–2329.

Frich, P., L. Alexander, P. Della-Martin, B. Gleason, M. Haylock, A. Klein-Tank, and T. Peterson, 2002: Global changes in climatic extremes during the 2nd half of the 20th century. *Clim. Res.*, **19**, 193–212.

Gamble, D., D. Parnell, and S. Curtis, 2008: Spatial variability of the Caribbean mid-summer drought and relation to North Atlantic high circulation. *Int. J. Climatol.*, **28**, 343–350.

Genio, A. D. and M.-S. Yao, 1993: Efficient cumulus parameterization for long-term climate studies: The GISS scheme. *The representation of cumulus convection in numerical models*, Amer. Meteor. Soc., No. 46 in Meteor. Monogr., 181–184.

Giannini, A., M. Cane, and Y. Kushnir, 2001: Interdecadal changes in the ENSO teleconnection to the Caribbean region and the North Atlantic oscillation. *J. Climate*, **14**, 2867–2879.

_____, Y. Kushnir, and M. Cane, 2000: Interannual variability of Caribbean rainfall, ENSO, and the Atlantic ocean. *J. Climate*, **13**, 297–311.

Gill, A., 1980: Some simple solutions for heat-induced tropical circulation. *Q. J. Roy. Meteor. Soc.*, **106**, 447–462.

Gregory, D. and P. Rowntree, 1990: A mass flux convection scheme with representation of cloud ensemble characteristics and stability dependent closure. *Mon. Wea. Rev.*, **118**, 1483–1506.

Huffman, G., R. Adler, M. Morrissey, D. Bolvin, S. Curtis, R. Joyce, B. McGavock, and J. Susskind, 2001: Global precipitation at one-degree daily resolution from multisatellite observation. *J. Hydrometeorol.*, **2**, 36–50.

Jury, M., 2008: Climate influences on dengue epidemics in Puerto Rico. *Int. J. Environ. Heal. R.*, **18**, 323–334.

_____, 2009a: An intercomparison of observational, reanalysis, satellite, and coupled model data on mean rainfall in the Caribbean. *J. Hydrometeorol.*, **10**, 413–430.

_____, 2009b: A quasi-decadal cycle in Caribbean climate. *J. Geophs. Res.*, **114**, D13102, doi:10.1029/2009JD011 741.

_____, B. Malmgren, and A. Winter, 2007: Subregional precipitation climate of the Caribbean and relationships with ENSO and NAO. *J. Geophys. Res.*, **112**, D16107, doi:10.1029/2006JD007 541.

Kanamitsu, M., W. Ebisuzaki, J. Woollen, S.-K. Yang, J. Hnilo, M. Fiorino, and G. L. Potter, 2002: NCEP-DOE AMIP-II reanalysis (R-2). *Bull. Amer. Meteor. Soc.*, **83**, 1631–1643.

Kikuchi, Y. and Y. Takayabu, 2003: Equatorial circumnavigation of moisture signal associated with the Madden-Julian oscillation (MJO) during boreal winter. *J. Meteor. Soc. Japan*, **81**, 851–869.

Klotzbach, P., 2010: On the Madden-Julian oscillation-Atlantic hurricane relationship. *J. Climate*, **23**, 282–293.

Lin, B., B. Wielicki, P. Minnis, L. Chambers, K.-M. Xu, Y. Hu, and A. Fan, 2006a: The effect of environmental conditions on tropical deep convective systems observed from the TRMM satellite. *J. Climate*, **19**, 5745–5761.

Lin, J.-L., 2007: The double-ITCZ problem in IPCC AR4 coupled GCMs: Ocean-atmosphere feedback analysis. *J. Climate*, **20**, 4497–4525.

_____, G. Kiladis, B. Mapes, K. Weickmann, K. Sperber et al., 2006b: Tropical intraseasonal variability in 14 IPCC AR4 climate models. Part I: Convective signals. *J. Climate*, **19**, 2665–2690.

Madden, R. and P. Julian, 1971: Detection of a 40-50 day oscillation in zonal wind in the tropical Pacific. *J. Atmos. Sci*, **28**, 702–708.

Magaña, V. and E. Caetano, 2005: Temporal evolution of summer convective activity over the Americas warm pools. *Geophys. Res. Lett.*, **32**, L02803, doi:10.1029/2004GL021 033.

_____, J. Amador, and S. Medina, 1999: The midsummer drought over Mexico and Central America. *J. Climate*, **12**, 1577–1588.

Maloney, E. and S. Esbensen, 2003: The amplification of East Pacific Madden-Julian oscillation convection and wind anomalies during June-November. *J. Climate*, **16**, 3482–3497.

_____, and D. Hartmann, 2000a: Modulation of eastern North Pacific hurricanes by the Madden-Julian oscillation. *J. Climate*, **13**, 1451–1460.

_____and _____, 2000b: Modulation of hurricane activity in the Gulf of Mexico by the Madden-Julian oscillation. *Science*, **287**, 2002–2004.

Mapes, B., P. Liu, and N. Buenning, 2005: Indian monsoon onset and Americas midsummer drought: Out-of-equilibrium responses to smooth seasonal forcing. *J. Climate*, **18**, 1109–1115.

Marshall, J., Y. Kushnir, D. Battisi, P. Chang, A. Czaja et al., 2001: North Atlantic climate variability: Phenomena, impacts and mechanisms. *Int. J. Climatol.*, **21**, 1863–1898.

Martin, E. and C. Schumacher, 2011a: The Caribbean low-level jet and its relationship with precipitation in the IPCC AR4 models. *J. Climate*, doi:10.1175/JCLID1100 134.1. In Press.

_____and _____, 2011b: Modulation of Caribbean precipitation by the Madden-Julian oscillation. *J. Climate*, **24**, 813–824.

_____and _____, 2011c: The relationship between warm pool precipitation, sea surface temperature, and large-scale vertical motion in IPCC AR4 models. *J. Atmos. Sci.*, Conditionally Accepted.

Matthews, A., 2000: Propagation mechanisms for the Madden-Julian oscillation. *Quart. J. Roy. Meteor. Soc.*, **126**, 2637–2652.

Mestas-Nuñez, A., D. Enfield, and C. Zhang, 2007: Water vapor fluxes over the Intras-Americas Sea: Seasonal and interannual variability and associations with rainfall. *J. Climate.*, **20**, 1910–1922.

Misra, V., S. Chan, R. Wu, and E. Chassignet, 2009: Air-sea interaction over the Atlantic warm pool in the NCEP CFS. *Geophys. Res. Lett.*, **36**, L15702, doi:10.1029/2009GL038 737.

Mo, K., M. Chelliah, M. Carrera, R. Higgins, and W. Ebisuzaki, 2005: Atmospheric moisture transport over the United States and Mexico as evaluated in the NCEP regional reanalysis. *J. Hydrometeorol.*, **6**, 710–728.

Moorthi, S. and M. Suarez, 1992: Relaxed Arakawa-Schubert. A parameterization of moist convection for general circulation models. *Mon. Wea. Rev.*, **120**, 978–1002.

Muñoz, E., A. Busalacchi, S. Nigam, and A. Ruiz-Barradas, 2008: Winter and summer structure of the Caribbean low-level jet. *J. Climate*, **21**, 1260–1276.

Neelin, J., M. Munnich, H. Su, J. Meyerson, and C. Holloway, 2006: Tropical drying trends in global warming models and observations. *Proc. Nat. Acad. Sci.*, **103**, 6110–6115.

Nordeng, T., 1994: Extended versions of the convective parameterization scheme at ECMWF and their impact on the mean and transient activity of the model in the tropics. ECMWF Tech. Memo 206, Reading, United Kingdom, 41 pp.

Pan, D.-M. and D. Randall, 1998: A cumulus parameterization with a prognostic closure. *Quart. J. Roy. Meteor. Soc.*, **124**, 949–981.

Peterson, T., M. Taylor, R. Demeritte, D. Dunacombe, S. Burton et al., 2002: Recent changes in climate extremes in the Caribbean region. *J. Geophys. Res*, **107**, D21, 4601, doi:10.1029/2002JD002 251.

Poveda, G. and O. Mesa, 2000: On the existence of Lloró (the rainiest locality on Earth): Enhanced ocean-land-atmosphere interaction by a low-level jet. *Geophys. Res. Lett.*, **27**, 1675–1678.

Rauscher, S., F. Kucharski, and D. Enfield, 2011: The role of regional SST warming

variations in the drying of Meso-America in future climate projections. *J. Climate*, **24**, 2003–2016.

Rayner, N., D. Parker, E. Horton, C. Folland, L. Alexander, D. Powell, E. Kent, and A. Kaplan, 2003: Global analyses of sea surface temperature, sea ice, and night marine air temperature since the late nineteenth century. *J. Geophs. Res.*, **108**, D14, 4407, doi:10.1029/2002JD002 670.

Richter, I. and S.-P. Xie, 2008: On the origin of equatorial Atlantic biases in coupled general circulation models. *Clim. Dyn.*, **31**, 587–598.

Russell, G., J. Miller, and D. Rind, 1995: A coupled atmosphere-ocean model for transient climate change studies. *Atmos.-Ocean*, **33**, 683–730.

Salby, M. and H. Hendon, 1994: Intraseasonal behavior of clouds, temperature and motion in the tropics. *J. Atmos. Sci.*, **51**, 2207–2224.

Serra, Y., G. Kiladis, and K. Hodges, 2010: Tracking and mean structure of easterly waves over the Intra-Americas Sea. *J. Climate*, **23**, 4823–4840.

Servain, J., 1991: Simple climatic indices for the tropical Atlantic ocean and some applications. *J. Geophys. Res.*, **96**, 15 137–15 146.

Simmons, A., S. Uppala, D. Dee, and S. Kobayashi, 2007: ERA-Interim: New ECMWF reanalysis products from 1989 onwards. *ECMWF Newsletter*, **110**, 25–35.

Sobel, A., C. Burleyson, and S. Yuter, 2011: Rain on small tropical islands. *J. Geophys. Res.*, **116**, D08102, doi:10.1029/2010JD014 695.

Sperber, K., 2003: Propagation and the vertical structure of the Madden-Julian oscillation. *Mon. Wea. Rev.*, **131**, 3018–3037.

Taylor, M., D. Enfield, and A. Chen, 2002: Influence of the tropical Atlantic versus the tropical Pacific on Caribbean rainfall. *J. Geophys. Res.-Oceans*, **107**, C9, 3127, doi:10.1029/2001JC001 097.

Tiedtke, M., 1989: A comprehensive mass flux scheme for cumulus parameterization in large-scale models. *Mon. Wea. Rev.*, **117**, 1779–1800.

Ting, M. and H. Wang, 2006: The role of the North American topography on the maintenance of the Great Plains summer low-level jet. *J. Atmos. Sci.*, **63**, 1056–1068.

Torrence, C. and G. Compo, 1998: A practical guide to wavelet analysis. *Bull. Am. Meteor. Soc.*, **79**, 61–78.

Turner, A. and J. Slingo, 2009: Uncertainties in future projections of extreme precipitation in the Indian monsoon region. *Atmos. Sci. Let.*, **10**, 152–158.

Vimont, D. and J. Kossin, 2007: The Atlantic meridional mode and hurricane activity. *Geophys. Res. Lett.*, **34**, L07 709, doi:10.1029/2007GL029 683.

Virji, H., 1981: A preliminary study of summertime tropospheric circulation patterns over South America from cloud winds. *Mon. Wea. Rev.*, **109**, 599–610.

Waliser, D., 1993: Comparison of the highly relective cloud and outgoing longwave radiation datasets for use in estimating tropical deep convection. *J. Climate*, **6**, 331–353.

Wang, C., 2007: Variability of the Caribbean low-level jet and its relations to climate. *Clim. Dyn.*, **29**, 411–422.

_____and D. Enfield, 2001: The tropical western hemisphere warm pool. *Geophys. Res. Lett.*, **28**, 1635–1638.

_____and S.-K. Lee, 2007: Atlantic warm pool, Caribbean low-level jet, and their potential impact on Atlantic hurricanes. *Geophys. Res. Lett.*, **34**, L02703, doi:10.1029/2006GL028 579.

_____, _____, and D. Enfield, 2008: Climate response to anomalously large and small Atlantic warm pools during the summer. *J. Climate.*, **21**, 2437–2450.

Wheeler, M. and H. Hendon, 2004: An all-season real-time multivariate MJO index: Development of an index for monitoring and prediction. *Mon. Wea. Rev.*, **132**, 1917–1932.

Whyte, F., M. Taylor, T. Stephenson, and J. Campbell, 2008: Features of the Caribbean low level jet. *Int. J. Climatol.*, **28**, 119–128.

Wilcox, E. and L. Donner, 2007: The frequency of extreme rain events in satellite rain-rate estimates and an atmospheric general circulation model. *J. Climate*, **20**, 53–69.

Zhang, C., 1993: Large-scale variability of atmopsheric deep convection in relation to sea surface temperature in the tropics. *J. Climate*, **6**, 1898–1913.

Zhang, G. and N. McFarlane, 1995: Sensitivity of climate simulations to the parameterization of cumulus convection in the Canadian Climate Centre general circulation model. *Atmos.-Ocean*, **33**, 407–446.

APPENDIX A

Table 1. List of IPCC AR4 models used in this study. Flux correction indicates those models using heat (H), water (W) or no (N) flux correction. AMIP indicates whether monthly AMIP data was available. Further model details, including references, can be found at the PCMDI website http://www-pcmdi.llnl.gov .

Center, Country	**Identification Name**	**Horizontal Resolution (lat,lon)**	**Z**	**Flux Correction**	**AMIP**
BCCR, Norway	BCCR	T63 (∼2.8°)	31	N	
CCCma, Canada	CCCMA	T32 (∼3.75°)	31	HW	
CCCma, Canada	CCCMA-T63	T63 (∼2.8°)	31	HW	
CNRM, France	CNRM	T63 (∼2.8°)	45	N	Y
CSIRO, Australia	CSIRO3.0	T63 (∼2.8°)	18	N	
CSIRO, Australia	CSIRO3.5	T63 (∼2.8°)	18	N	
GFDL, USA	GFDL2.0	2° x 2.5°	24	N	
GFDL, USA	GFDL2.1	2° x 2.5°	24	N	Y
GISS, USA,	GISS-AOM	4° x 3°	12	N	
GISS, USA,	GISS-EH	4° x 5°	20	N	
GISS, USA,	GISS-ER	4° x 5°	20	N	Y
IAP, China	IAP	2.8° x 2.8°	26	N	Y
INGV/MPI, Italy/Germany	INGV	T106 (∼1.125°)	19	N	

Table 1 – continued

Center, Country	**Identification Name**	**Horizontal Resolution (lat,lon)**	**Z**	**Flux Correction**	**AMIP**
INM, Russia	INMCM	4° x 5°	21	W	Y
IPSL, France	IPSL	2.5° x 3.75°	19	N	Y
CCSR, Japan	MIROC-HI	T106 (∼1.125°)	56	N	Y
CCSR, Japan	MIROC-MED	T42 (∼2.8°)	20	N	Y
MIUB, Germany/Korea	MIUB	T30 (∼3.75°)	19	HW	
MPI, Germany	MPI	T63 (∼2.8°)	31	N	Y
MRI, Japan	MRI	T42 (∼2.8°)	30	HW	Y
NCAR, USA	NCAR-CCSM	T85 (∼1.4°)	26	N	Y
NCAR, USA	NCAR-PCM	T42 (∼2.8°)	26	N	Y
UKMO, UK	UKMO-HADCM	3.75° x 2.5°	19	N	
UKMO, UK	UKMO-HADGEM	1.875° x 1.25°	38	N	Y

Table 2. List of deep convective parameterizations, groups and closure and trigger mechanisms for IPCC AR4 models. ZM denotes the Zhang and McFarlane (1995) parameterization and group. CBB denotes cloud-based buoyancy closure scheme and RH relative humidity.

Model	**Convective Parameterization**	**Group**	**Closure/Trigger**
BCCR	Bougeault (1985)	Bulk	Kuo
CCCMA	Zhang and McFarlane (1995)	ZM	CAPE
CCCMA-T63	Zhang and McFarlane (1995)	ZM	CAPE
CNRM	Bougeault (1985)	Bulk	Kuo
CSIRO3.0	Gregory and Rowntree (1990)	Bulk	CBB
CSIRO3.5	Gregory and Rowntree (1990)	Bulk	CBB
GFDL2.0	Moorthi and Suarez (1992)	Spectral	CAPE/Threshold
GFDL2.1	Moorthi and Suarez (1992)	Spectral	CAPE/Threshold
GISS-AOM	Russell et al. (1995)	Other	CAPE
GISS-EH	Genio and Yao (1993)	Bulk	CBB
GISS-ER	Genio and Yao (1993)	Bulk	CBB
IAP	Zhang and McFarlane (1995)	ZM	CAPE
INGV	Tiedtke (1989); Nordeng (1994)	Bulk	CAPE
INMCM	Betts (1986)	Other	CAPE
IPSL	Emmanuel (1991)	Other	CAPE

Table 2 – continued

Model	**Convective Parameterization**	**Group**	**Closure/Trigger**
MIROC-HI	Pan and Randall (1998)	Spectral	CAPE/RH
MIROC-MED	Pan and Randall (1998)	Spectral	CAPE/RH
MIUB	Tiedtke (1989); Nordeng (1994)	Bulk	CAPE/Moisture convergence
MPI	Tiedtke (1989); Nordeng (1994)	Bulk	CAPE/Moisture convergence
MRI	Pan and Randall (1998)	Spectral	CAPE
NCAR-CCSM	Zhang and McFarlane (1995)	ZM	CAPE
NCAR-PCM	Zhang and McFarlane (1995)	ZM	CAPE
UKMO-HADCM	Gregory and Rowntree (1990)	Bulk	CBB
UKMO-HADGEM	Gregory and Rowntree (1990)	Bulk	CBB

Table 3. Regression coefficients (mm day^{-1} per ms^{-1}) between the annual CLLJ index and the Caribbean area-averaged precipitation anomaly. Bold (italic) values are significant at the 95 % (99 %) significance level.

Name	**CMIP**	**AMIP**
Observations	**-2.57**	**-2.57**
cccma	0.43	
cccma-t63	-0.04	
cnrm	0.2	**-2.57**
csiro3.0	-1.38	
csiro3.5	***-3.29***	
gfdl2.0	0.47	
gfdl2.1	-0.52	**-2.21**
iap	-1.79	***-3.03***
ingv	***-4.04***	
inmcm	***-3.21***	-1.9
ipsl	-1.75	**-2.50**
miroc-hi	-2.00	-1.74
miroc-med	-0.45	**-2.17**
mpi	***-4.32***	***-3.02***
mri	***-3.13***	**-2.61**
ncar-ccsm	-0.07	***-2.90***
ncar-pcm	**-2.44**	***-4.81***
ukmo-hadcm	-0.49	
ukmo-hadgem	-0.42	***-3.13***

Table 4. Regression coefficients between the CLLJ index and the GPLLJ index for observations by month. Values in bold are significant at the 95 % significance level and values in bold and italic are significant at the 99 % significance level.

Month	
Jan	***2.82***
Feb	**2.67**
Mar	***3.58***
Apr	***3.31***
May	1.98
Jun	**2.17**
Jul	**2.59**
Aug	1.66
Sep	***4.18***
Oct	1.42
Nov	-1.02
Dec	1.02

Table 5. Mean and standard deviation (in parentheses) of the CLLJ index composited by phases and season.

Season	**Phases 1+2**	**Phases 3+4**	**Phases 5+6**	**Phases 7+8**
Annual	-1.50 (3.12)	0.73 (3.09)	1.46 (2.80)	-0.46 (3.31)
DJF	-1.73 (3.67)	0.63 (3.01)	1.36 (2.99)	-0.90 (2.88)
MAM	-1.31 (2.63)	0.97 (3.09)	1.45 (3.06)	-1.15 (3.77)
JJA	-1.52 (2.54)	0.92 (1.83)	1.62 (1.98)	0.76 (2.22)
SON	-1.47 (3.91)	0.54 (3.65)	1.49 (2.77)	-0.27 (3.95)

APPENDIX B

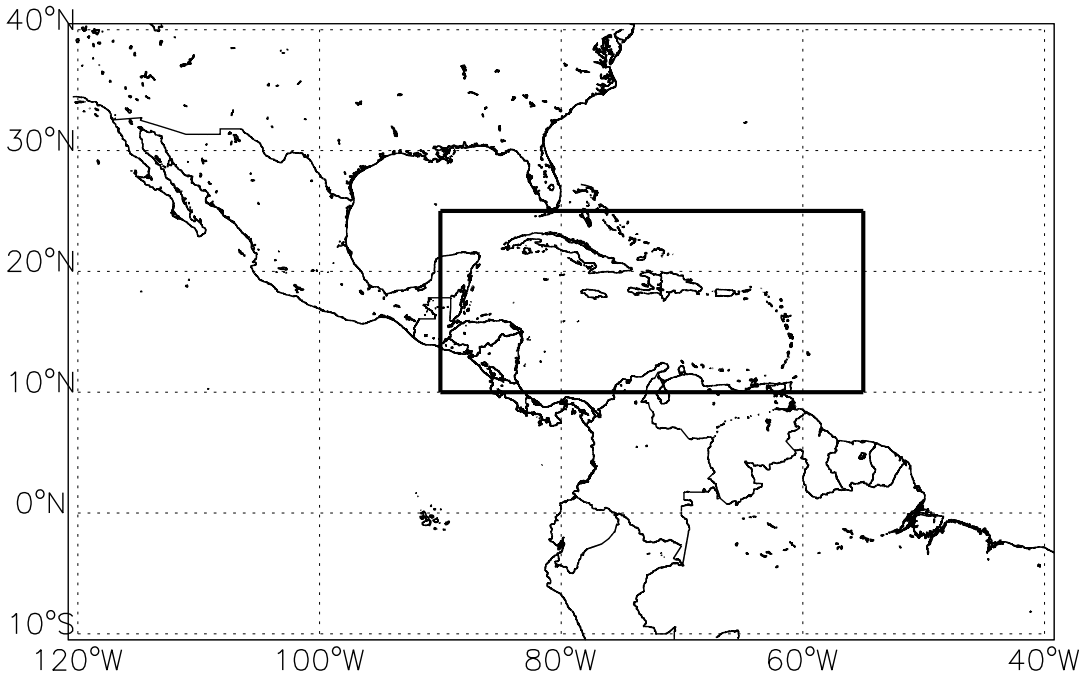

Fig. 1. Regional map of Caribbean and surrounding. Black box indicates region for Caribbean area-averaging.

Fig. 2. Annual mean SST (from HadISST), beginning at 26.5°C with intervals of 1°C. Black boxes indicate averaging regions for the West Pacific and Caribbean.

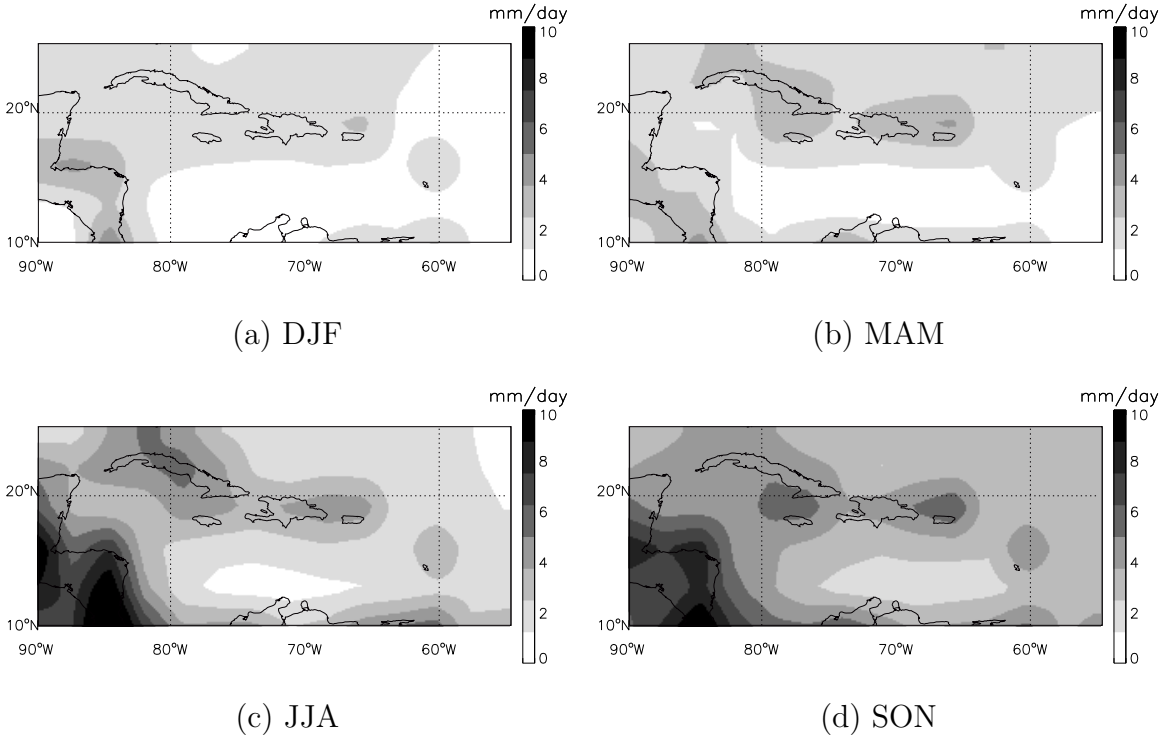

(a) DJF (b) MAM

(c) JJA (d) SON

Fig. 3. Seasonal mean GPCP monthly (1979-2008) precipitation rates for the Caribbean region.

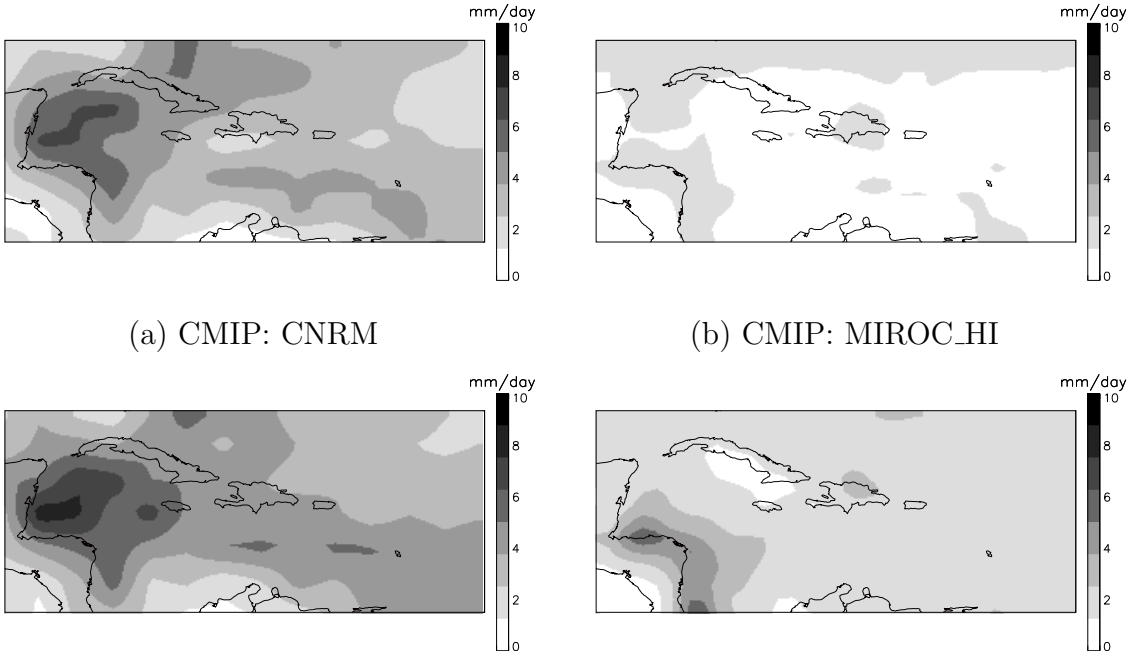

(a) CMIP: CNRM (b) CMIP: MIROC_HI

(c) AMIP: CNRM (d) AMIP: MIROC_HI

Fig. 4. Seasonal DJF mean monthly precipitation rates for the Caribbean region for four different simulations.

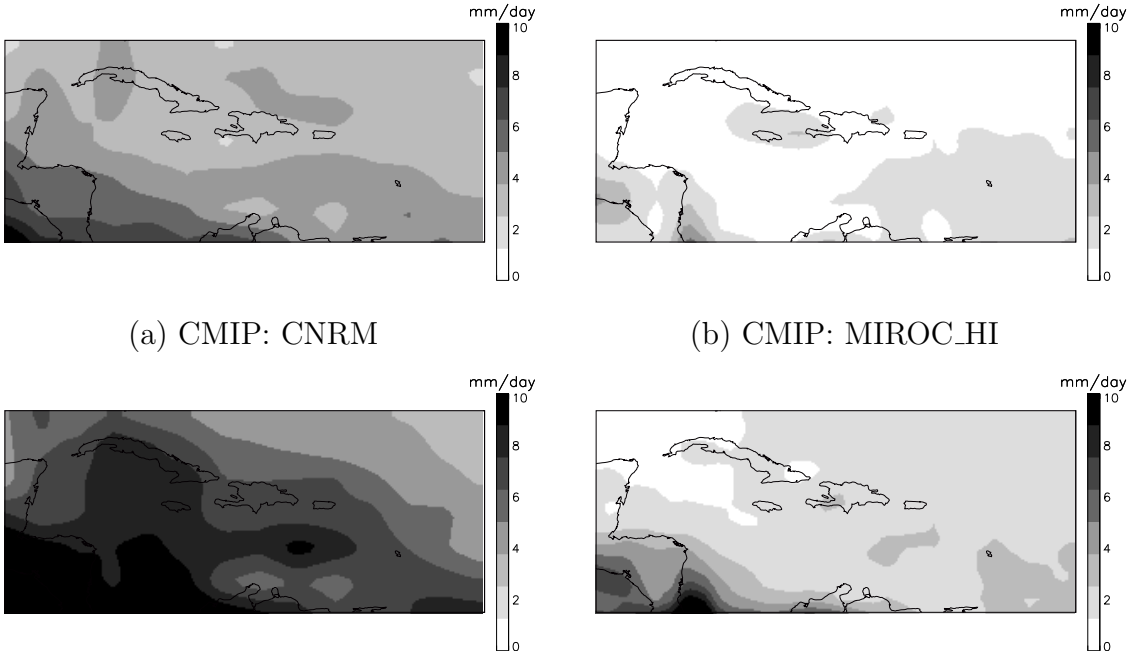

(a) CMIP: CNRM (b) CMIP: MIROC_HI

(c) AMIP: CNRM (d) AMIP: MIROC_HI

Fig. 5. Same as Fig. 4 but for JJA.

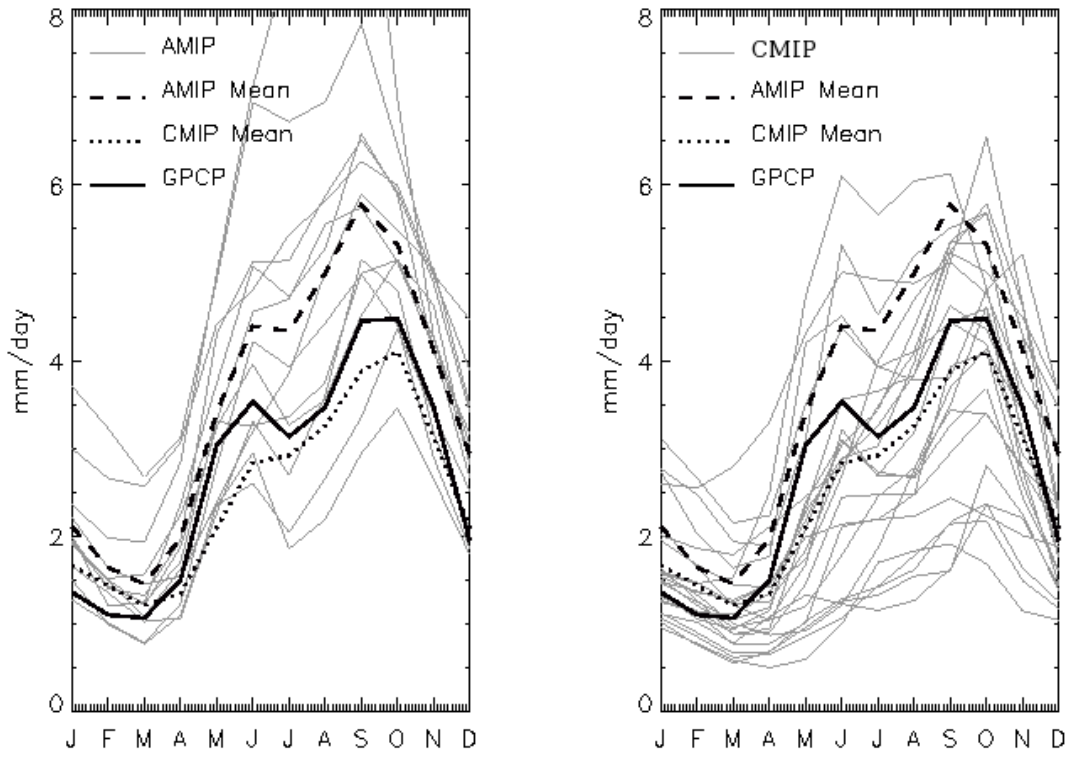

Fig. 6. Annual cycle of Caribbean area-averaged monthly precipitation from GPCP data in addition to CMIP and AMIP models. On both panels are GPCP (1979-2008) observations (solid), CMIP model mean (dotted) and AMIP model mean (dashed). Left panel shows individual AMIP models (grey) and right panel shows individual CMIP models (grey).

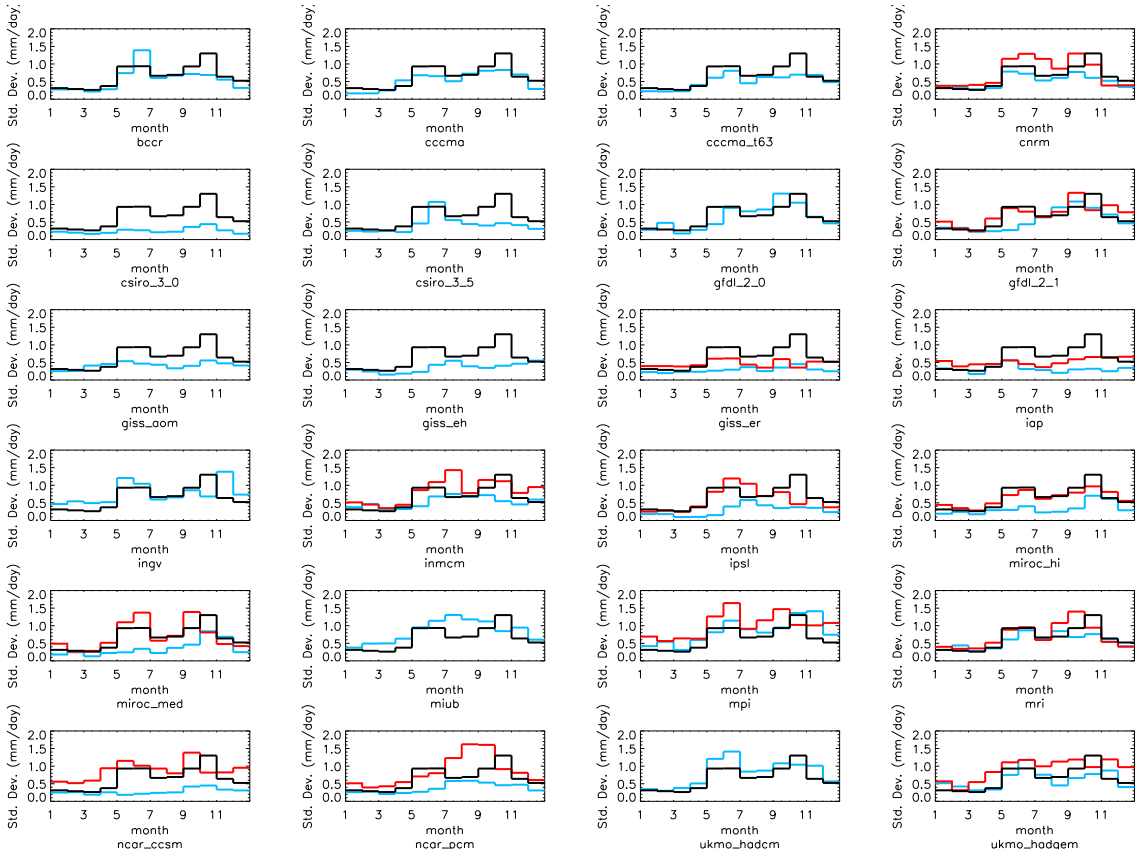

Fig. 7. Annual cycle of monthly standard deviations of area-averaged Caribbean precipitation for observations (black), CMIP (blue) and AMIP (red where available) models.

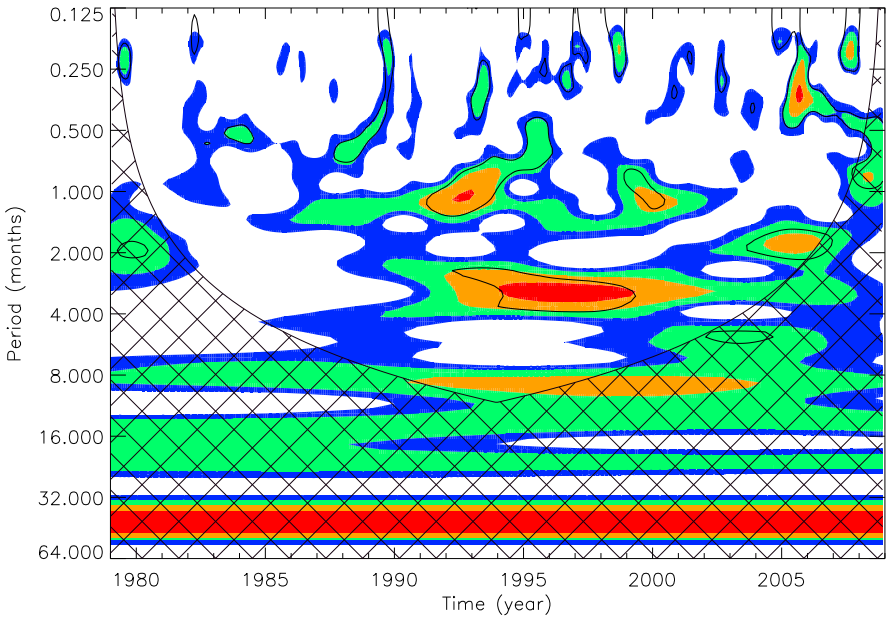

Fig. 8. Wavelet analysis of GPCP monthly data (annual cycle removed). Colors show power contours at 0.5, 1, 2, 4 $(\text{mm/day})^2$ and black contours show 90 % significance level. Black hatched area shows cone of influence where power is unreliable due to the finite length of the time series.

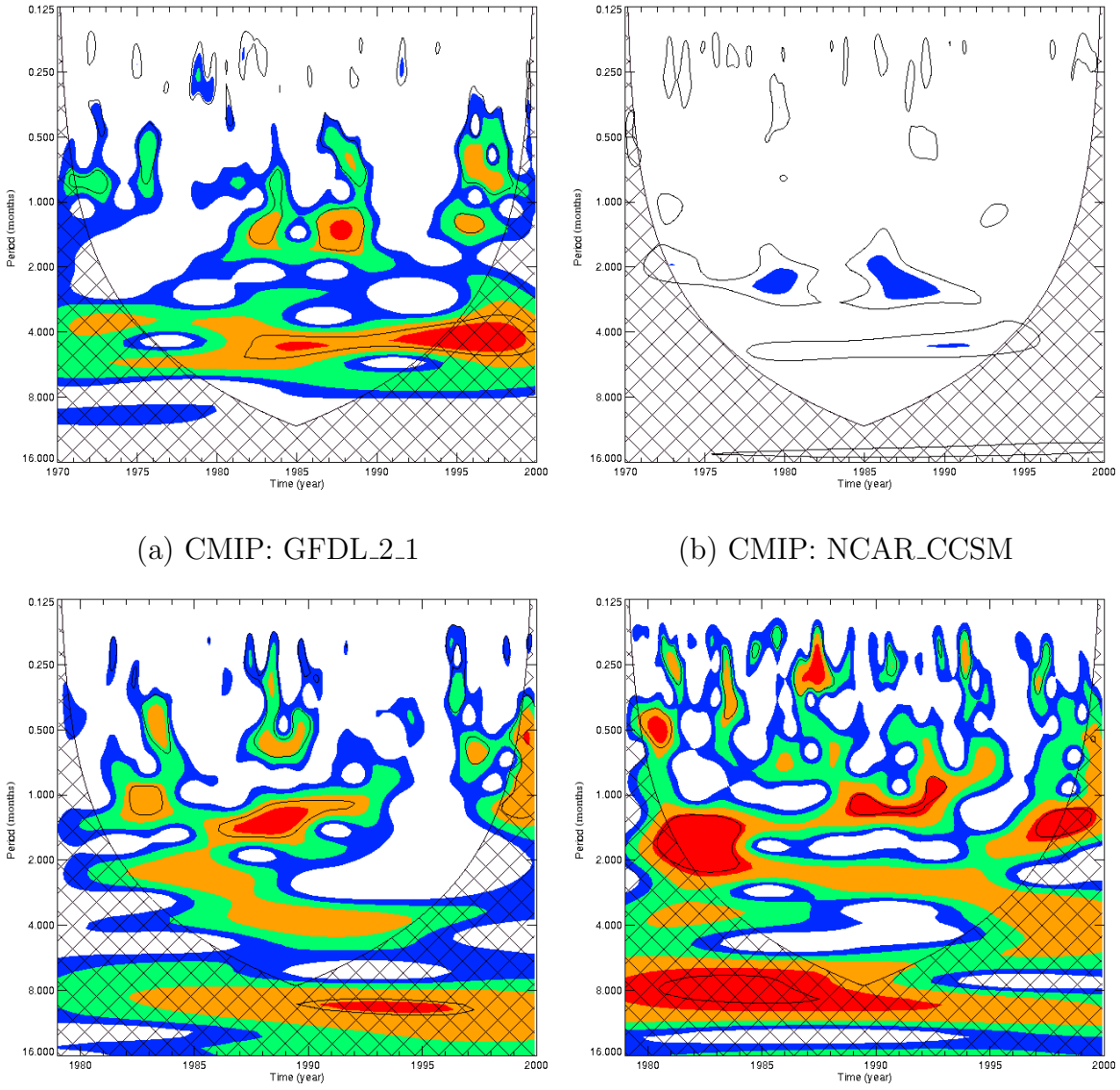

(a) CMIP: GFDL_2_1

(b) CMIP: NCAR_CCSM

(c) AMIP: GFDL_2_1

(d) AMIP: NCAR_CCSM

Fig. 9. Same as Fig. 8 but for four IPCC AR4 simulations (2 CMIP and 2 AMIP) as labeled.

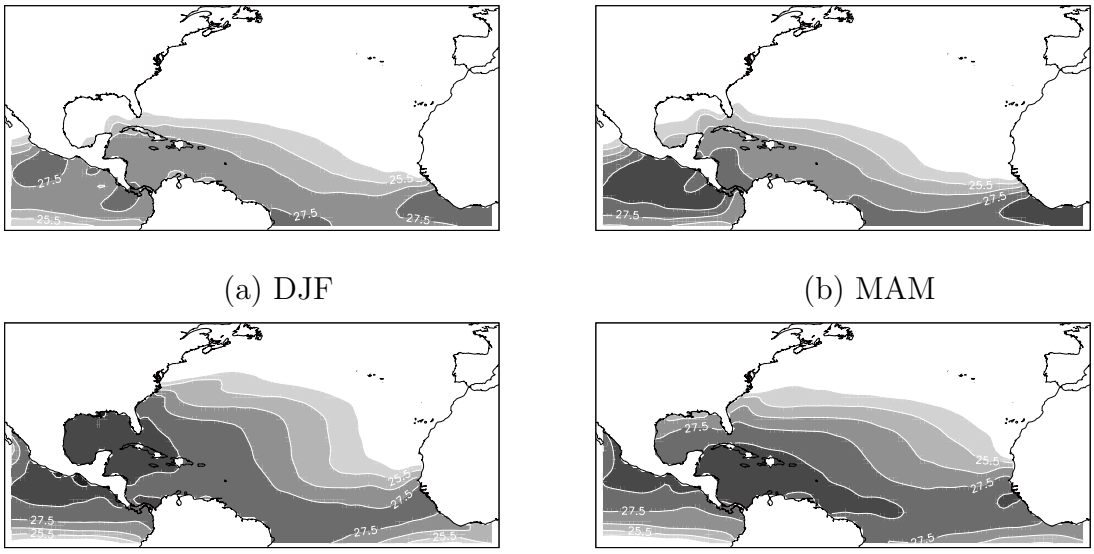

(a) DJF (b) MAM

(c) JJA (d) SON

Fig. 10. Seasonal mean SST values from HadISST dataset. Contour interval is 1°C beginning at 24.5°C.

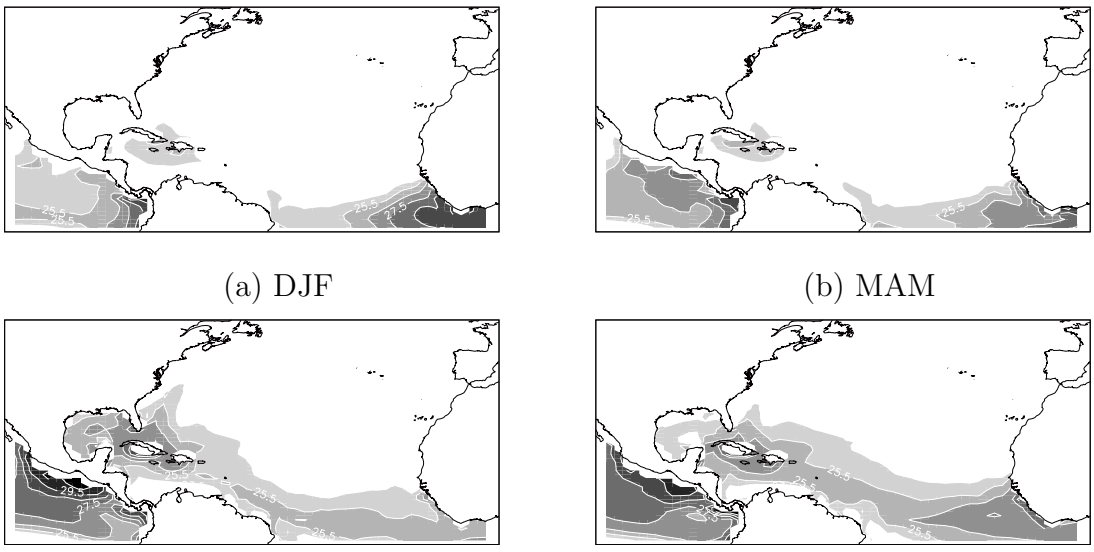

(a) DJF (b) MAM

(c) JJA (d) SON

Fig. 11. Same as Fig. 10 but for the CSIRO_3_0 CMIP simulation.

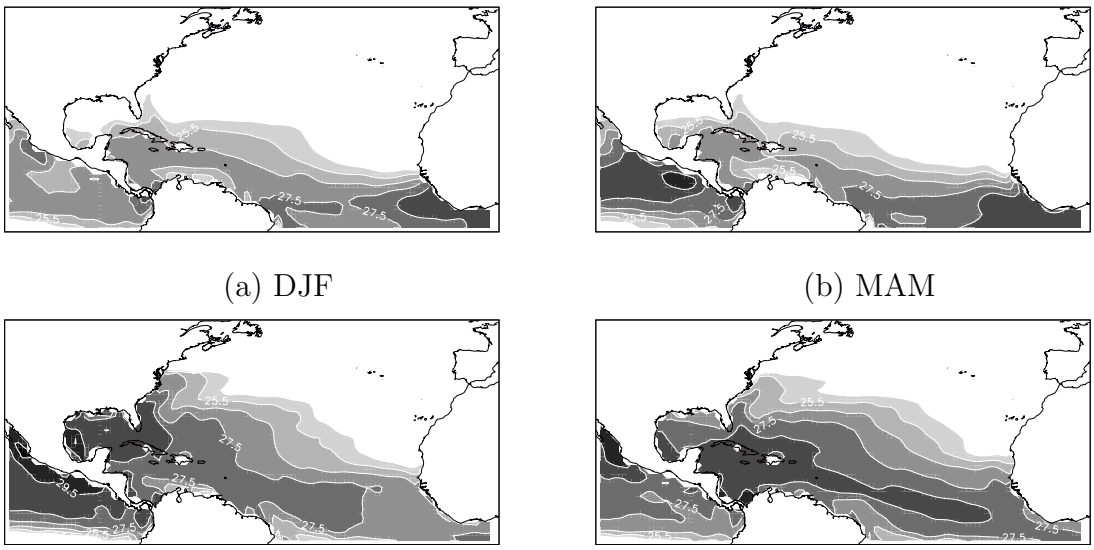

(a) DJF (b) MAM

(c) JJA (d) SON

Fig. 12. Same as Fig. 10 but for the MPI CMIP simulation.

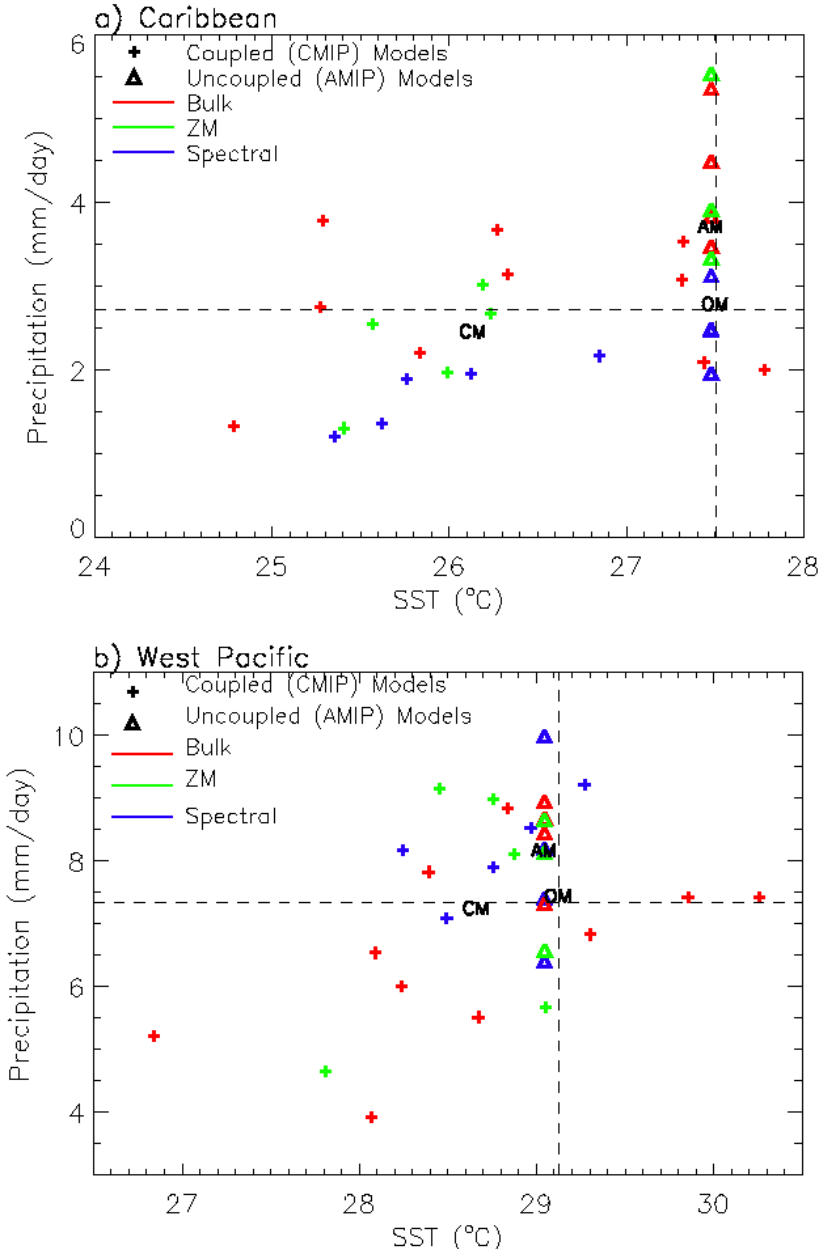

Fig. 13. Scatter plot of a) Caribbean, and b) West Pacific (10^oS-5^oN, 130-165^oE) area-averaged sea surface temperature (^oC) and precipitation (mm/day). Observations (GPCP and HadISST) are shown by 'OM', with the CMIP multi-model ensemble mean marked as 'CM' and the AMIP multi-model ensemble mean shown by 'AM'. Shapes indicate model type and colors convective parameterization type as shown. Horizontal and vertical lines indicate observed mean precipitation and SST values respectively.

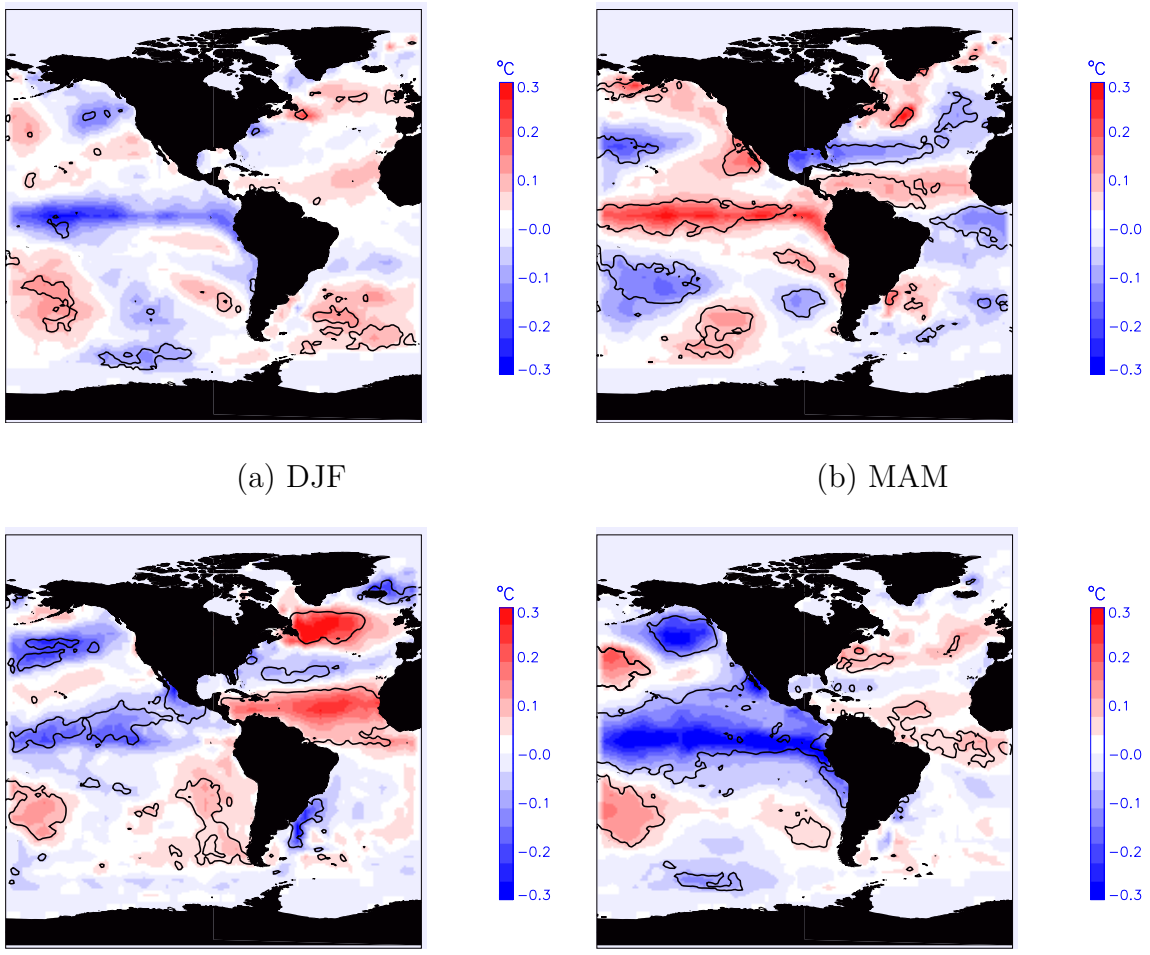

(a) DJF (b) MAM

(c) JJA (d) SON

Fig. 14. Regression coefficients (°C per mm/day) of SST regressed onto Caribbean area-averaged precipitation calculated by season. Long term linear trends are removed from SST time series. Black lines indicate regions where the correlation coefficient is significantly different from zero at the 95 % confidence level.

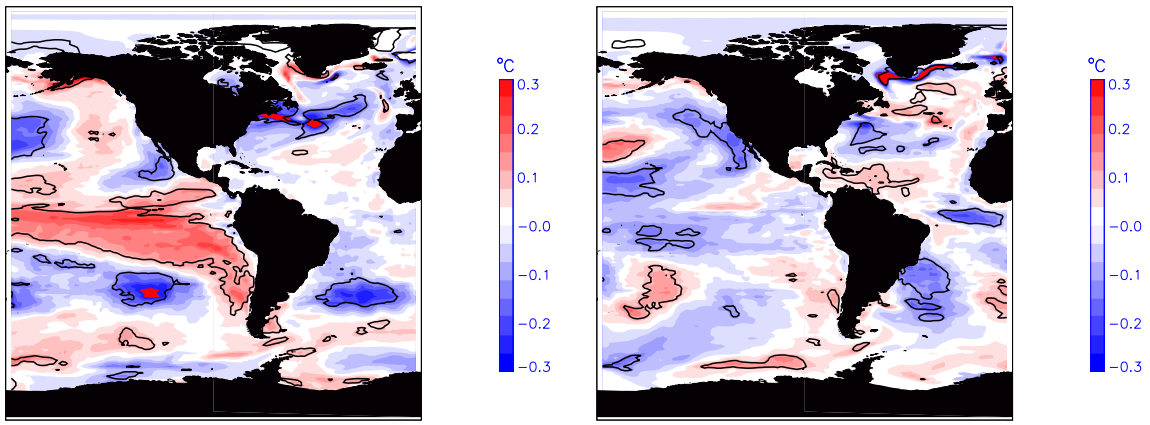

(a) DJF (b) MAM

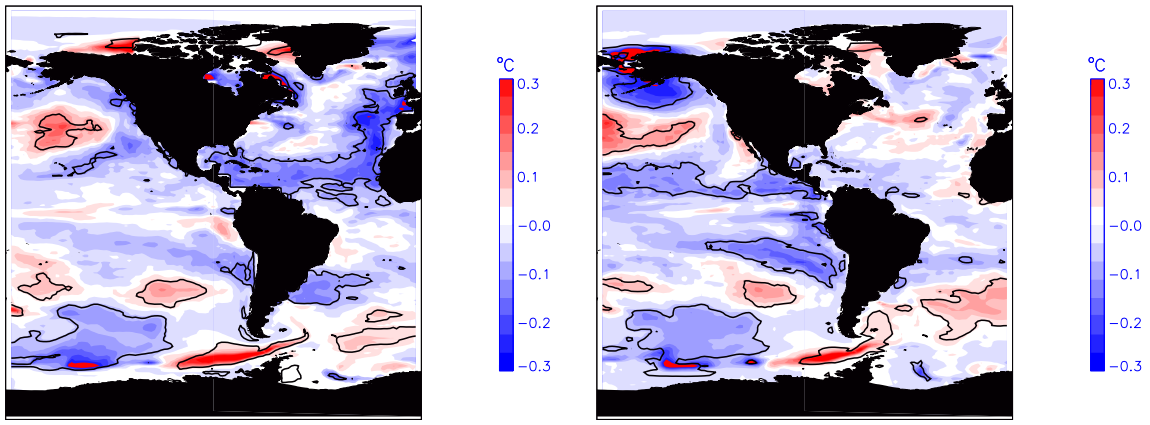

(c) JJA (d) SON

Fig. 15. Same as Fig. 14 but for MIROC_MED CMIP simulation.

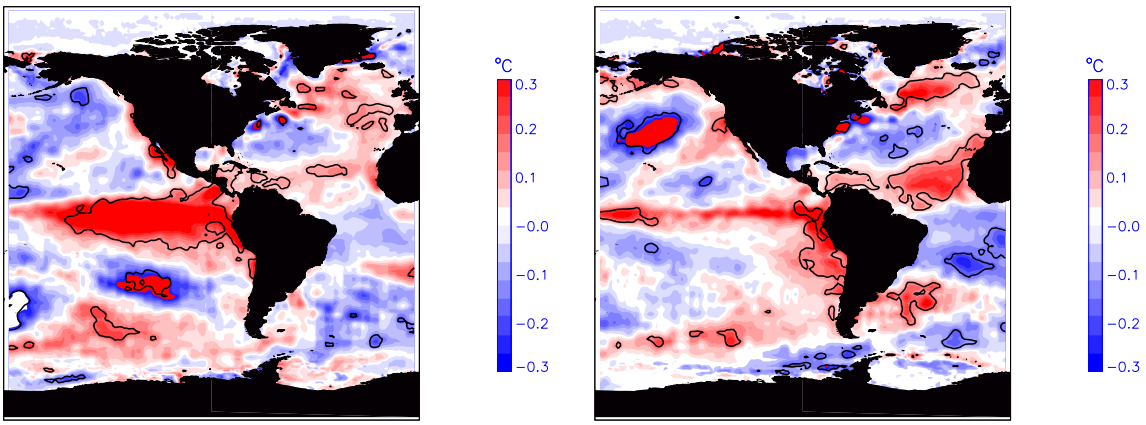

(a) DJF (b) MAM

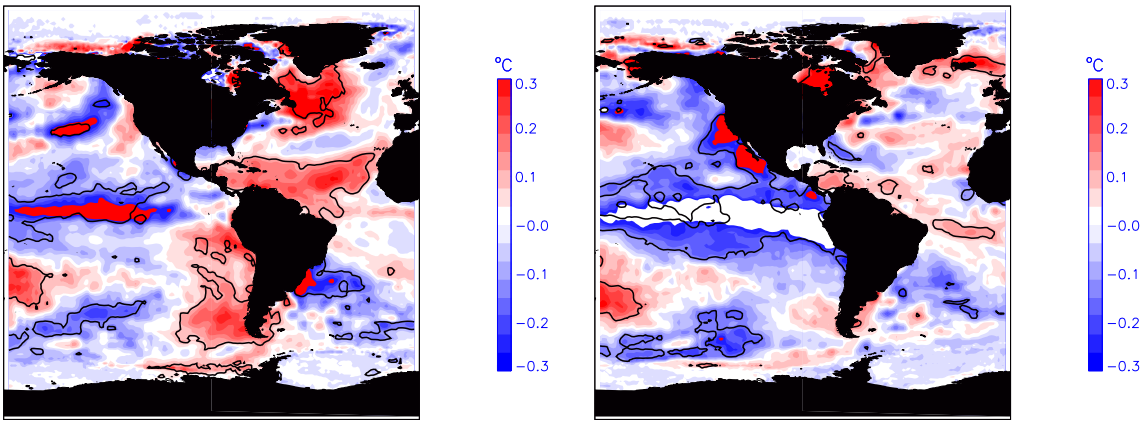

(c) JJA (d) SON

Fig. 16. Same as Fig. 14 but for MIROC_MED AMIP simulation.

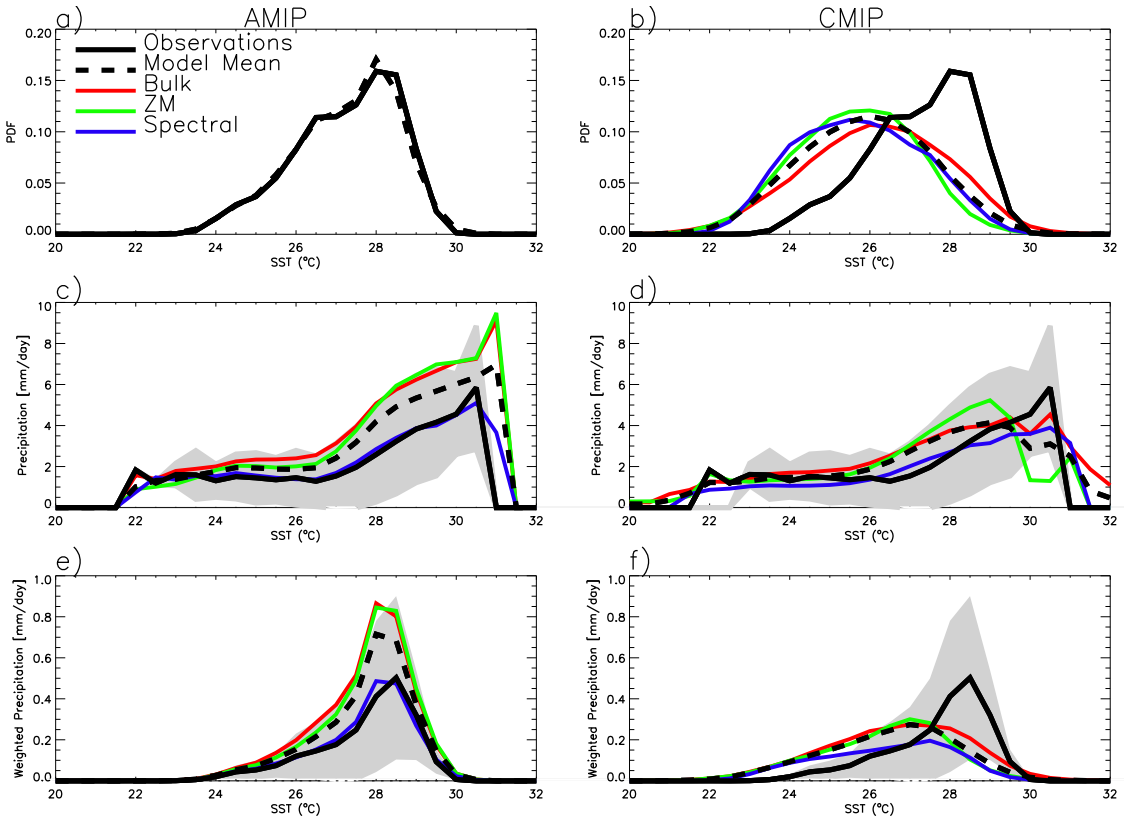

Fig. 17. Regime sorting analysis of Caribbean area-averaged (10-25^{o}N, 55-90^{o}W) precipitation by SST for AMIP (left, a-c) and CMIP (right, d-f) models and observations (solid black line). a), d) Probability distribution function (PDF) of SST. b), e) Precipitation composited by SST. c), f) composited precipitation (b) weighted by the PDF of SST (a). Convective parameterization group multi-model means indicated by colored lines as shown in panel a). Multi-model ensemble mean shown by dashed black line. Grey shading indicates plus/minus one standard deviation from observations.

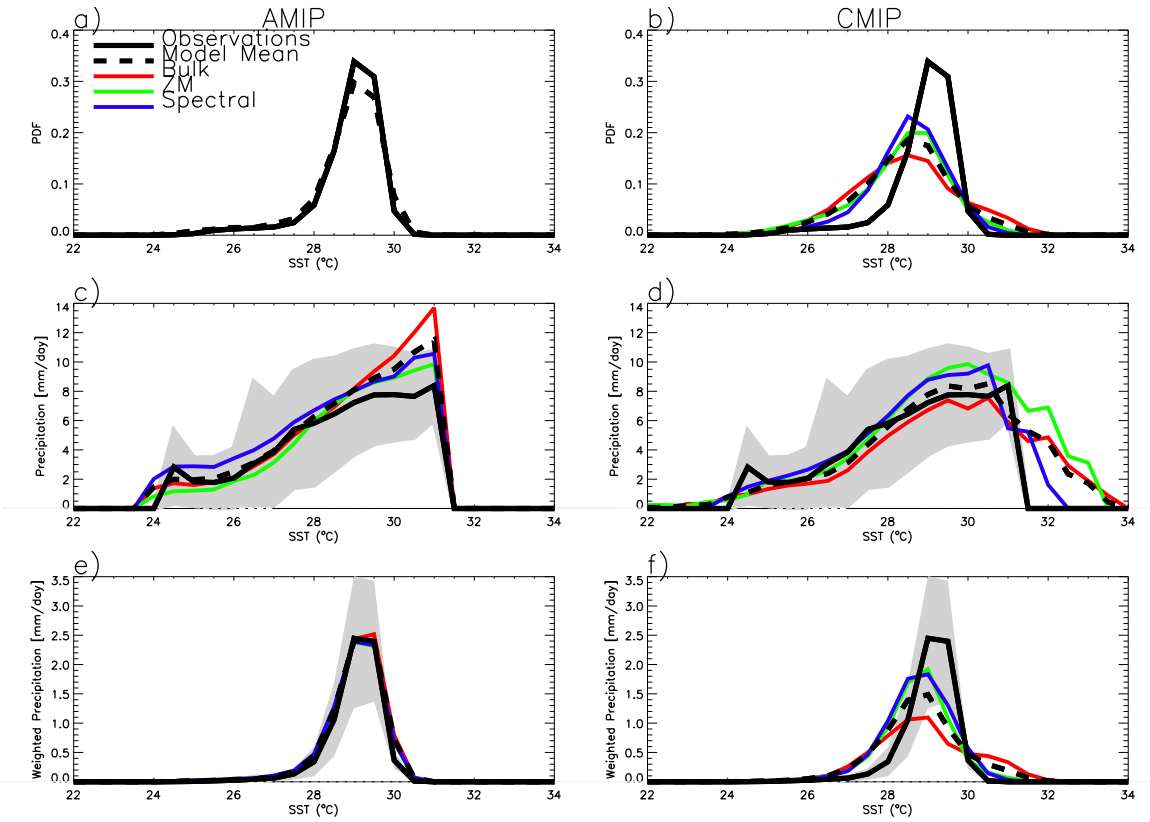

Fig. 18. Same as in Figure 17 but for the West Pacific (10^{o}S-5^{o}N, 130-165^{o}E).

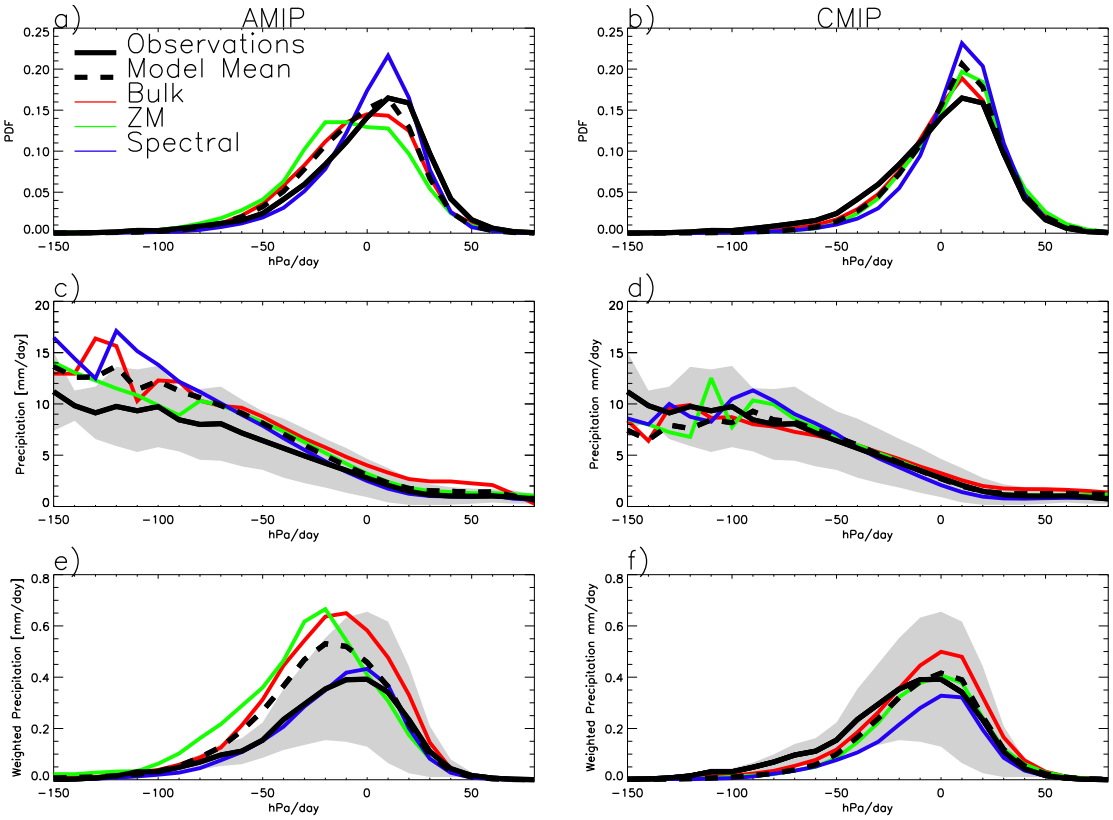

Fig. 19. Same as in Figure 17 but replacing regime sorting by SST with ω_{500} (hPa/day).

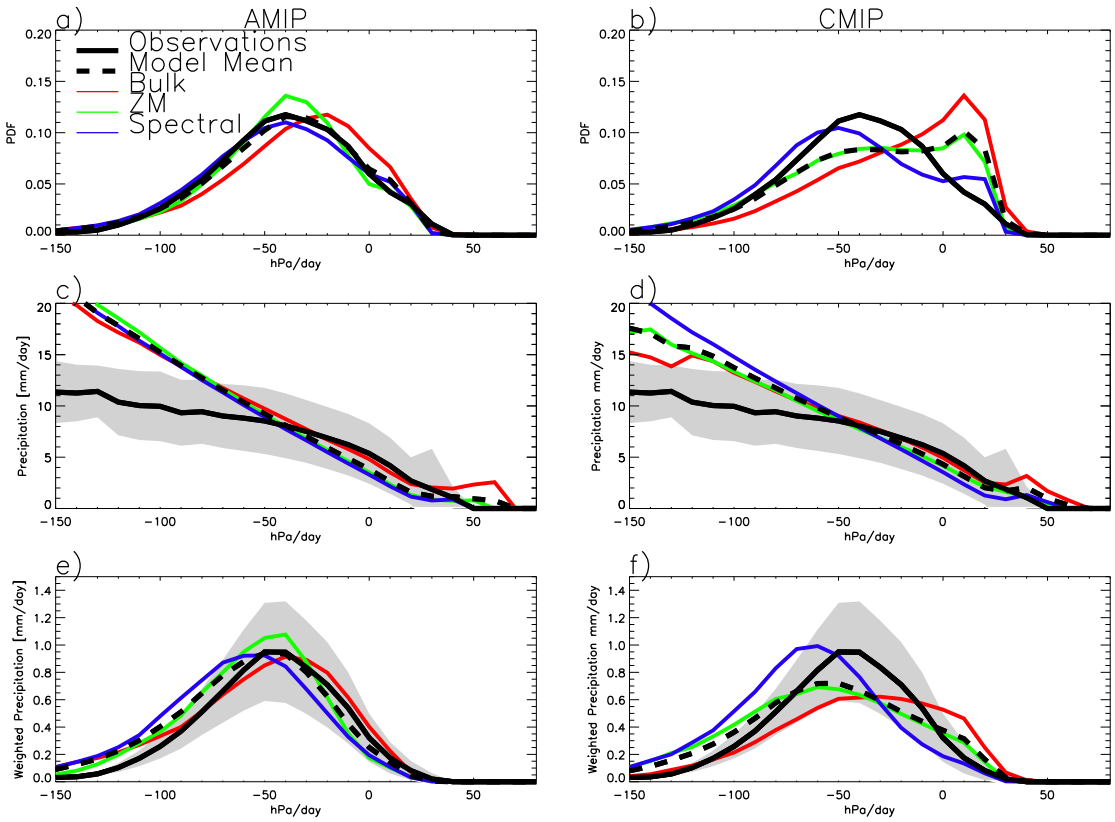

Fig. 20. Same as in Figure 18 but replacing regime sorting by SST with ω_{500} (hPa/day).

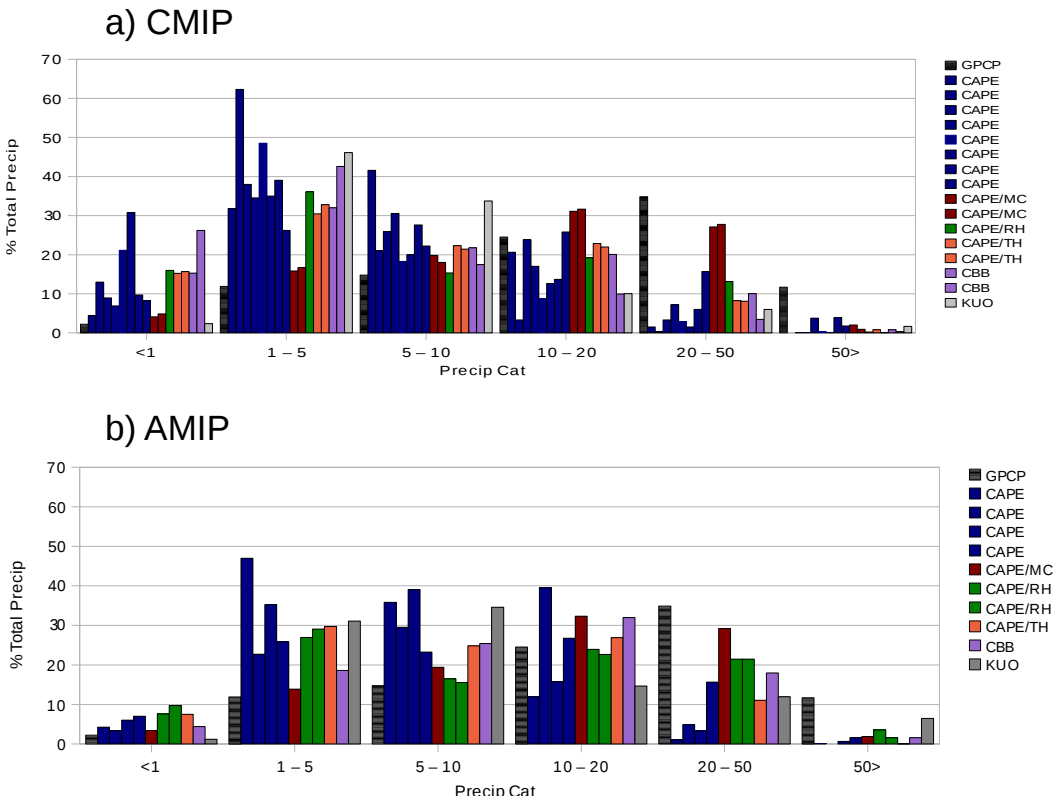

Fig. 21. Percent contribution to the total annual precipitation from different daily precipitation rate categories (in mm/day) for GPCP observations (black bars) and a) CMIP ensemble members and b) AMIP ensemble members. Colored bars represent one of 6 types of closure/trigger mechanism; CAPE, CAPE and moisture convergence (CAPE/MC), CAPE and relative humidity (CAPE/RH), CAPE and threshold (CAPE/TH), cloud-base buoyancy (CBB) and Kuo.

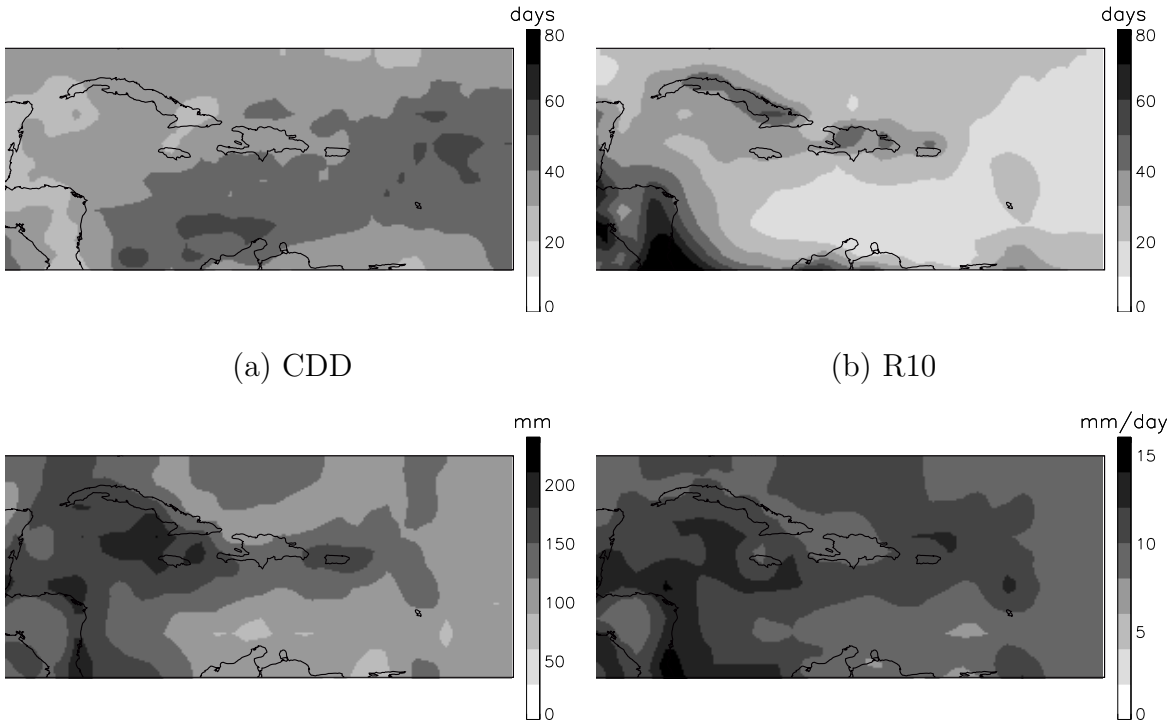

(a) CDD (b) R10

(c) R5D (d) SDII

Fig. 22. Maps of extreme indices as calculated from GPCP daily data (1997-2008). a) Consecutive dry days, b) Number of days with rainfall greater than 10 mm, c) Maximum 5 day rainfall total and d) Simple daily intensity index.

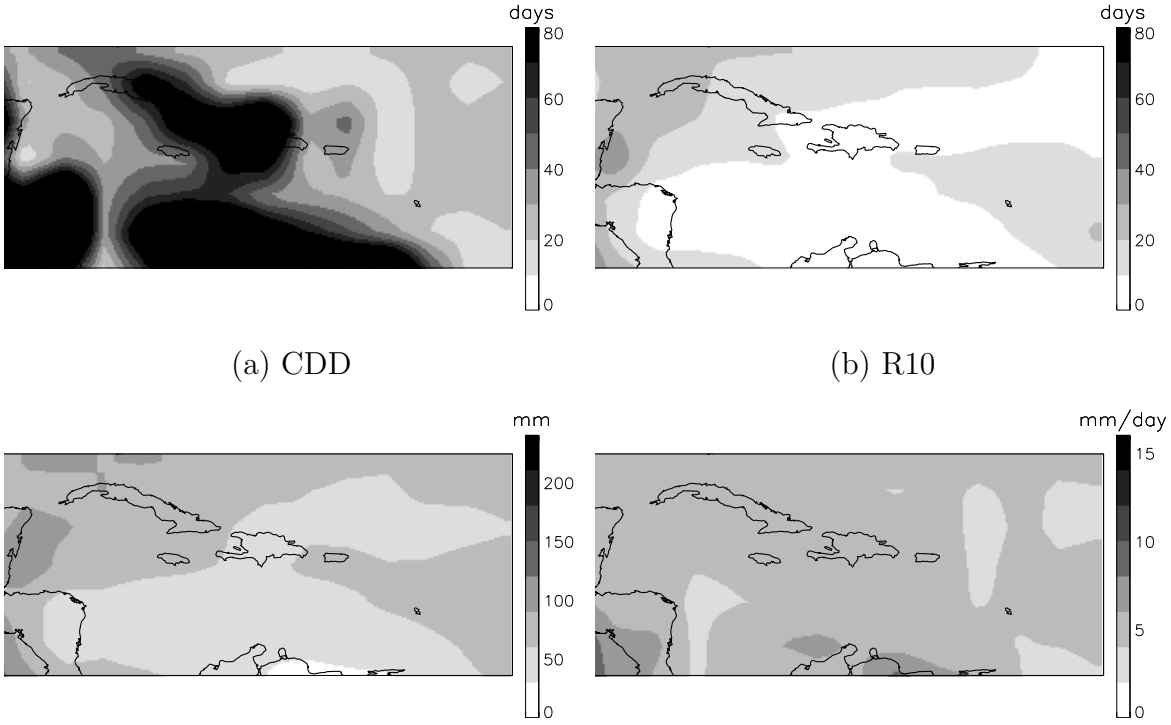

(a) CDD (b) R10

(c) R5D (d) SDII

Fig. 23. Same as Fig. 22 but for GFDL_2_1 CMIP simulation.

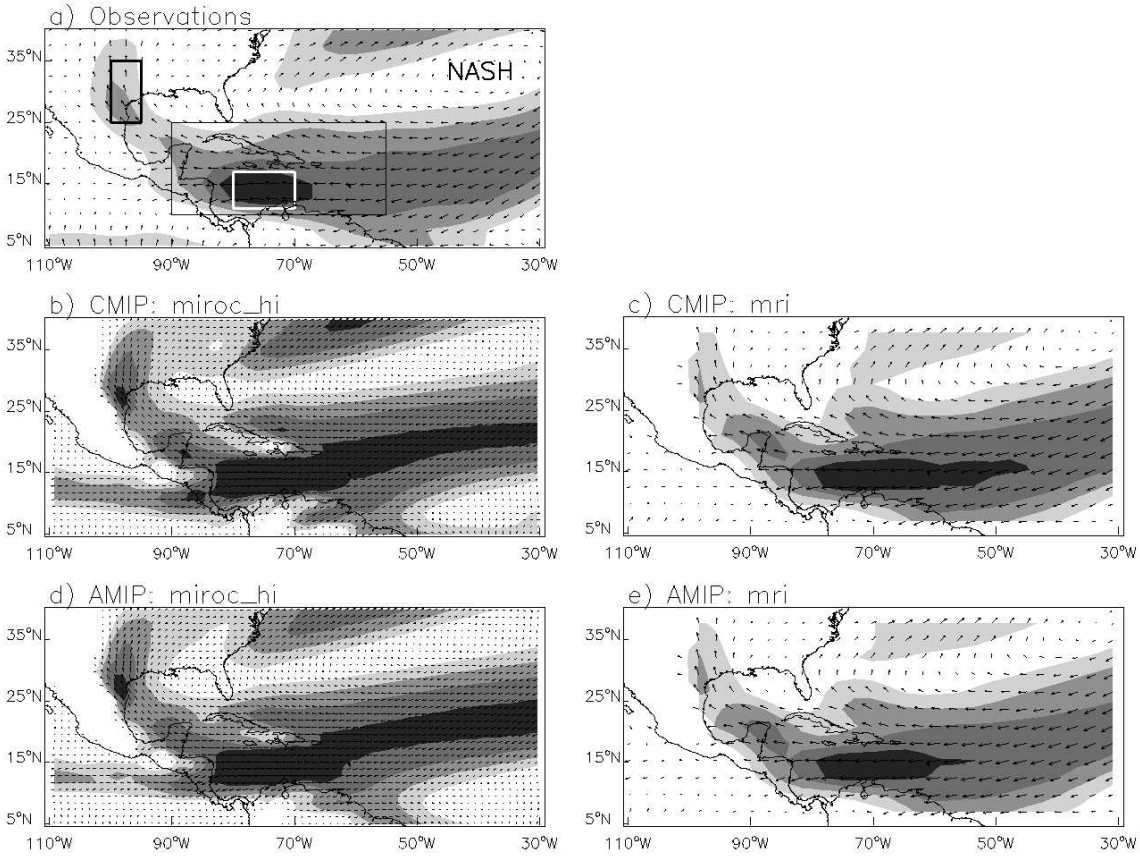

Fig. 24. Seasonal mean JJA 925 hPa wind speed (shaded contours, 2, 4, 6, 8, 10 ms^{-1}) and direction (vectors) from a) NCEP/DOE reanalysis II and four different IPCC AR4 simulations: (b, c) coupled CMIP simulations and, (d, e) uncoupled AMIP simulations. Only two models, miroc_hi (b, d) and mri (c, e) are shown for brevity. In panel a, the white box indicates region for calculating the CLLJ index and thick black box the region for calculating the GPLLJ index. Thin black box indicates averaging region for Caribbean area-averaged quantities. NASH indicates the approximate climatological center of the North Atlantic Subtropical High.

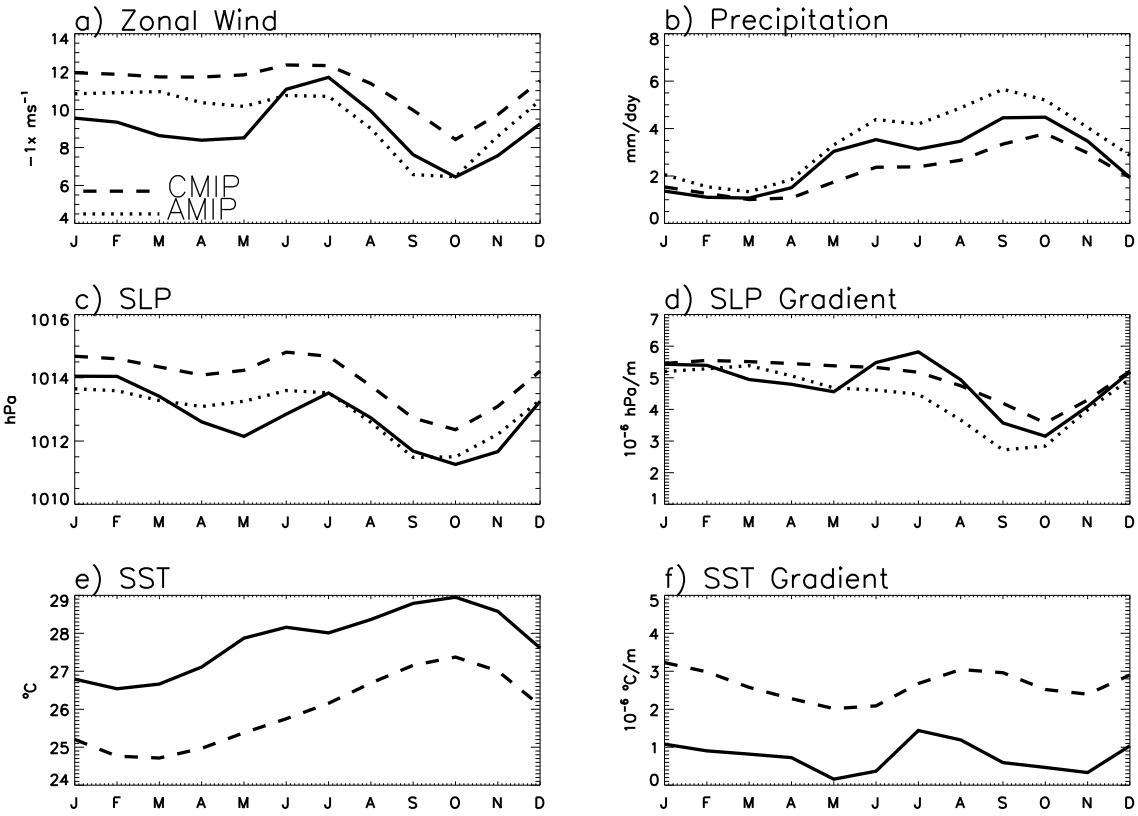

Fig. 25. Observed (solid), CMIP mean (dashed) and AMIP mean (dotted) annual cycle of various quantities. Averaging area for precipitation (b) is 90-55°W, 10-25°N (thin black box, Fig. 24), zonal wind (a), SLP (c) and SLP gradient (d), 12.5-17.5°N, 70-80°W (white box, Fig. 24), SST (e) and SST gradient (f), 12-16°N, 70-80°W.

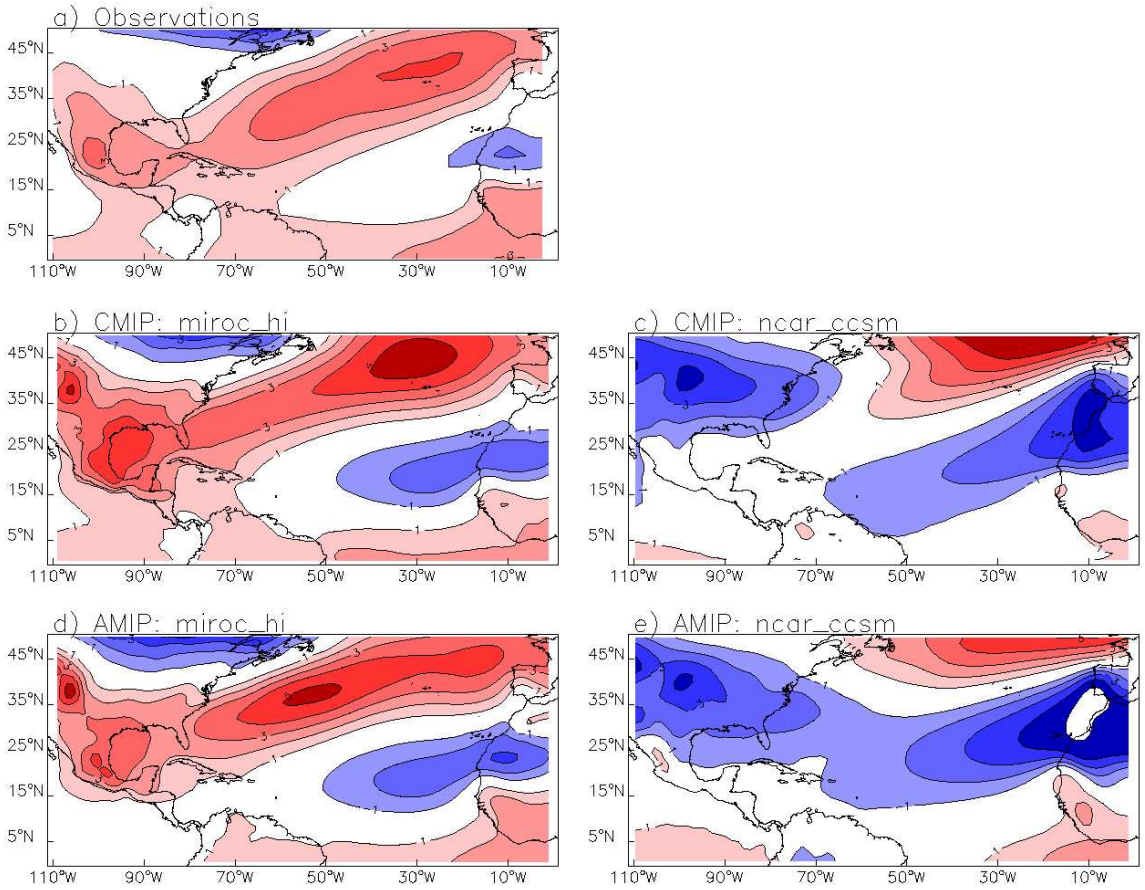

Fig. 26. July minus May SLP difference (hPa). Contours at -4, -3, -2, -1, 1, 2, 3, 4 hPa with positive indicating an increase in SLP between May and July. Observations (a) are shown in conjunction with example output from two models, miroc_hi (b, d) and ncar_ccsm (c, e). Output from both CMIP (b, c) and AMIP (d, e) simulations are shown for each model.

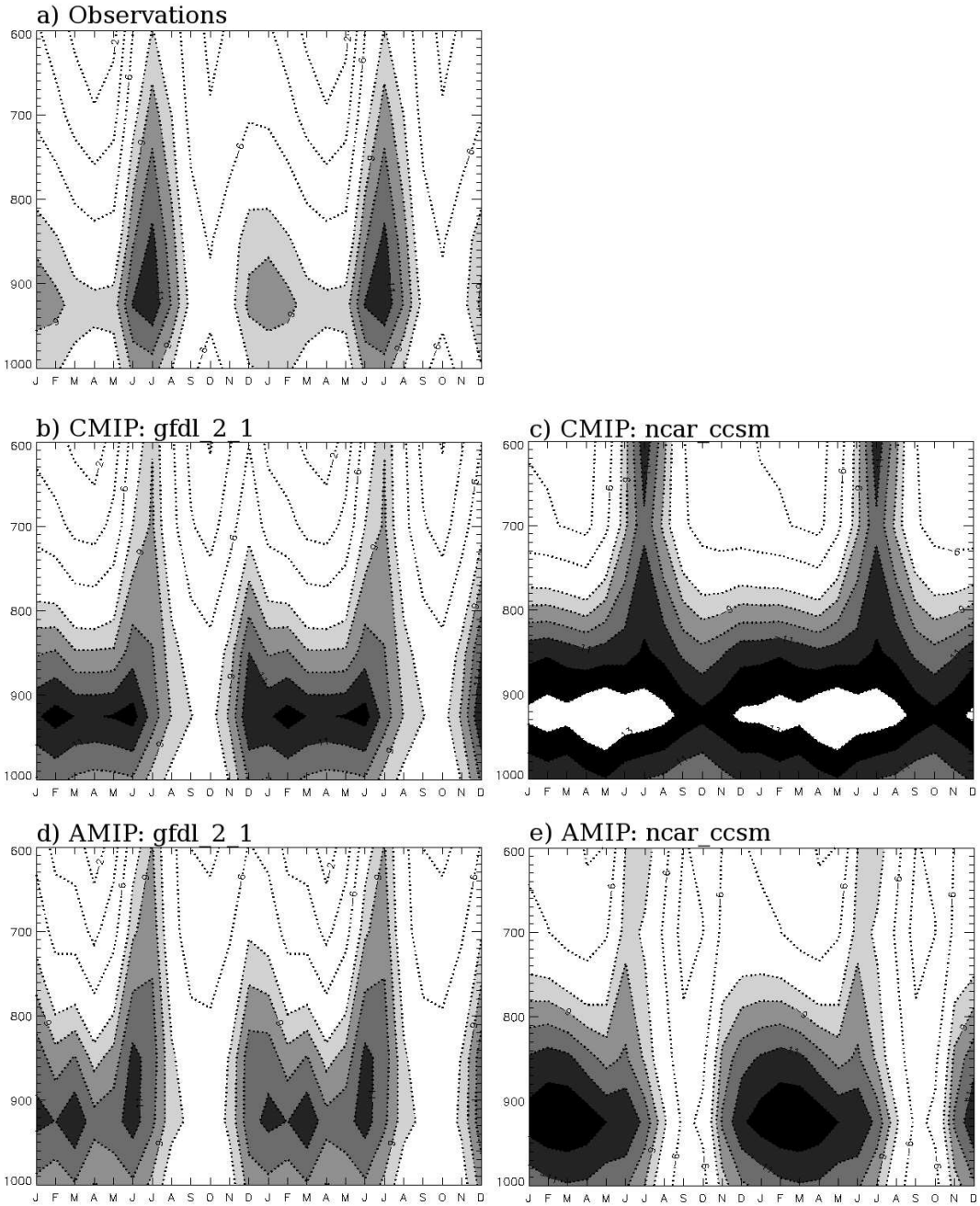

Fig. 27. Annual cycle (repeated twice) of the vertical (1000 - 600 hPa) profile of zonal wind averaged over the CLLJ index area (white box, Fig. 24). The contour interval is 2 ms^{-1} up to -8 ms^{-1} and 1 ms^{-1} at higher wind speeds. Shading begins at -8 ms^{-1} and dotted contours indicate easterly winds. As in Fig. 26, observations (a) are shown in conjunction with example output from two models, gfdl_2_1 (b, d) and ncar_ccsm (c, e). Output from both CMIP (b, c) and AMIP (d, e) simulations are shown for each model.

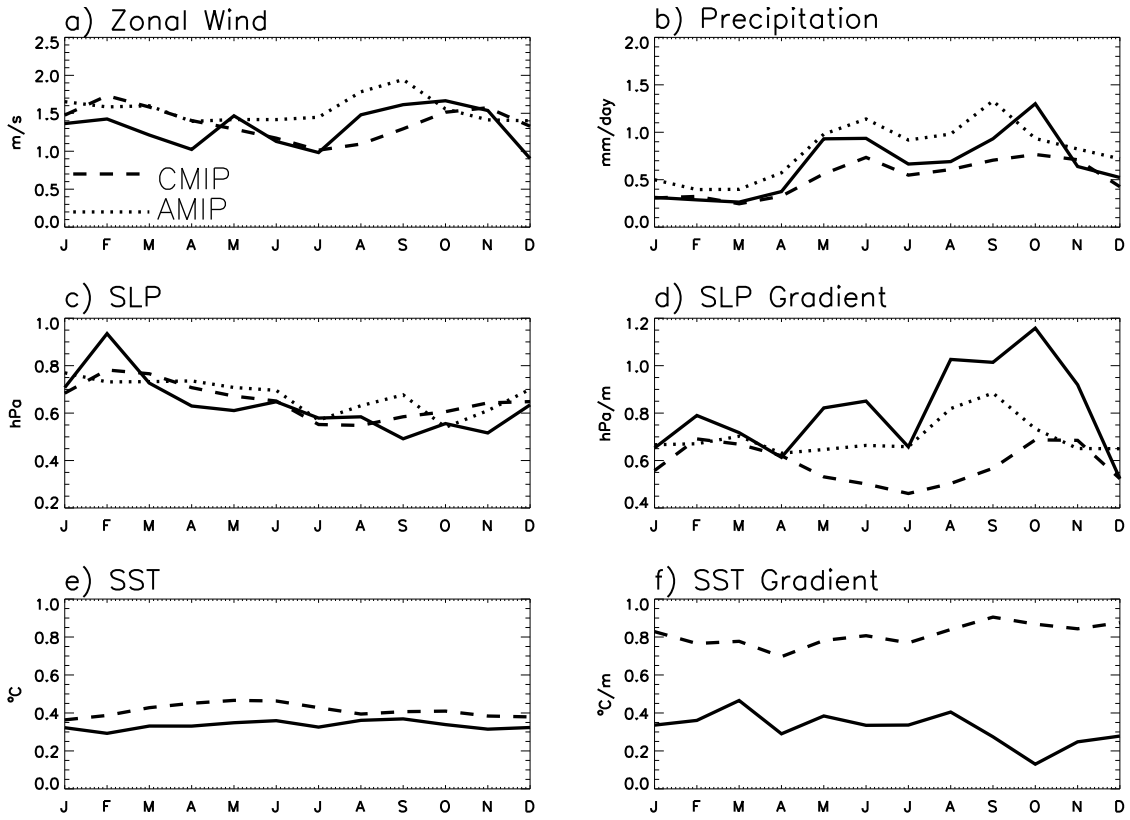

Fig. 28. As in Fig. 25 but for standard deviations.

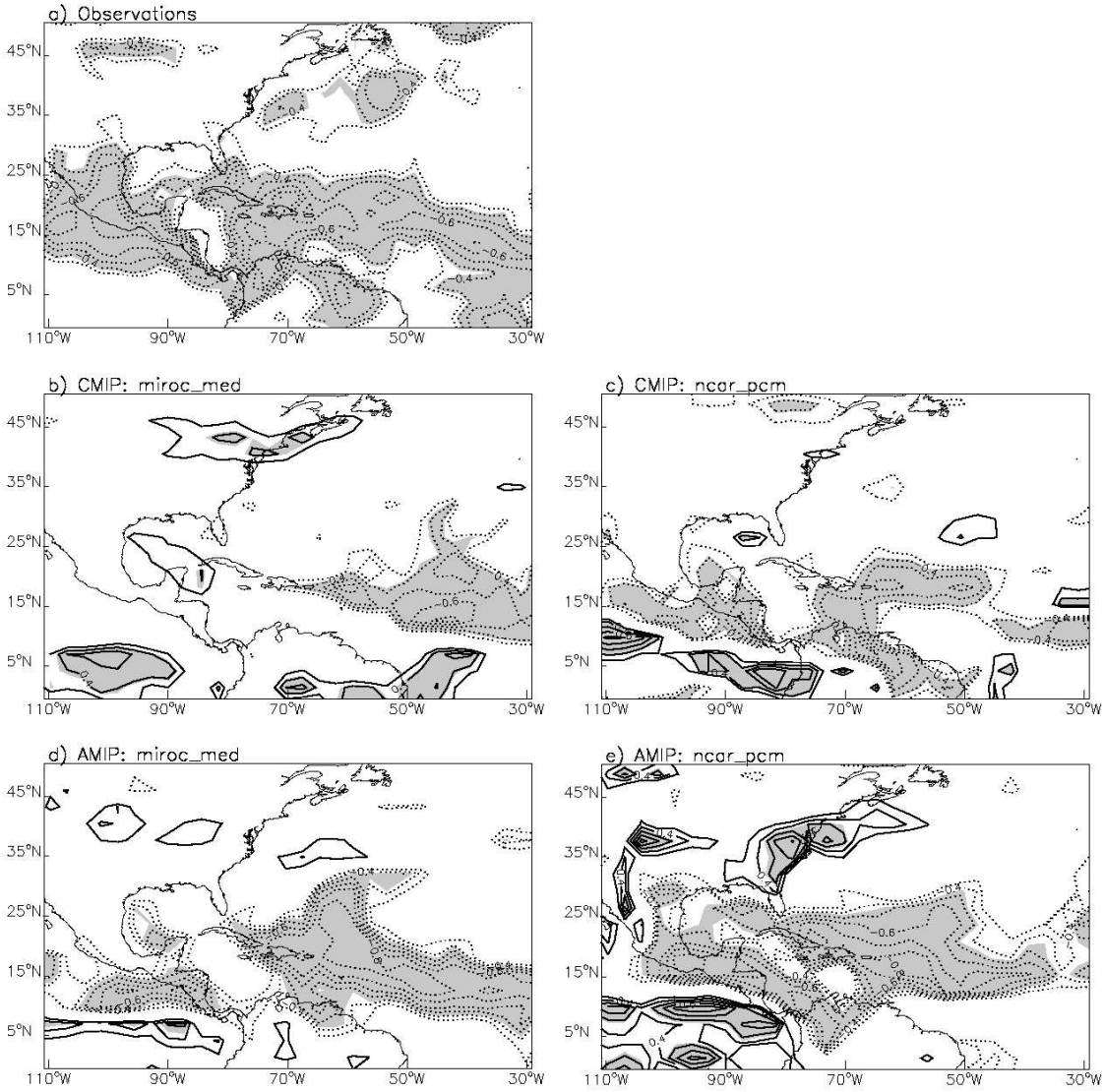

Fig. 29. Maps of correlation coefficients between precipitation anomalies and CLLJ index for August. (a) Observations, (b, c) CMIP output and (d, e) AMIP output. Model output presented from (b, d) miroc_med and (c, e) ncar_pcm. Contour interval is 0.1, with negative correlations dashed (indicating increased precipitation anomalies with reduced CLLJ strength) and positive correlations solid. Shading indicates correlations significantly different from zero at the 95 % confidence level.

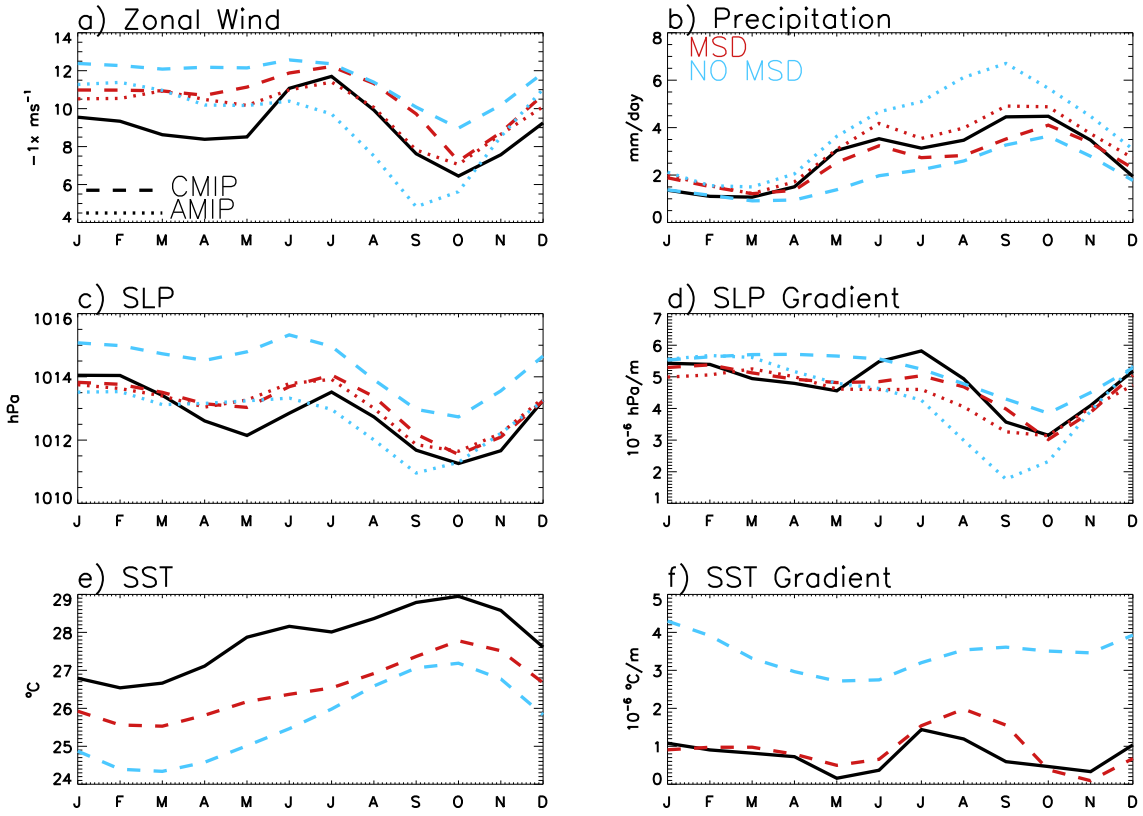

Fig. 30. Observed (solid), CMIP mean (dashed) and AMIP mean (dotted) annual cycle of quantities shown in Fig. 25. Red lines show means of models that captured the MSD and blue lines show means of models without a MSD.

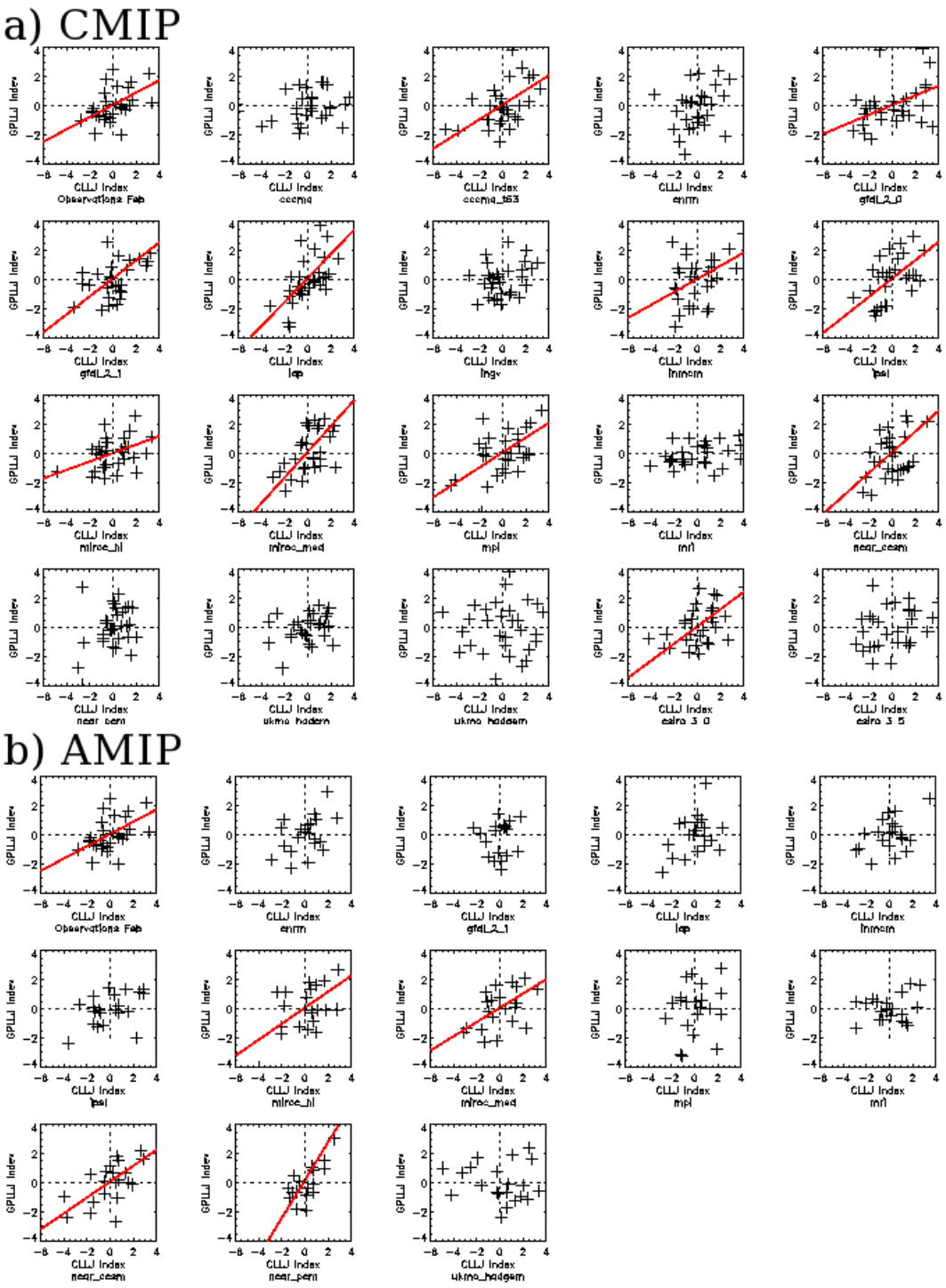

Fig. 31. Scatter plots between February CLLJ and GPLLJ indices for a) CMIP models and b) AMIP models. Observations are shown in top left panel of a) and b). Regression line (red) is shown only if significant at the 95 % level (based on student's t-test). Averaging areas for indices as shown in Fig. 24.

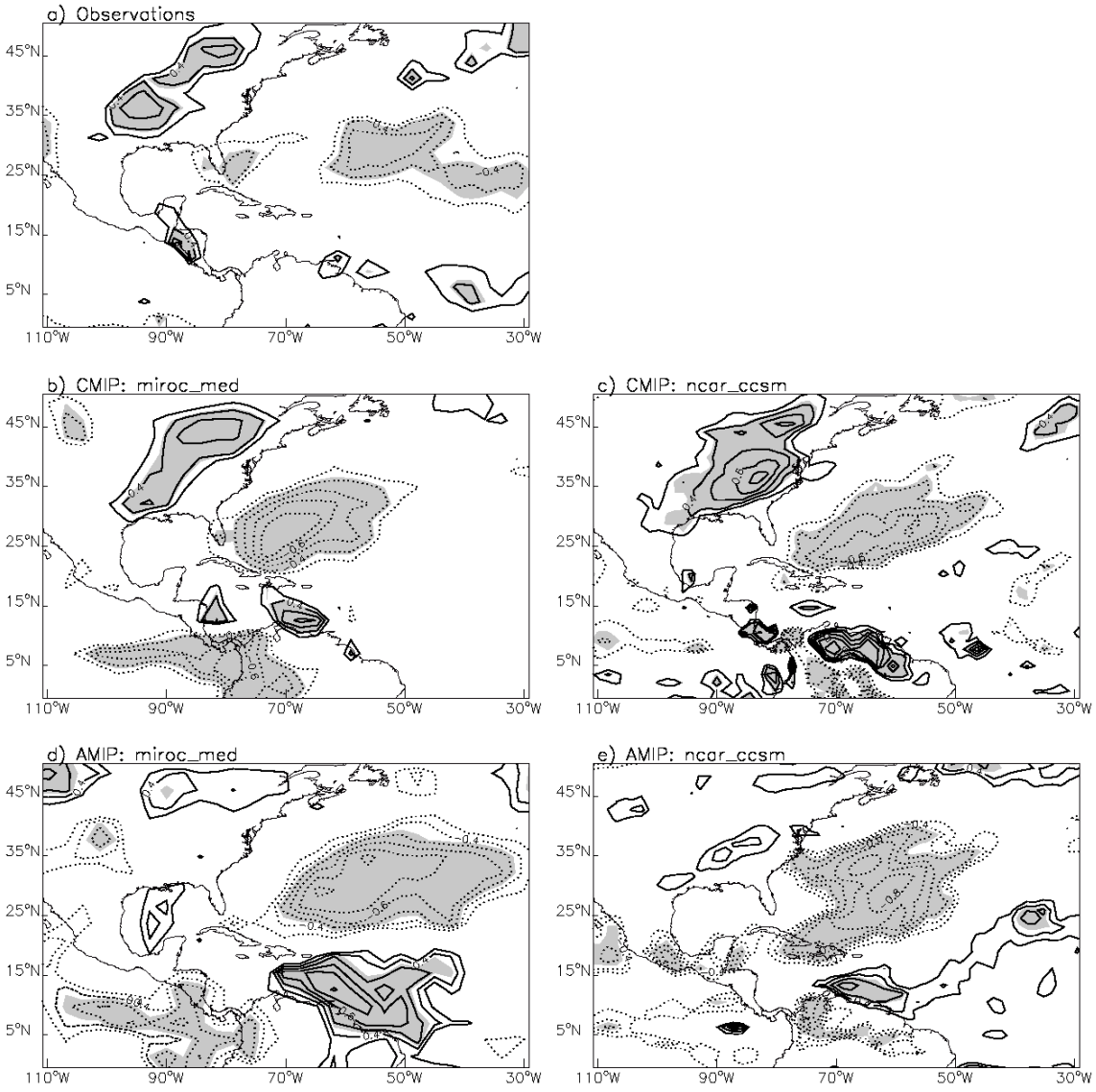

Fig. 32. Same as Fig. 29 but for February and ncar_pcm is replaced by ncar_ccsm.

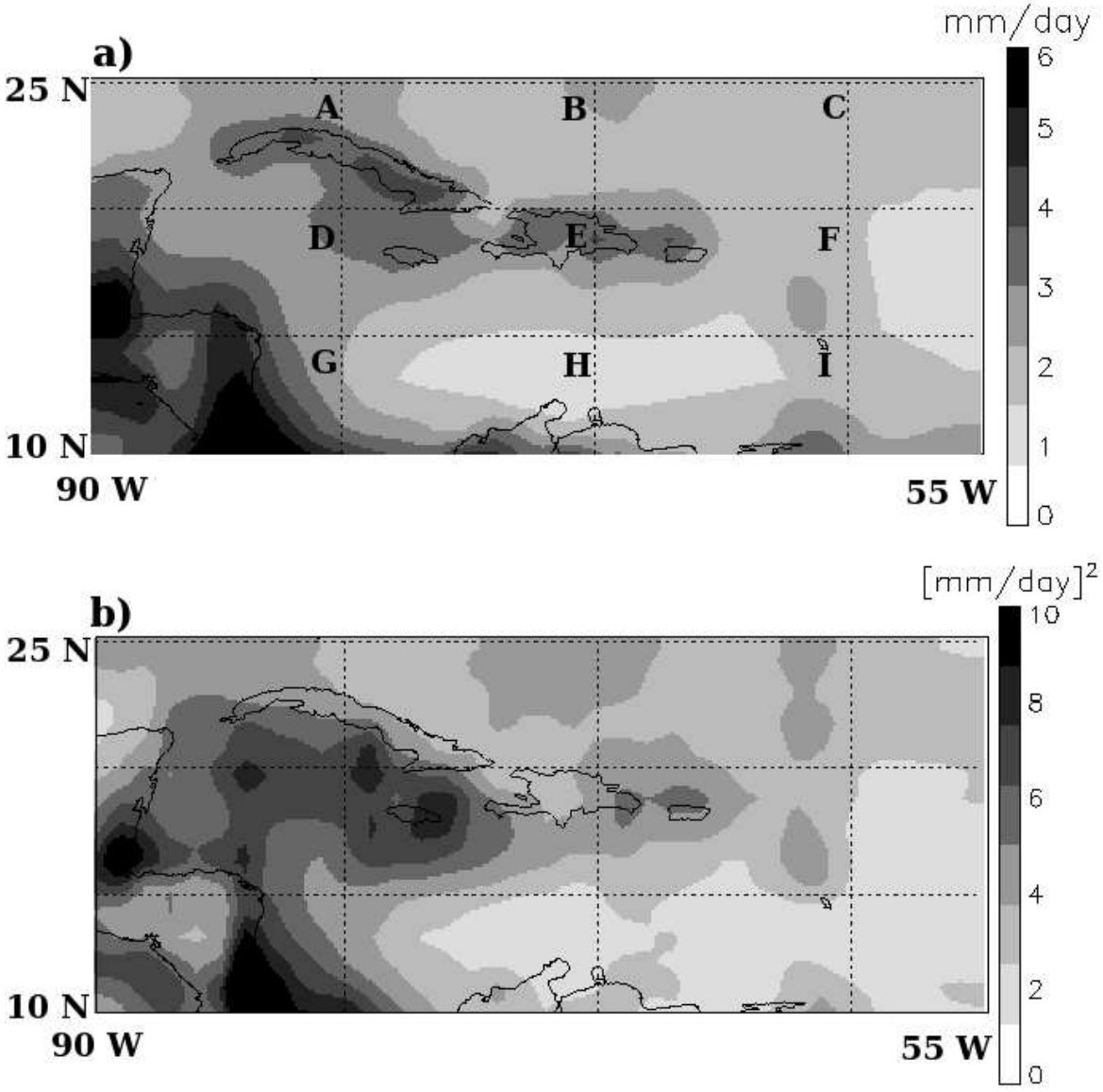

Fig. 33. a) Annual averaged precipitation (1997-2008) in mm day^{-1} from GPCP daily data. Letters in upper right corner of each 5^ox10^o box indicate averaging regions for spectral analysis. b) Instraseasonal variance (30-90 days) of annual precipitation in (mm day^{-1})^2).

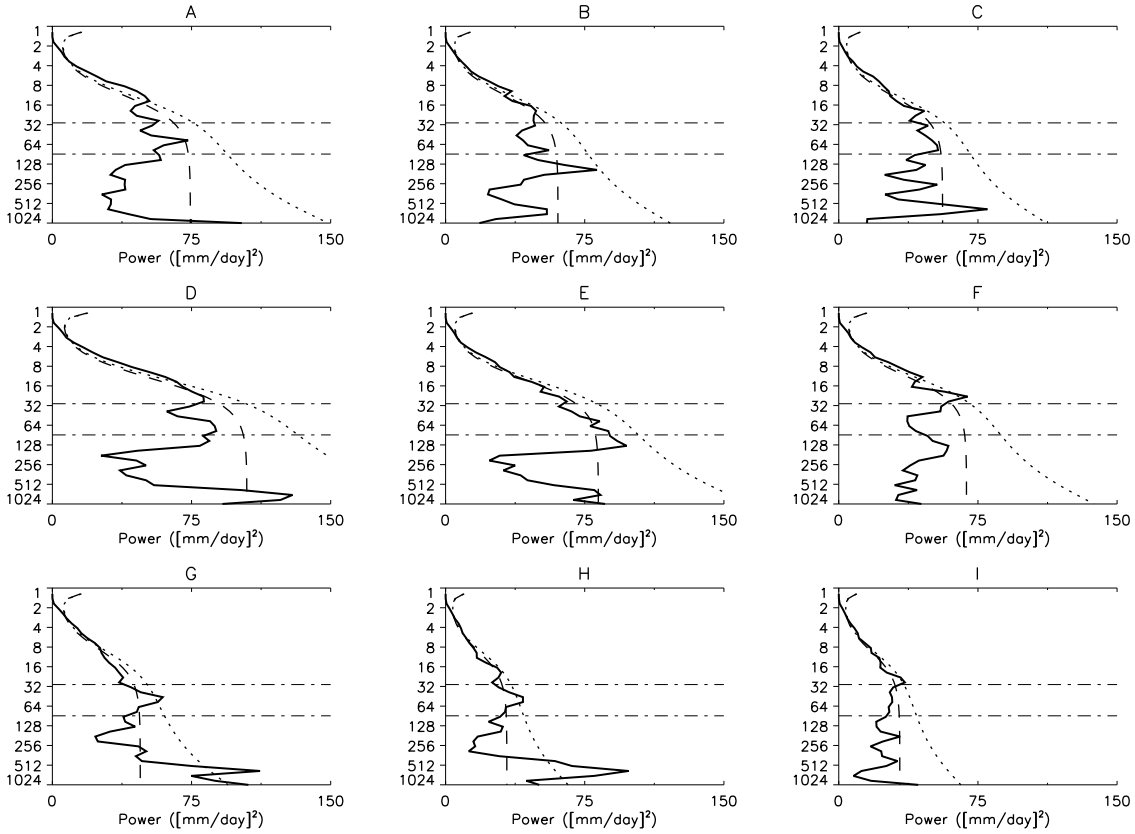

Fig. 34. Spectral analysis of area averaged precipitation anomalies. A through I correspond to averaging regions shown in Fig. 33. In each figure, the precipitation (solid), red noise (dashed) and 90 % significance (dotted) spectra are shown. Dash-dot lines in each panel delineate 30 and 90 day periods.

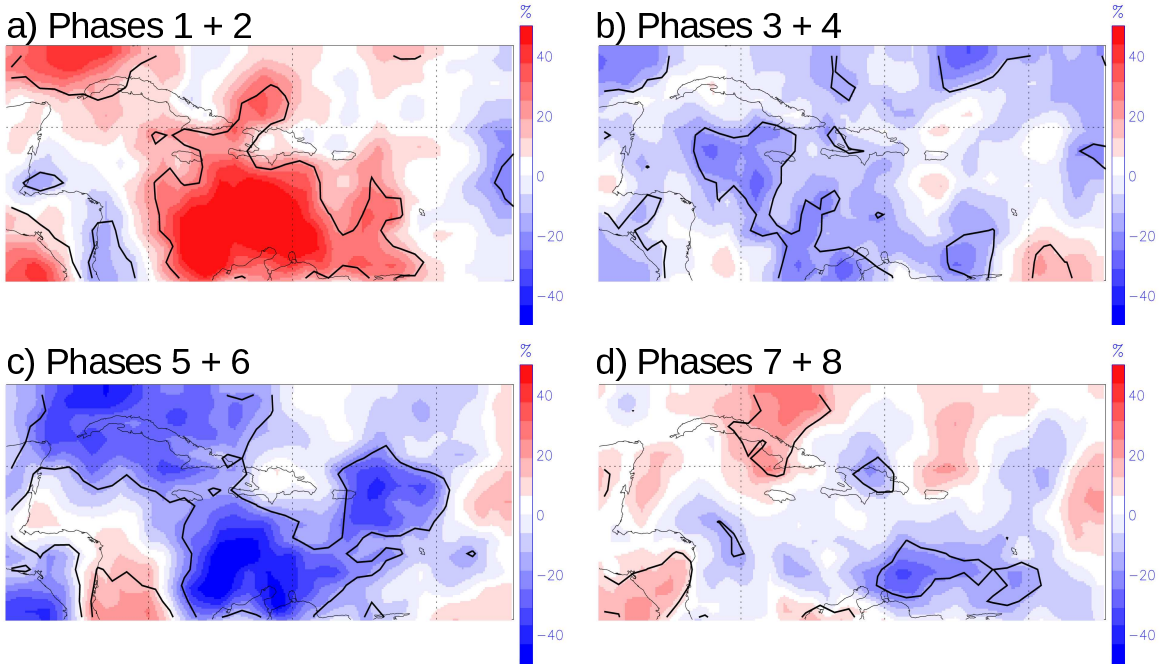

Fig. 35. Precipitation anomalies from the annual cycle (as percent change from annual average mean precipitation) composited by phase of the MJO, a) phases 1 and 2, b) phases 3 and 4, c) phases 5 and 6, and d) phases 7 and 8. Thick black lines show 90 % significance as calculated by a simple t-test.

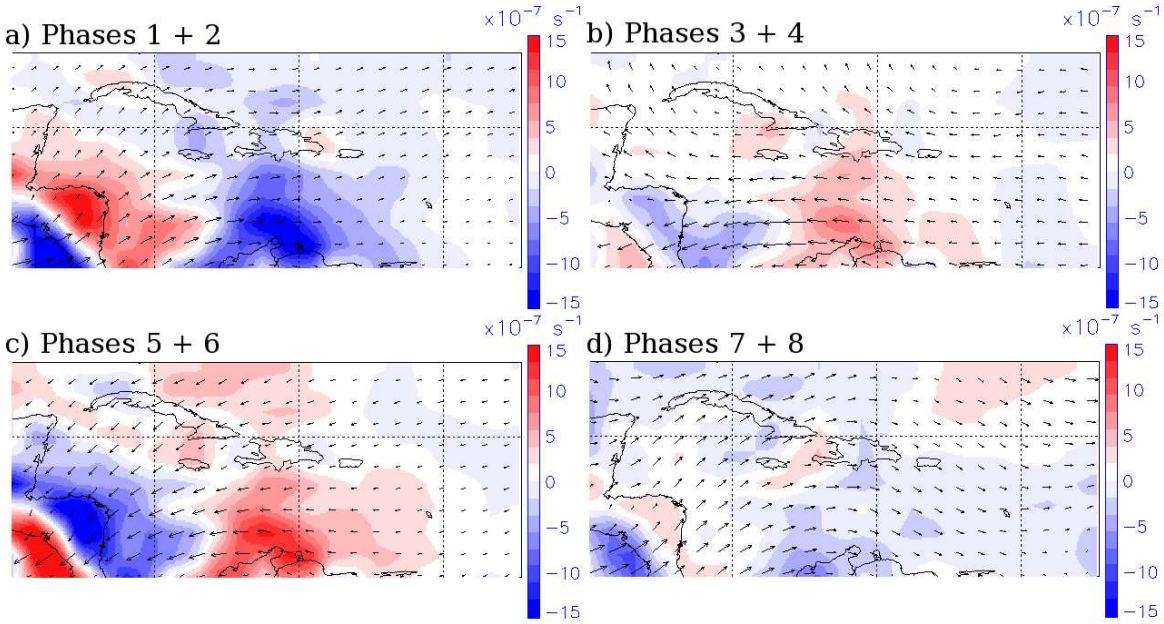

Fig. 36. Low-level (925 hPa) divergence anomalies (shading) and winds (vectors) for a) phases 1 and 2, maximum wind vector 2.9 m s^{-1}, b) phases 3 and 4, maximum wind vector 1.1 m s^{-1}, c) phases 5 and 6, maximum wind vector 2.8 m s^{-1}, and d) phases 7 and 8, maximum wind vector 1.1 m s^{-1}.

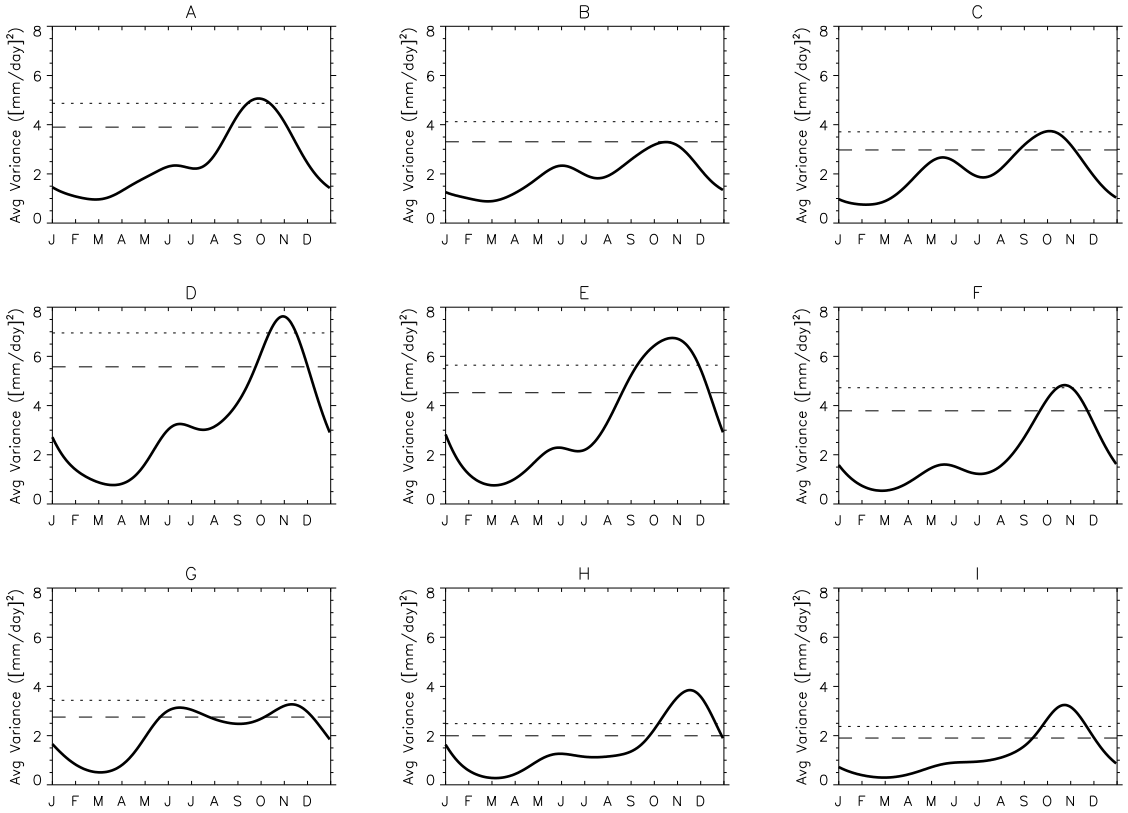

Fig. 37. Seasonal cycle of area-averaged precipitation anomaly variance (solid) in the intraseasonal period (30-90 days). A through I correspond to averaging regions shown in Fig. 33. Dashed and dotted lines indicate 80 and 90 % significance levels above red noise respectively.

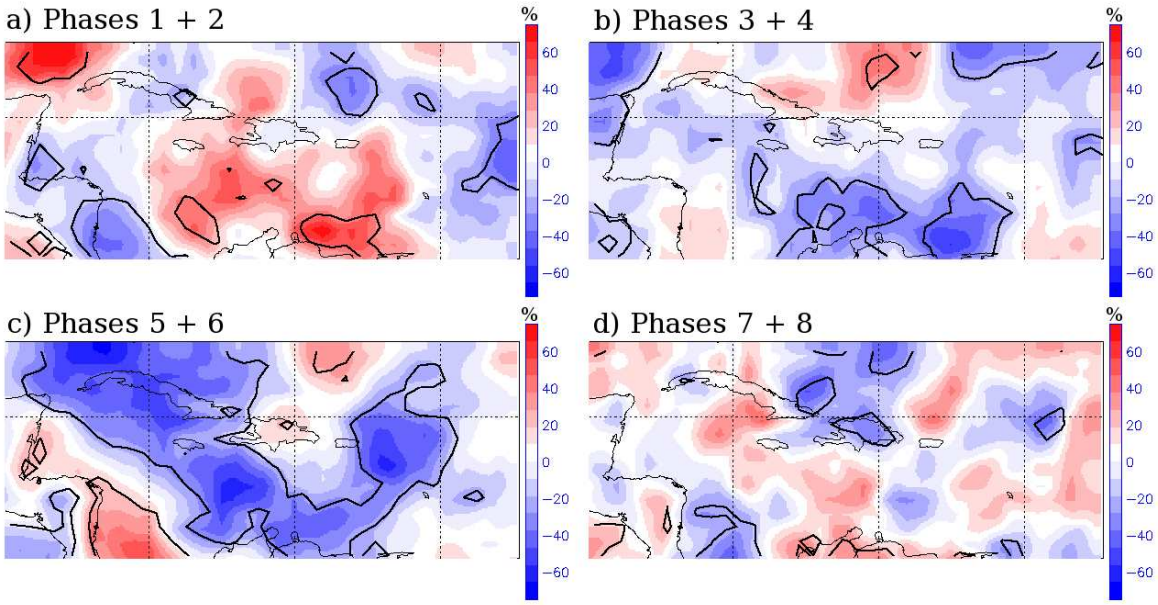

Fig. 38. As Fig. 35 but for SON only.

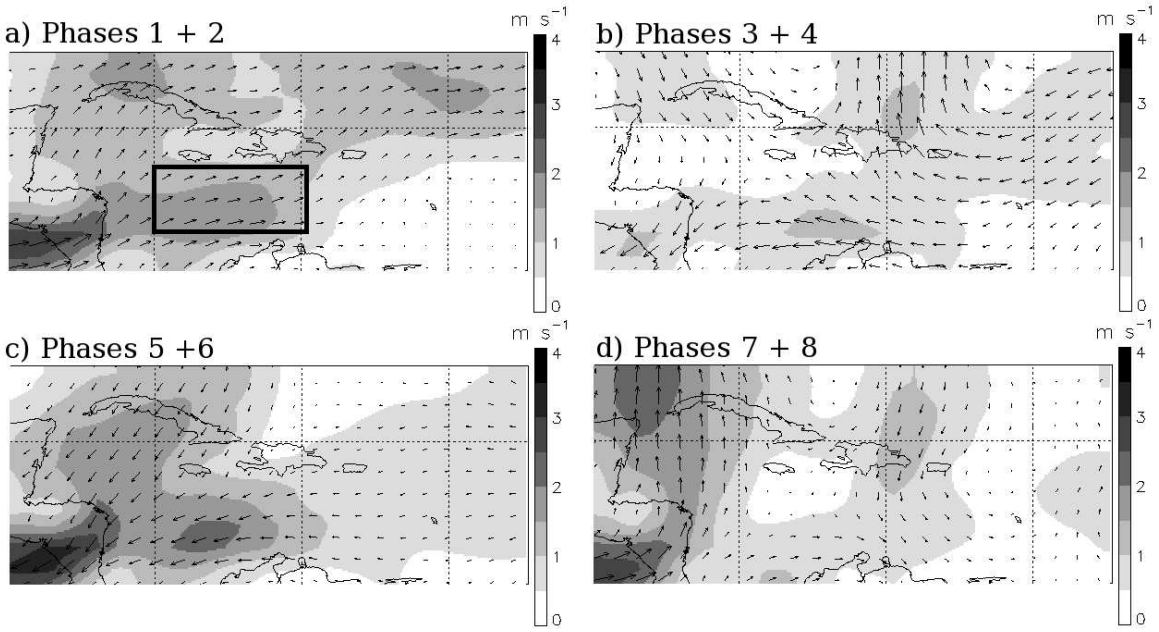

Fig. 39. Seasonal wind speed (shading, m s^{-1}) and direction (vectors) anomalies composited by phase of the MJO for SON. Box in (a) indicates region for calculating CLLJ index.

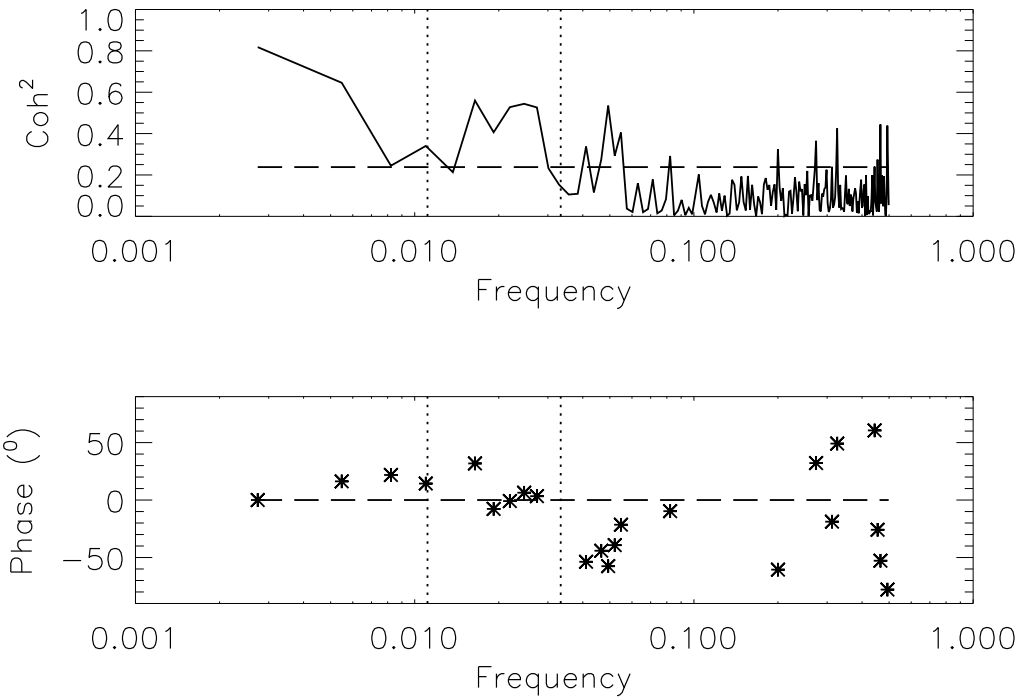

Fig. 40. Upper panel: Coherence squared between time series of jet index and Caribbean area averaged precipitation anomalies. Dashed line shows 95 % significance line. Lower panel: Phase between the two time series. Phase is only shown where coherence squared is significant with dashed line indicating zero phase difference. Dotted lines in each panel indicates frequencies corresponding to instraseasonal periods of 30 and 90 days

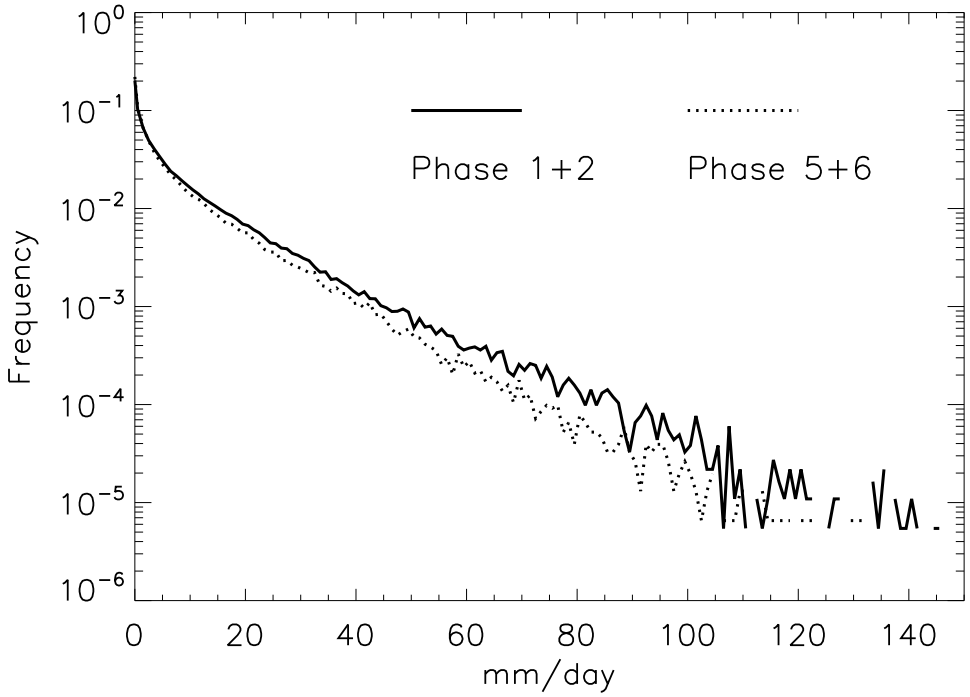

Fig. 41. Probability distribution functions of total precipitation (mm day^{-1}) across all seasons and years at each grid point, composited by either phase 1 and 2 (solid line) or phase 5 and 6 (dotted line).

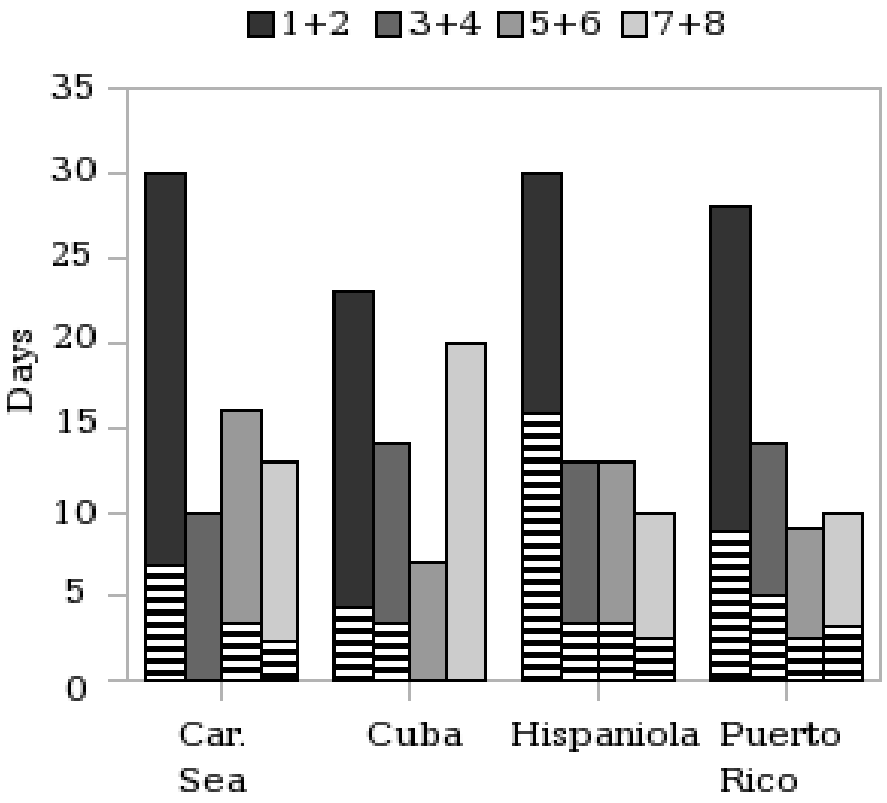

Fig. 42. Number of days in each phase of the MJO for 100 highest rain rate days (across all seasons and years) at four Caribbean locations. Only days with strong MJO events are included. Striped bars indicate the number of days in each phase at each location that were directly associated with tropical storms.

APPENDIX C

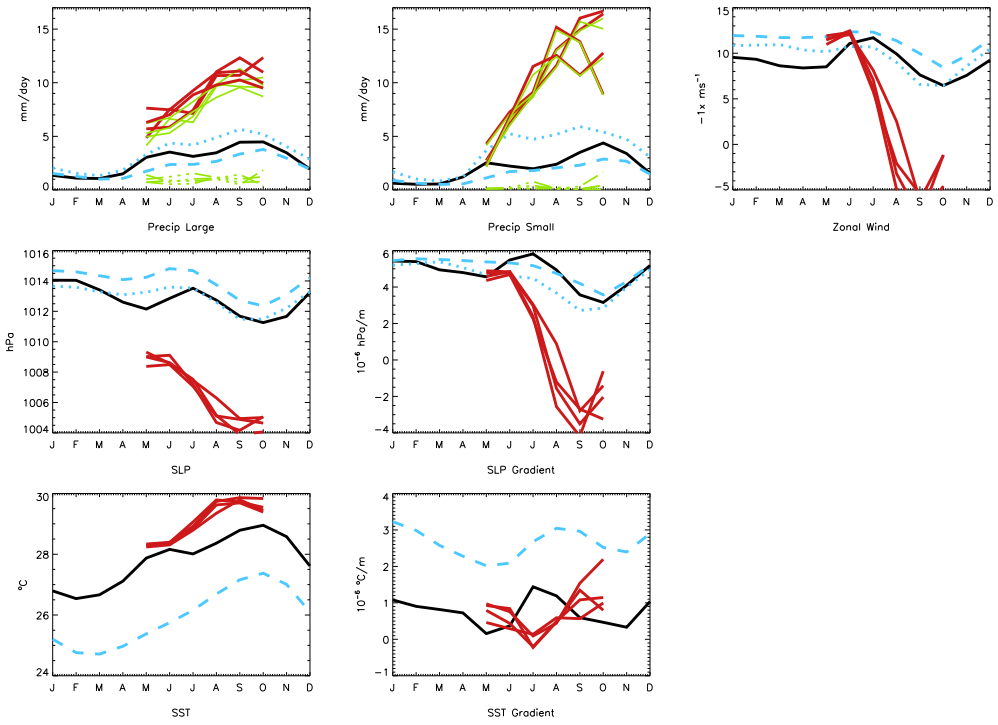

Fig. 43. Seasonal cycle of seven variables related to the CLLJ. Precipitation large (mm/day, 10-25°N, 55-90°W); Precipitation small (mm/day, 11-17°N, 70-80°W), zonal wind (-1 x m/s,12.5-17.5°N, 70-80°W), Sea Level Pressure and Sea Level Pressure gradient (hPa, 10^{-6} hPa/m, 12.5-17.5°N, 70-80°W), SST and SST gradient (°C, 10^{-6}°C/m, 12-16°N, 70-80°W). Black lines are observations/reanalysis, blue dashed are CMIP, blue dotted are AMIP and red are WRF-ROMS ensemble members. In the precipitation plots, the solid green shows cumulus rain (from convective parameterization) and dashed-dotted green shows grid scale precipitation (from microphysics parameterization).

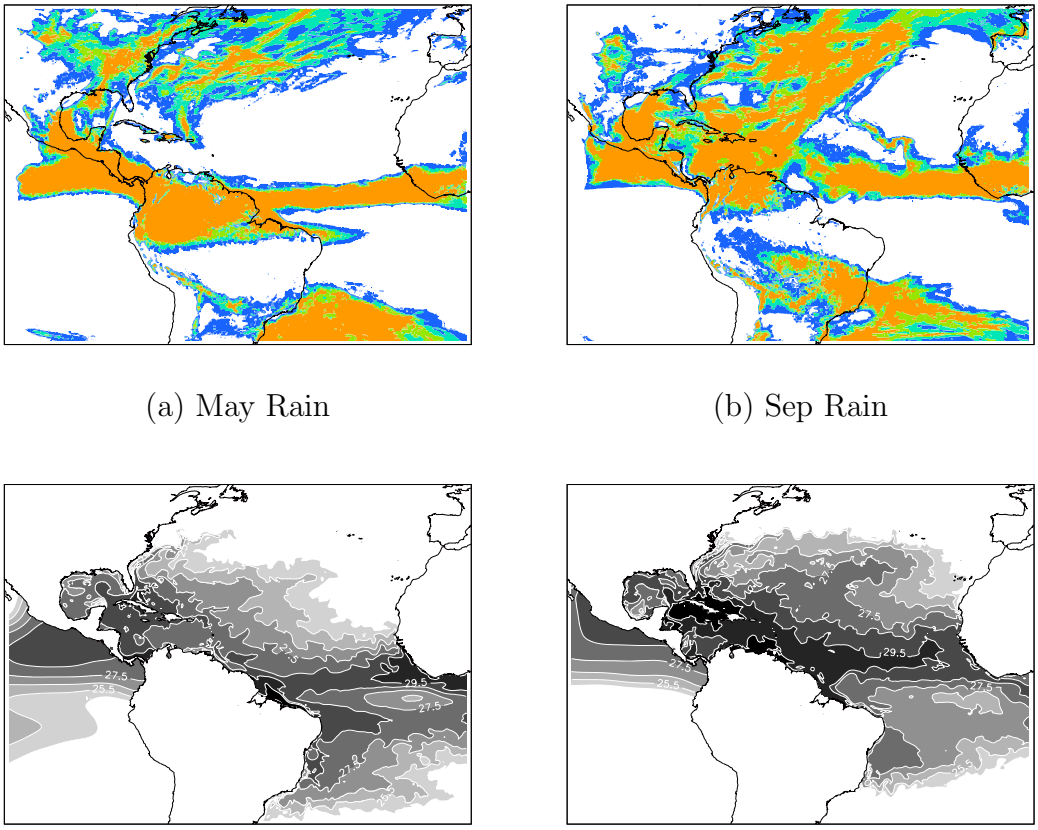

(a) May Rain

(b) Sep Rain

(c) May SST

(d) Sep SST

Fig. 44. Monthly mean quantities for May and September from one ensemble of WRF-ROMS coupled regional model. Rainfall from contours are 2,4,6,8 mm/day and SST contours every 1°C beginning at 23.5°C

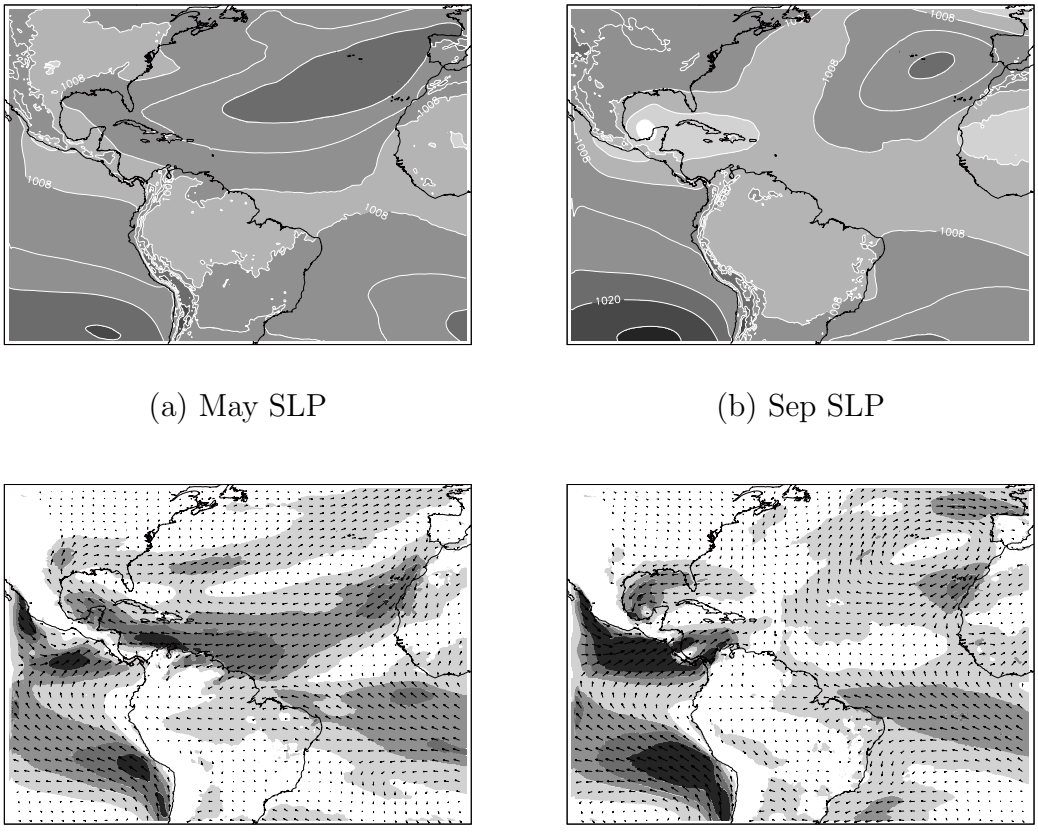

(a) May SLP

(b) Sep SLP

(c) May 925 hPa Wind

(d) Sep 925 hPa Wind

Fig. 45. Monthly mean quantities for May and September from one ensemble of WRF-ROMS coupled regional model. SLP contours every 4 hPa, and wind vectors are plotted every 10th point with speed contours at 2,4,6,8,10,12 m/s.

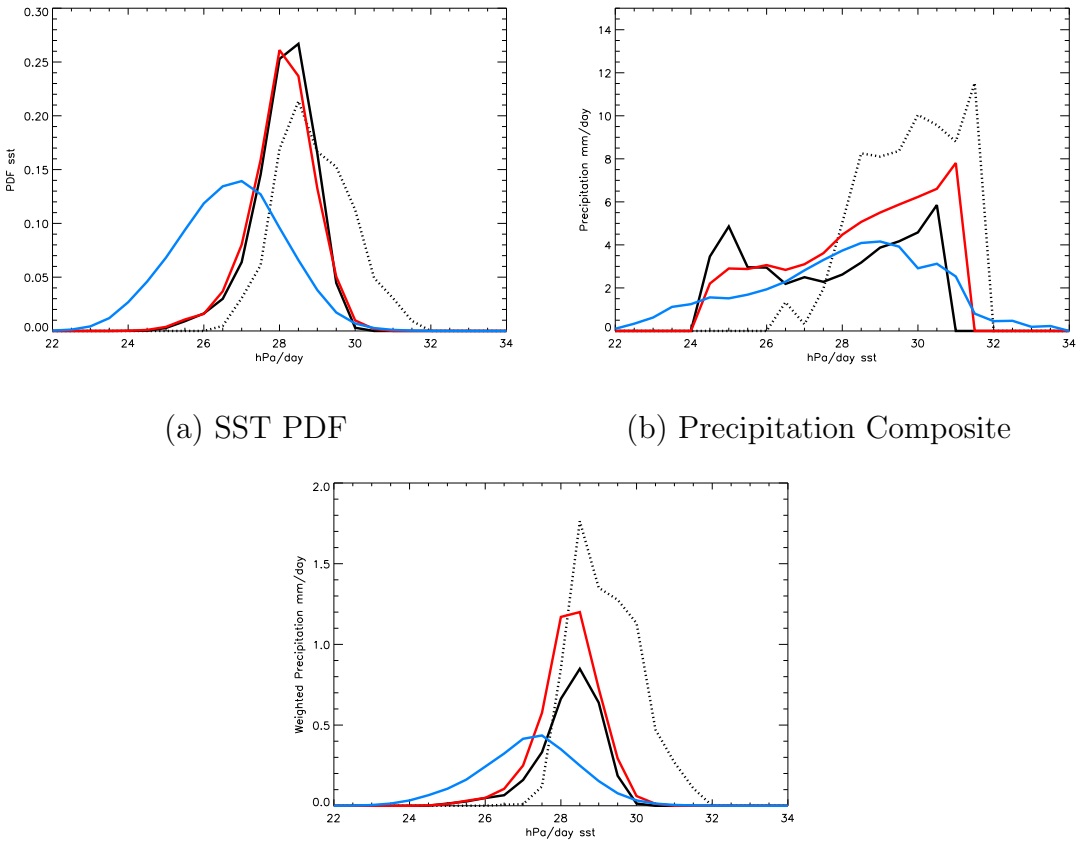

(a) SST PDF

(b) Precipitation Composite

(c) Precipitation Weighting

Fig. 46. Regime sorting analysis by SST for one ensemble of WRF-ROMS coupled model. Black line indicates observations, red line AMIP model mean, blue line CMIP model mean and dashed black line WRF-ROMS simulation. All calculations are for May through October only.

VITA

Elinor Ruth Martin

Department of Atmospheric Sciences

Texas A&M University

3150 TAMU

College Station, TX 77843-3150

B.Sc., Meteorology with a year in Oklahoma, 2005, University of Reading

M.S., Atmospheric Science, 2007, Colorado State University

Ph.D., Atmospheric Sciences, 2011, Texas A&M University